

Room-Temperature Synthesis of Transition Metal Clusters and Main Group Polycations from Ionic Liquids

DISSERTATION

zur Erlangung des akademischen Grades

Doctor rerum naturalium

(Dr. rer. nat.)

vorgelegt

**der Fakultät Mathematik und Naturwissenschaften
der Technischen Universität Dresden**

von

M. Phil. Ejaz Ahmed

geboren am 06.07.1978 in Attock, Pakistan

Eingereicht am 11.07.2011

Die Dissertation wurde in der Zeit von 04/2007 bis
06/2011 an der Fachrichtung Chemie und Lebensmittelchemie angefertigt.

Tag der Verteidigung: 06.12.2011

1. Gutachter: Prof. Dr. Michael Ruck

2. Gutachter: Prof. Dr. Johannes Beck

Dedicated to my dear brother

Muhammad Arshad

Contents

1. Homo- and Heteroatomic Polycations of Groups 15 and 16.....	1
1.1. Synthesis in Inorganic Solvents.....	3
1.1.1. Homoatomic Polycations from Inorganic Solvents	3
1.1.2. Heteroatomic Polycations from Inorganic Solvents.....	6
1.2. High-Temperature Synthesis in Melts and by Chemical Vapor Transport.....	8
1.2.1. Homoatomic Polycations from High-Temperature Synthesis.....	9
1.2.2. Heteroatomic Polycations from High-Temperature Synthesis.....	13
1.3. Synthesis in Organic Solvents.....	15
1.4. Synthesis in Ionic Liquids	17
1.4.1. Homoatomic Polycations from Ionic Liquids	17
1.4.2. Heteroatomic Polycations from Ionic Liquids	18
1.5. Chemistry of Polynuclear Transition Metals Complexes in Ionic Liquids.....	21
1.5.1. Binuclear Complexes	22
1.5.2. Trinuclear Complexes	24
1.5.3. Tetranuclear Complexes.....	26
1.5.4. Pentanuclear Complexes	28
1.5.5. Hexanuclear and High-Nuclearity Complexes.....	30
2. Experimental.....	33
2.1. Synthesis.....	33
2.2. X-Ray Crystallography.....	33
2.3. Magnetic Susceptibility Measurements.....	34
2.4. Raman Spectroscopy	34
2.5. Quantum Chemical Calculations.....	34
3. Synthesis and Characterization of Polycationic Bismuth Cluster Compounds.....	36
3.1. Synthesis of $\text{Bi}_5[\text{AlCl}_4]_3$	36
3.2. Synthesis of Bi_6Cl_7	36
3.3. Results and Discussion	36
4. Synthesis and Characterization of Polycationic Tellurium Cluster Compounds	42
4.1. Synthesis of $[\text{Mo}_2\text{Te}_{12}]\text{I}_6$	42
4.2. Synthesis of $\text{Te}_4[\text{AlCl}_4]_2$	42
4.3. Synthesis of $\text{Te}_4[\text{Bi}_6\text{Cl}_{20}]$	42
4.4. Synthesis of $\text{Te}_6[\text{WOCl}_4]_2$	42

4.5. Synthesis of $\text{Te}_8[\text{Bi}_4\text{Cl}_{14}]$	43
4.6. Results and Discussion	43
5. Synthesis and Characterization of $\text{Sn}[\text{SnCl}][\text{W}_3\text{Cl}_{13}]$	55
5.1. Synthesis of $\text{Sn}[\text{SnCl}][\text{W}_3\text{Cl}_{13}]$	55
5.2. Results and Discussion	55
6. Synthesis and Characterization of Molybdenum Cluster Compounds.....	60
6.1. Synthesis of $\text{Bi}[\text{Mo}_5\text{Cl}_{13}]\text{Cl}$	60
6.2. Synthesis of $\text{BiCl}[\text{Mo}_6\text{Cl}_{14}]$	60
6.3. Results and Discussion	60
7. Synthesis and Characterization of $[\text{Sb}_{10}\text{Se}_{10}][\text{AlCl}_4]_2$	67
7.1. Synthesis of $[\text{Sb}_{10}\text{Se}_{10}][\text{AlCl}_4]_2$	67
7.2. Results and Discussion	67
8. Synthesis and Characterization of $\text{Te}_4[\text{Bi}_{0.74}\text{Cl}_4]$	79
8.1. Synthesis of $\text{Te}_4[\text{Bi}_{0.74}\text{Cl}_4]$	79
8.2. Results and Discussion	79
9. Conclusion and Outlook	90
10. Acknowledgment	94
11. References	95
12. Publications	107

1. Homo- and Heteroatomic Polycations of Groups 15 and 16

The first synthesis of a chalcogen polycation was possibly carried out in 1798, when *Klaproth* described that tellurium gradually dissolves in sulfuric acid to give a red solution [1]. Following him, in the early 19th century, *Bucholz* and *Magnus* prepared colored solution for sulfur and selenium in sulfuric acid and oleum respectively [2]. It took more than 150 years until the true nature of the species responsible for such coloration was interpreted when *Bjerrum et al.* and *Gillespie et al.* confirmed spectroscopically that the species are polycations, e.g. Te_4^{2+} , S_4^{2+} , or Se_4^{2+} [3, 4]. However, the first chalcogen polycation was isolated in 1962 by *Bartlett et al.* by reacting oxygen and PtF_6 , yielding $\text{O}_2[\text{PtF}_6]$ containing the oxygen polycation O_2^+ [5]. Later, X-ray crystallographic studies proved the existence and revealed the shape of other chalcogen polycations thereby opening the way to an understanding of the relations between composition, charge, structure, and bonding.

As far as the polycations of group 15 are concerned, the early investigations into the nature of “BiCl” led to the discovery of the first bismuth polycation Bi_9^{5+} . In 1908, *Eggink* carried out the reduction of bismuth trichloride with elemental bismuth to synthesize “BiCl” [2]. About 60 years later, X-ray crystallographic investigations by *Corbett* and co-workers revealed the true composition to be $\text{Bi}_{24}\text{Cl}_{28} = \text{Bi}_6\text{Cl}_7$ [6, 7]. In the crystal structure they found tri-capped trigonal prismatic Bi_9^{5+} polycations accompanied by chlorido-bismuthate(III) anions.

In the early 1970s, *Paul et al.* and *Gillespie et al.* provided spectroscopic evidence for antimony, arsenic and phosphorus homoatomic polycations by analyzing different colored solutions, obtained by oxidizing the respective element in protic acids or liquid SO_2 [8, 9]. However, the first structurally characterized nitrogen polycation appeared in 2001, when *Christe et al.* managed to isolate N_5^+ from anhydrous HF solution [10a]. A while later, *Kloo* and co-workers obtained an antimony polycation Sb_8^{2+} from Ga/GaCl₃-benzene media in 2004 [10b]. In addition to homoatomic, a number of heteroatomic polycations were also reported by several research groups.

There are plenty of well-established methods for the synthesis of such polycations, all of which need strongly polar media such as H_2SO_4 , anhydrous HF, HSO_3F , liquid SO_2 , molten salts, e.g. $\text{Na}[\text{AlCl}_4]$, or GaX_3 -benzene media ($X = \text{Br}, \text{Cl}$). The particular species are

converted to the polycationic clusters through; (i) oxidation using appropriate oxidants such as AsF_5 , SbF_5 , WCl_6 , or MoOCl_4 [11, 13], (ii) synproportionation in the presence of a strong halogenide ion acceptor such as AlX_3 , ZrX_4 or BiX_3 ($X = \text{Cl, Br, I}$) [13–15], and (iii) reduction with elemental Ga or oxidation by GaX_3 in benzene ($X = \text{Cl, Br}$) [16].

Recently room temperature ionic liquids (RTIL) have been introduced as a new alternative reaction medium for the synthesis of polycations and cluster compounds [17–23].

A number of review articles on the synthesis of polycations have been published by *Gillespie* and co-workers, in which they highlighted the route using highly acidic media or liquid SO_2 and elucidated the structures of the several polycations [11]. *Corbett* reviewed the homoatomic polycations of main group elements synthesized through the molten salts approach [14c]. In 1989, *Passmore* et al. discussed in detail the nature of bonding and charge delocalization in some of the unusual non-classically bonded homoatomic polycations [24]. The latest reviews date from 2000: *Passmore* and co-workers surveyed all known homoatomic polycations of the chalcogens and halogens, studied their bonding, reaction kinetics and thermodynamics to estimate the stabilities using Born-Fajans-Haber cycles [25]. Meanwhile, *Beck* contributed two review articles, first in 1994, on the preparation of chalcogen polycations via chemical vapor transport (CVT) [12], a new synthetic route leading to novel polycations [13a], and second in 1997, in which he treated the chalcogens polycations with respect to their structure and bonding according to the Zintl concept [13b]. In 1999, *Kloo* et al. reviewed different preparation routes for the naked clusters of the post-transition elements and explained their structure and bonding [26]. A review article on sub-valent bismuth compounds was published by *Ruck* in 2001, which covers the whole spectrum from partially oxidized porous metals, through one- and two-dimensional metals, to semiconducting ionic or molecular cluster compounds including new bismuth polycations [27]. In 2004, two comprehensive accounts were presented separately by *Krossing* and *Sheldrick*, focusing on the cages and clusters of the group 15 elements and chalcogens respectively [28, 29]. They concentrated mainly on the bonding and geometries of the isolated cationic, neutral, and anionic homoatomic cages and clusters.

The last 12 years have provided four new homoatomic polycations, i.e. N_5^+ , Bi_5^+ , Bi_6^{2+} , Sb_8^{2+} , and 15 new heteroatomic polycations with hitherto unprecedented structures e.g. $(\text{S}_4\text{N}_5)^+$, $(\text{Bi}_4\text{E}_4)^{4+}$ ($E = \text{S, Se, Te}$), ${}^1[\text{Sb}_2\text{Te}_2]^+$, $(\text{Pd}@\text{Bi}_{10})^{4+}$, $(\text{Au}@\text{Bi}_{10})^{5+}$, $(\text{Bi}_{10}\text{Au}_2)^{6+}$, $(\text{Bi}_8\text{Si}_2)^{3+}$, $(\text{Sb}_7\text{S}_8\text{Br}_2)^{3+}$, ${}^2[\text{A}_2\text{Te}_2\text{Br}]^+$ ($A = \text{Bi, Sb}$), $(\text{As}_3\text{S}_5)^+$, $(\text{Bi}_3\text{GaS}_5)^{2+}$, and $(\text{Sb}_{10}\text{Se}_{10})^{2+}$

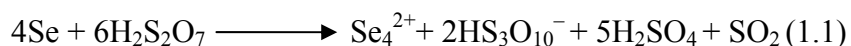
[Table 1.1]. The synthetic schemes for the polycationic clusters are regrettably limited, because they need large, weakly basic, weakly coordinating and non oxidizing anions to stabilize them in solution and in solid state. Until now, four different successful preparative methods have been reported in literature.

1.1. Synthesis in Inorganic Solvents

The superacid route to polycationic clusters was first introduced by *Klaproth* for the synthesis of Te_4^{2+} by the oxidation of the elemental tellurium in concentrated sulfuric acid where one-component superacids were used both as the oxidizing agent and as the source of the necessary weak Lewis base [1]. The superacids are practical and successful for the synthesis of clusters in solution but several difficulties are associated with crystallization and recovery of solid cluster phases [30]. *Gillespie, Passmore* and co-workers put their efforts to overcome these difficulties by using highly oxidizing agents like pentafluorides of antimony and, even better, arsenic in superacids or inert solvents (most often liquid SO_2) to prepare ligand-free “naked” clusters of post-transition elements. This method proved to be very promising and resulted in the fabrication of several new compounds containing variety of polycationic clusters of chalcogens, bismuth, and halogens [11, 24, 25].

1.1.1. Homoatomic Polycations from Inorganic Solvents

Numerous homoatomic polycations were synthesized using superacidic media and liquid SO_2 . They were characterized spectroscopically in solution and through X-ray crystallography in the form of solid phases. The tetraatomic cations E_4^{2+} ($E = \text{S}, \text{Se}, \text{Te}$) were the earliest to be characterized. In 1971, the first compound $\text{Se}_4[\text{HS}_2\text{O}_7]_2$ was crystallized from oleum in the form of orange needles containing Se_4^{2+} polycations. Originally, the synthesis was performed according to *Klaproth* by the oxidation of selenium in disulfuric acid [31], equation (1.1).



Other chalcogen polycationic compounds were more difficult to isolate from the solution, and it was in early 1980s that the colorless crystals of $\text{S}_4[\text{AsF}_6]_2 \cdot 0.6\text{SO}_2$ were obtained by reacting S_8 with AsF_5 in the presence of traces of bromine in liquid SO_2 . Hence, the square planar and discrete molecular entity S_4^{2+} was finally characterized [32]. The tellurium homologue Te_4^{2+} had already been isolated in 1970 as $\text{Te}_4[\text{AlCl}_4]_2$ through a melting

reaction and its crystal structure was determined by *Corbett* and co-workers [14b]. The same polycation was also found in $\text{Te}_4[\text{SbF}_6]_2$ as dark red crystals by reacting a mixture of tellurium and germanium with SbF_5 in liquid SO_2 [33]. The tetraatomic E_4^{2+} polycations show charge delocalization and are incompatible with the Zintl concept. The E_4^{2+} polycations carry 22 valence electrons and, according to the Zintl concept, they should contain two double and two triple bound chalcogen atoms in a butterfly conformation where both positive charges are formally localized. Instead, the E_4^{2+} cations show delocalization, which was confirmed by a series of theoretical investigations at different computational levels [34]. The considerable aromatic π stabilization of E_4^{2+} cations was concluded from all calculations.

The trigonal prismatic Te_6^{4+} polycation had appeared first in 1979 as $\text{Te}_6[\text{AsF}_6]_4 \cdot 2\text{AsF}_3$ and $\text{Te}_6[\text{AsF}_6]_4 \cdot 2\text{SO}_2$ by the oxidation of elemental tellurium with AsF_5 in AsF_3 or liquid SO_2 (Figure 1.1a) [35]. Te_6^{4+} is also an example of non-classical structure which has 32 valence electrons. In accordance with the Zintl concept, the number of triple bonded Te atoms should be reduced from six to four but Te_6^{4+} shows the phenomenon of bond delocalization and therefore adopts a non-classical structure.

The heptaatomic tellurium polycation is known as the repetition unit of the polymeric chain $\infty[\text{Te}_7^{2+}]$. $\text{Te}_7[\text{AsF}_6]_2$ was synthesized by reacting $\text{Te}_4[\text{AsF}_6]_2$ with $\text{Fe}(\text{CO})_5$ in liquid SO_2 , in which the iron carbonyl is presumably responsible for the reduction of Te_4^{2+} to Te_7^{2+} . The infinite chain of the polycation consists of six-membered tellurium rings connected through bridging, triply bonded tellurium atoms, which carry the formal positive charges and represent a Zintl precise structure (Figure 1.4d) [36].

The eight-membered E_8^{2+} homologues of sulfur and selenium polycations were also prepared. They have similar bicyclic structures derived from the crown shaped ring of the neutral S_8 or Se_8 molecules. Flipping one atom from the *exo* to the *endo* position, excluding an electron pair and deformation of the ring to an oval leads to a bicyclic structure which shows slight distortion from C_s symmetry. The S_8^{2+} polycation was obtained in 1971 as $\text{S}_8[\text{AsF}_6]_2$ by the oxidation of sulfur with AsF_5 in HF (Figure 1.1c) [37], but the crystallization of compounds containing Se_8^{2+} polycations was finally successful in 1987, when elemental tellurium and selenium were oxidized by AsF_5 in liquid SO_2 to get dark green crystals of $(\text{Te}_6)(\text{Se}_8)[\text{AsF}_6]_6 \cdot \text{SO}_2$ [38]. However, Se_8^{2+} had already been isolated through molten salts approach as $\text{Se}_8[\text{AlCl}_4]_2$ and structurally characterized by *Corbett* et al. in 1969 [39].

The Se_{10}^{2+} polycation was found as a six-membered twisted ring that is linked across the 1,4- positions by a chain of four Se atoms leading to a bicyclo[4.2.2]decane type structure. It was prepared by oxidizing selenium with AF_5 ($A = \text{As}, \text{Sb}$) in liquid SO_2 [40]. The Se_{10}^{2+} polycation has an electron-precise, localized bond structure (Figure 1.1d).

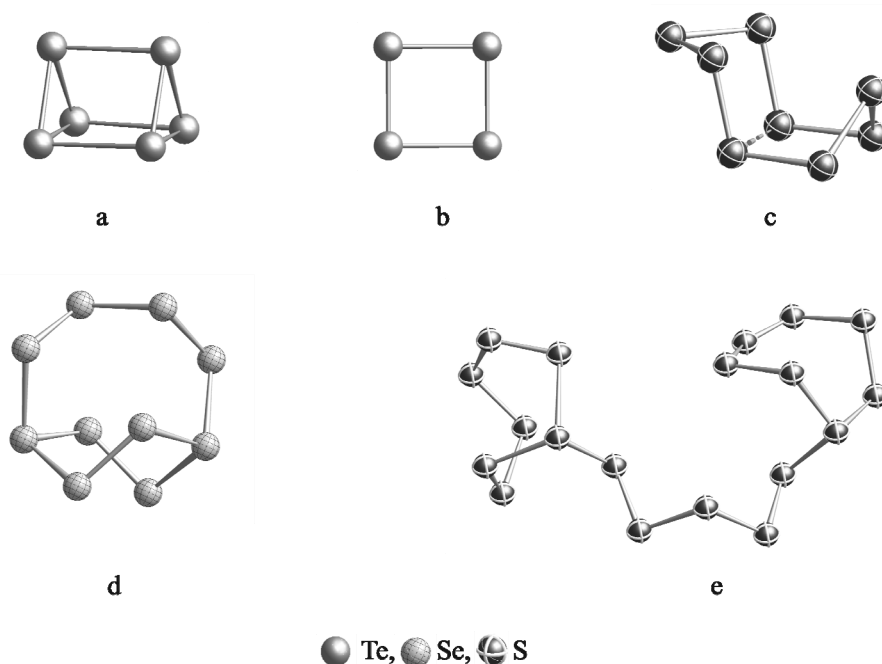


Figure 1.1: The structures of the homoatomic polycations (a) Te_6^{4+} (b) Te_4^{2+} (c) S_8^{2+} (d) Se_{10}^{2+} , and (e) S_{19}^{2+} .

S_{19}^{2+} is the heaviest homoatomic polycation synthesized by this approach, here by reacting elemental sulfur with AsF_5 in a mixture of SO_2ClF and liquid SO_2 [41]. Its structure consists of two seven-membered rings in the chair conformation connected by a S_5 -chain (Figure 1.1e). The three bonded sulfur atoms hold the formal positive charges and adopt a classical structure.

Besides the spectroscopic evidences for arsenic (e.g. As_4^{2+} , As_2^{2+}), phosphorus (P_8^{2+} , P_4^{2+}), and antimony (Sb_8^{2+} , Sb_4^{2+}) polycations in protic acids or liquid SO_2 [8, 9], the trigonal bipyramidal Bi_5^{3+} remained the only group 15 polycation that could be isolated by this route and characterized. It was obtained as $\text{Bi}_5[\text{AsF}_6]_3 \cdot 2\text{SO}_2$ by the oxidation of elemental bismuth with AsF_5 in liquid SO_2 [42] equation (1.2).



1.1.2. Heteroatomic Polycations from Inorganic Solvents

Besides plenty of homoatomic polycations of groups 15 and 16, a small number of heteroatomic polycations have been discovered. Among them, polycations that are built by two different kinds of chalcogen atoms (E) represent the largest group. *Gillespie et al.* synthesized a variety of such mixed polycations from liquid SO_2 or in a liquid mixture of $\text{SO}_2/\text{ClF}/\text{SO}_2$ and structurally characterized them by means of X-ray crystallography.

For the square (E_4)²⁺ polycations, a number of mixed group 16 polycations were isolated e.g. $(\text{Te}_2\text{Se}_2)^{2+}$, $(\text{Te}_3\text{Se})^{2+}$, or $(\text{S}_3\text{Se})^{2+}$ [43]. The non-classical (E_4)²⁺ polycations show significant deviations from the square-planar conformation. They were obtained as salts of either fluorido-stibates(III) or fluorido-arsenates(III) by reacting the respective elements with SbF_5 or AsF_5 in liquid SO_2 .

The six-membered (E_6)²⁺ species are also known, e.g. $(\text{Te}_3\text{S}_3)^{2+}$, $(\text{Te}_2\text{S}_4)^{2+}$ or $(\text{Te}_x\text{Se}_{6-x})^{2+}$ [44], they are almost isostructural having a six-membered ring in boat-conformation (Figure 1.2b, 1.2f). A series of heteroatomic $(\text{Te}_x\text{Se}_{6-x})^{2+}$ polycations were prepared as described above, but for the synthesis of $(\text{Te}_3\text{S}_3)^{2+}$ two different methods were applied using liquid SO_2 as the reaction medium: (i) by reacting $\text{Te}_4[\text{AsF}_6]_2$ and $\text{S}_8[\text{AsF}_6]_2$, (ii) by reacting a mixture of Te/S with AsF_5 . All six-membered heteroatomic (E_6)²⁺ cations follow the Zintl concept and exhibit classical structures with localized bonds.

Only two interchalcogen (E_8)²⁺ polycations, $(\text{Te}_4\text{S}_4)^{2+}$ and $(\text{Te}_2\text{Se}_6)^{2+}$, were obtained by this synthetic route. The $(\text{Te}_2\text{Se}_6)^{2+}$ polycation has a bicyclo[2.2.2]octane structure with the two tellurium atoms occupying the bridgehead positions. The triple bonded tellurium atoms bear the formal positive charges and reveal an electron-precise structure (Figure 1.2g). Dark brown crystals of $(\text{Te}_2\text{Se}_6)(\text{Te}_2\text{Se}_8)[\text{AsF}_6]_4 \cdot (\text{SO}_2)_2$ resulted from the reaction of tellurium, selenium, and sulfur with AsF_5 in liquid SO_2 [45]. The realgar-like $(\text{Te}_4\text{S}_4)^{2+}$ polycation was prepared by a reaction of a mixture of tellurium and tin powder with AsF_5 in liquid SO_2 [46]. For the cage structures, normally a count of 44 valence electrons is realized, however, the $(\text{Te}_4\text{S}_4)^{2+}$ cation has two extra electrons. According to the Zintl concept, for the four triple bonded Te atoms, the cage structure should bear a positive charge $(\text{Te}_4\text{S}_4)^{4+}$. Consequently, the $(\text{Te}_4\text{S}_4)^{2+}$ cation structure was suggested with a pair of delocalized electrons trapped inside the cluster (Figure 1.2a).

The ten-membered (E_{10})²⁺ heteroatomic polycations, such as (Te_2Se_8)²⁺, ($\text{Te}_{3.7}\text{Se}_{6.3}$)²⁺ or, ($\text{Te}_{4.5}\text{Se}_{5.5}$)²⁺, are the heaviest species synthesized employing this route [45, 47]. The structure of these cations is similar to Se_{10}^{2+} (Figure 1.2e).

Very few heteroatomic polycations that contain elements of groups 15 and 16 are known. The mixed arsenic/chalcogen polycations, (As_3S_4)⁺ and (As_3Se_4)⁺, were also found by Gillespie et al. [48a]. For the synthesis of (As_3S_4)⁺, they treated β - As_4S_4 with AsF_5 or SbF_5 to get the corresponding salts, while in case of (As_3Se_4)⁺, the related amounts of 1:1 or 4:3 As-Se-melts were reacted with either AsF_5 or SbF_5 . Both (As_3S_4)⁺ and (As_3Se_4)⁺ cations have C_s symmetry and are isostructural to P_4S_3 or P_7^{3-} [49], which can be considered to be derived from a tetrahedron of three arsenic atoms and one sulfur or selenium atom with three of its edges bridged by sulfur or selenium atoms (Figure 1.2c). These heteroatomic polycations show classical, electron-precise structures. Some mixed nitrogen/sulfur polycations were also reported e.g. (SN)⁺, (SNS)⁺, (S_4N_4)²⁺, (S_6N_4)²⁺, or (S_5N_5)⁺, they were isolated from liquid SO_2 , HSO_3Cl , or SOCl_2 using a variety of counter ions like $[\text{Al}(\text{OC}(\text{CF}_3)_3)_4]^-$, AlCl_4^- , SbF_6^- , AsF_6^- , or SbCl_6^- etc. [48b–48e].

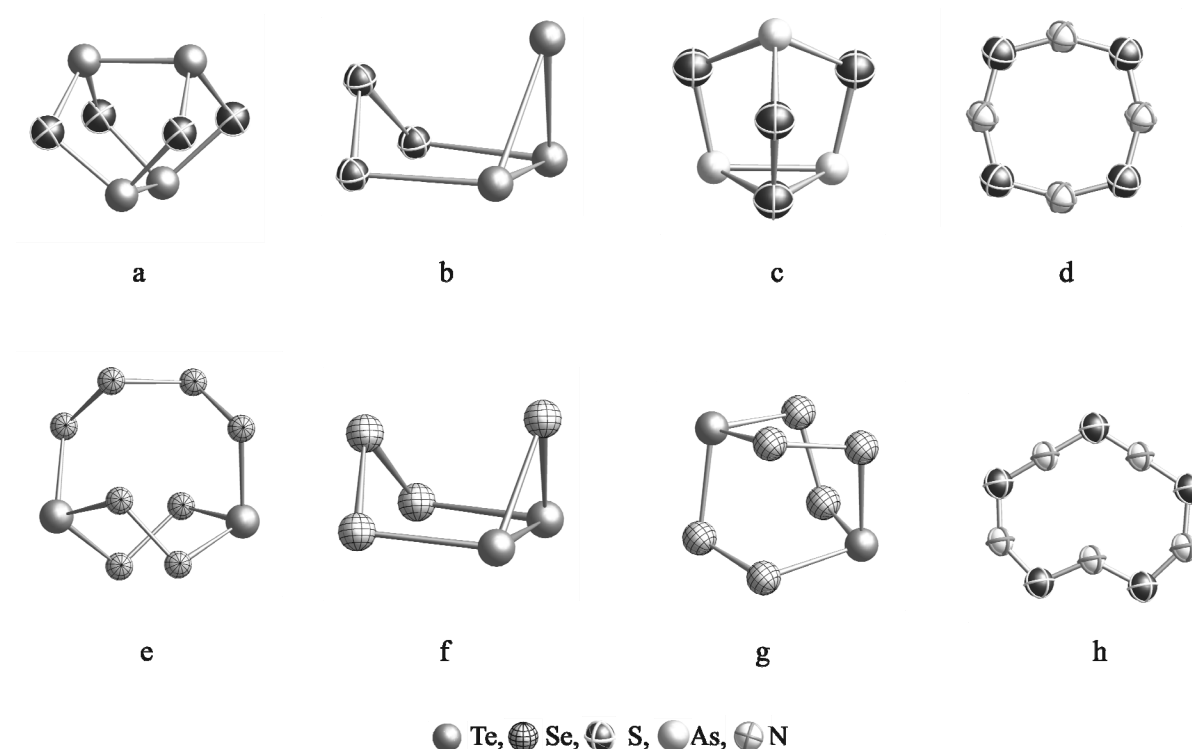


Figure 1.2: The structures of the heteroatomic polycations (a) (Te_4S_4)²⁺ (b) (Te_3S_3)²⁺ (c) (As_3S_4)⁺ (d) (S_4N_4)²⁺ (e) (Te_2Se_8)²⁺ (f) (Te_2Se_4)²⁺ (g) (Te_2Se_6)²⁺, and (h) (S_5N_5)⁺.

The phenomenon of bond delocalization was observed in such heteroatomic polycations

(Figure 1.2d, 1.2h). The use of strong oxidizing agents like AsF_5 or SbF_5 for the post-transition metal cluster synthesis has numerous advantages, e.g. reactions may be carried out in protic acids or in liquid SO_2 at ambient or lower temperature. In addition, the reaction by-products and the solvents are volatile and can be easily separated from the product. However, there are some demerits, which undermine this synthetic approach, e.g. the use of highly toxic AsF_5 or SbF_5 . Moreover, the production of less-volatile by-product SbF_3 on reduction is also a troublesome because it can accept F^- ions to form SbF_6^- or $\text{Sb}_2\text{F}_{11}^-$ as counter-ions. In this perspective, clean syntheses have frequently been made difficult or impossible by coprecipitation of the SbF_3 or by mixed oxidation state anion formation between SbF_5 , SbF_3 , and F^- ions. Otherwise reactions, which lead to a solid residue, yielded contaminated products because of the very low volatility of SbF_3 [30]. Moreover, this type of synthesis requires sophisticated glassware, and chemicals like AsF_5 which are very expensive.

1.2. High-Temperature Synthesis in Melts and by Chemical Vapor Transport

The early investigation into the nature of the subchloride “ BiCl ” fascinated synthetic chemists to explore a new approach to prepare, isolate and characterize the polycationic cluster compounds. This inspiration resulted in the discovery of the high temperature route or molten salts approach, which was mainly developed by *Corbett* and co-workers [14]. This route gifted not only novel polycations, but also assisted to isolate known species, which were not yet well characterized. Low-melting halogenides with melting points above room temperature (e.g. SbCl_3 : mp = 73 °C, AlCl_3 : mp = 193 °C, or GaCl_3 : mp = 80 °C) were used as the reaction media. The most frequently used method to synthesize polycations in melts is the synproportionation, which also proved helpful to solve the issue of “ BiCl ”. The single crystals analysis proved the existence of $\text{Bi}_{24}\text{Cl}_{28} = \text{Bi}_6\text{Cl}_7$ instead of BiCl , which has a structure consisting of tri-capped trigonal prismatic Bi_9^{5+} polycations accompanied by chlorido-bismuthate(III) anions (Figure 1.3e) [6, 7]. Later, *Krebs* et al. managed to modify the scheme by altering the proportion of molten salts to isolate other bismuth polycations [50]. A major obscurity with the synproportionation reaction is that the number of redox reactions that can take place is limited.

Beck brought key improvement in this scheme, which shows apparently similarities to the traditional molten salt route, but it avoids the limitations of synproportionations. This upgraded and advanced strategy is known as chemical vapor transport (CVT), in which a

volatile, high-valent transition metal halogenide acts both as halide acceptor and as oxidizing agent [13a]. *Ruck* et al. further expanded the scope of the higher temperature route by incorporating transition metals in the structure of the bismuth polycations [51]. To summarize, by the higher temperature route, besides known polycations, novel homo- and heteroatomic polycations of groups 15 and 16 also became accessible.

1.2.1. Homoatomic Polycations from High-Temperature Synthesis

Employing the high temperature synthetic route allowed the isolation and subsequent structure determination of polycationic compounds. Bi_5^{3+} and Bi_8^{2+} polycations were first reported by *Bjerrum* et al. in 1967 during the spectrochemical investigation of bismuth metal in dilute solutions of BiCl_3 in liquid NaCl-AlCl_3 and KCl-ZnCl_2 mixtures [52]. *Corbett* attempted to crystallize $\text{Bi}_5[\text{AlCl}_4]_3$ and $\text{Bi}_8[\text{AlCl}_4]_2$ from NaAlCl_4 melts but due to slow equilibration, supercooling phenomena, and problems with twinning, no suitable single-crystals were obtained in the early investigations [14a]. *Krebs* and co-workers reconsidered and refined this synthetic route successfully to obtain good quality single-crystals, which allowed a better structural characterization of the salts $\text{Bi}_5[\text{AlCl}_4]_3$ and $\text{Bi}_8[\text{AlCl}_4]_2$. The Bi_5^{3+} polycation proved to possess trigonal bipyramidal conformation, while Bi_8^{2+} is a square antiprism. (Figure 1.3a, 1.3d) [50].

Later, the square pyramidal Bi_5^+ and the distorted octahedral Bi_6^{2+} polycations were found simultaneously in the compounds $\text{Bi}_{34}\text{Ir}_3\text{Br}_{37}$ and $\text{Bi}_{12-x}\text{MX}_{13-x}$ ($M = \text{Rh, Ir; } X = \text{Cl, Br; } x \leq 1$) (Figure 1.3b, 1.3c) [53]. A better structural characterization of the Bi_6^{2+} cation, as a distorted octahedron with an opened edge, became possible with the discovery of $\text{Bi}_6[\text{PtBi}_6\text{Cl}_{12}]$ [54].

Modified Wade's rules have proven to be a very convenient tool for qualitative estimation of the geometries of homoatomic bismuth clusters, where the 6s electrons form the lone pairs and only the 6p electrons are used in cluster bonding. The geometries of the well-known bismuth polycations are found to be in agreement with the prescribed skeletal electrons (SE) e.g. Bi_5^+ (*nido*, 14 SE) [53], Bi_5^{3+} (*closo*, 12 SE) [14a, 15, 16b, 16c, 50a], Bi_6^{2+} (*nido*, 16 SE) [53, 54], Bi_8^{2+} (*arachno*, 22 SE) [50b, 55], Bi_{10}^{4+} (*arachno*, 26 SE) [51b–51f]. However, according to Wade's rules, the Bi_9^{5+} polycation with 22 SE should adopt a *nido* conformation with the shape of a monocapped square antiprism (C_{4v}), while in most of the crystal structures it is found to be rather close to the tri-capped trigonal prism (D_{3h}), that is a

closo polyhedron (Figure 1.3e) [6, 7, 50c, 56]. Quite recently, for the first time a C_{4v} symmetric Bi_9^{5+} polycation was reported in $\text{Bi}_{18}\text{Sn}_7\text{Br}_{24}$ and $\text{Bi}_9[\text{BiPb}_2\text{Br}_{12}]$ [57]. In agreement with Wade's rules and quantum chemical calculations, the homoatomic *nido* cluster Bi_9^{5+} is a monocapped square antiprism (C_{4v}) (Figure 1.3f).

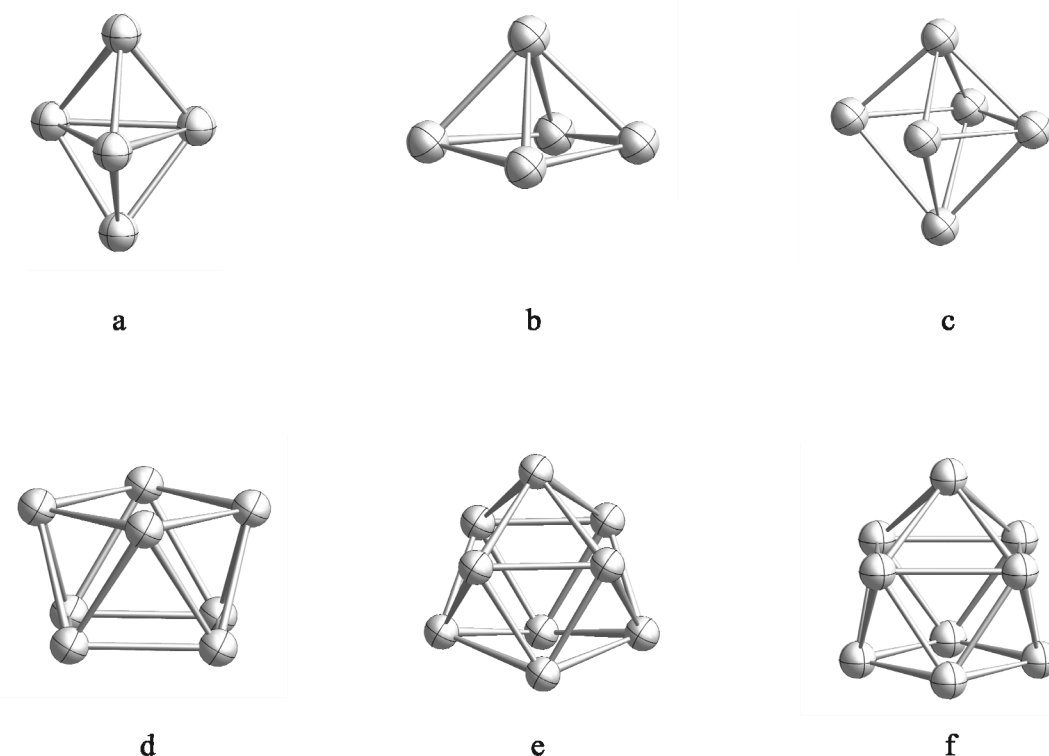


Figure 1.3: The structures of the bismuth homoatomic polycations (a) Bi_5^{3+} (b) Bi_5^+ (c) Bi_6^{2+} with an open edge (d) Bi_8^{2+} (e) Bi_9^{5+} : a tri-capped trigonal prism (D_{3h}), and (f) Bi_9^{5+} : a monocapped square antiprism (C_{4v}).

The square-planar Te_4^{2+} polycation was first isolated by the molten salts approach in 1971 in the form of dark red or violet crystals of $\text{Te}_4[\text{AlCl}_4]_2$ and $\text{Te}_4[\text{Al}_2\text{Cl}_7]_2$ [14b]. Other known square-planar Se_4^{2+} species were also obtained easily by this route [58].

The boat-shaped Te_6^{2+} polycation was trapped in $\text{Te}_6[\text{WOCl}_4]_2$ through CVT (Figure 1.4a) [59a]. A polymeric form, the $^1[\text{Te}_6^{2+}]$ polycation, has been found in $\text{Te}_6[\text{MCl}_6]_2$ ($M = \text{Zr}, \text{Hf}$) [60]. In this case, five-membered rings are connected via single tellurium atoms to a chain (Figure 1.4b). Like trigonal prismatic Te_6^{4+} polycation, Te_6^{2+} also shows a non-classical structure with delocalized bonds but for the polymeric form $^1[\text{Te}_6^{2+}]$, the Zintl concept can be applied to explain the relation between charge and structure. In the cationic chain, there are two threefold coordinated Te atoms, which exhibit three bonds and carry formally the positive charge.

The Te_7^{2+} has been known merely as a polymeric cation. In $\text{Te}_7[\text{AsF}_6]_2$, the infinite chain of the polycation consists of six-membered tellurium rings connected through bridging tellurium atoms (Figure 1.4d) [36], while in $\text{Te}_7[\text{MOX}_4]X$ ($M = \text{Nb}, \text{W}; X = \text{Cl}, \text{Br}$) the ${}^1[\text{Te}_7^{2+}]$ strands are made up from centrosymmetric planar Te_7 -groups linked by a *spiro* fragment of Te-Te bonds to give a folded band [61]. The structure has been rationalized as containing four triple bonded Te atoms bearing a formal positive charge, the central Te atom is in a tetra-coordination with two lone pairs *trans* to each other and having a formal charge of -2 . As a result, the polycation was interpreted as Te_7^{2+} (Figure 1.4c).

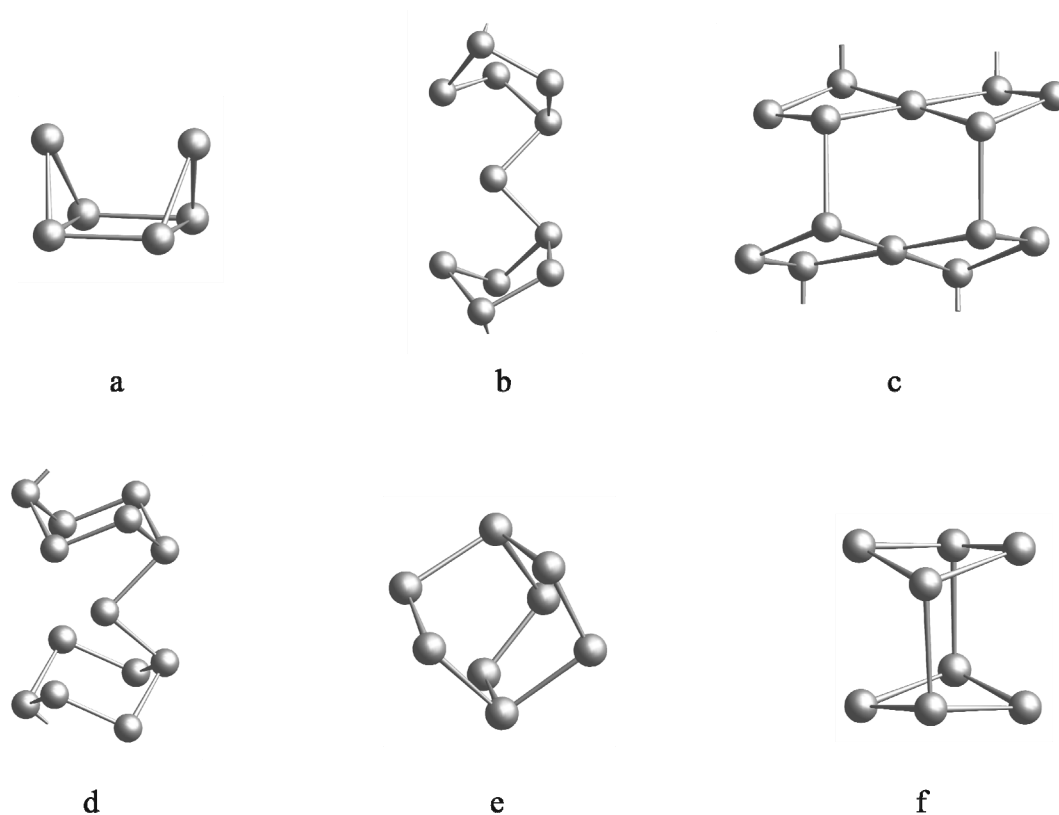


Figure 1.4: The structures of the tellurium homoatomic polycations: (a) Te_6^{2+} , (b) ${}^1[\text{Te}_6^{2+}]$ chain, (c) folded band of ${}^1[\text{Te}_7^{2+}]$, (d) polymeric ${}^1[\text{Te}_7^{2+}]$, (e) Te_8^{2+} , and (f) Te_8^{4+} : a cube with two open edges.

The Te_8^{2+} polycations are found in different conformations. In $\text{Te}_8[\text{WCl}_6]_2$, it shows a bicyclic structure composed of two five-membered rings each in an envelope conformation (Figure 1.5a) [62], while a quasi-bicyclic *exo-endo* conformed Te_8^{2+} ring similar to S_8^{2+} was characterized in $\text{Te}_8[\text{ReCl}_6]$ (Figure 1.1c) [63]. Moreover, a bicyclo[2.2.2]octane structure for Te_8^{2+} polycation has also been described in the compounds $(\text{Te}_6)(\text{Te}_8)[\text{MCl}_6]_4$ ($M = \text{W}, \text{Nb}$) (Figure 1.4e) [13b]. An other structural isomer of Te_8^{2+} has been discovered in $\text{Te}_8[\text{U}_2\text{Br}_{10}]$ and $\text{Te}_8[\text{Bi}_4\text{Cl}_{14}]$, which contain polymeric chains ${}^1[\text{Te}_8^{2+}]$ of six-membered tellurium rings

in chair conformation connected through Te_2 bridge (Figure 1.5b) [64]. Te_8^{4+} , a higher oxidized polycation stabilized in the salt $\text{Te}_8[\text{VOCl}_4]_2$, can be interpreted as a dimer formed by a pair of coplanar Te_4^{2+} rings. In fact, the Te_8^{4+} forms a deformed cube with two opened edges, leaving four of the eight Te atoms triple bonded (Figure 1.4f) [65]. Among different Te_8^{n+} forms, the bicyclo[2.2.2]octane-type Te_8^{2+} , the higher oxidized Te_8^{4+} , and polymeric chain found in $\text{Te}_8[\text{U}_2\text{Br}_{10}]$ and $\text{Te}_8[\text{Bi}_4\text{Cl}_{14}]$ show classical, Zintl precise structures and possess tri-coordinated tellurium atoms bearing the formal positive charges.

The octaselenium Se_8^{2+} polycation was first obtained through synproportionation in 1971 in the form of dark reddish brown crystals of $\text{Se}_8[\text{AlCl}_4]_2$ [66]. Se_8^{2+} is isostructural to S_8^{2+} and possesses a cyclic structure with approximately C_s symmetry (Figure 1.1c).

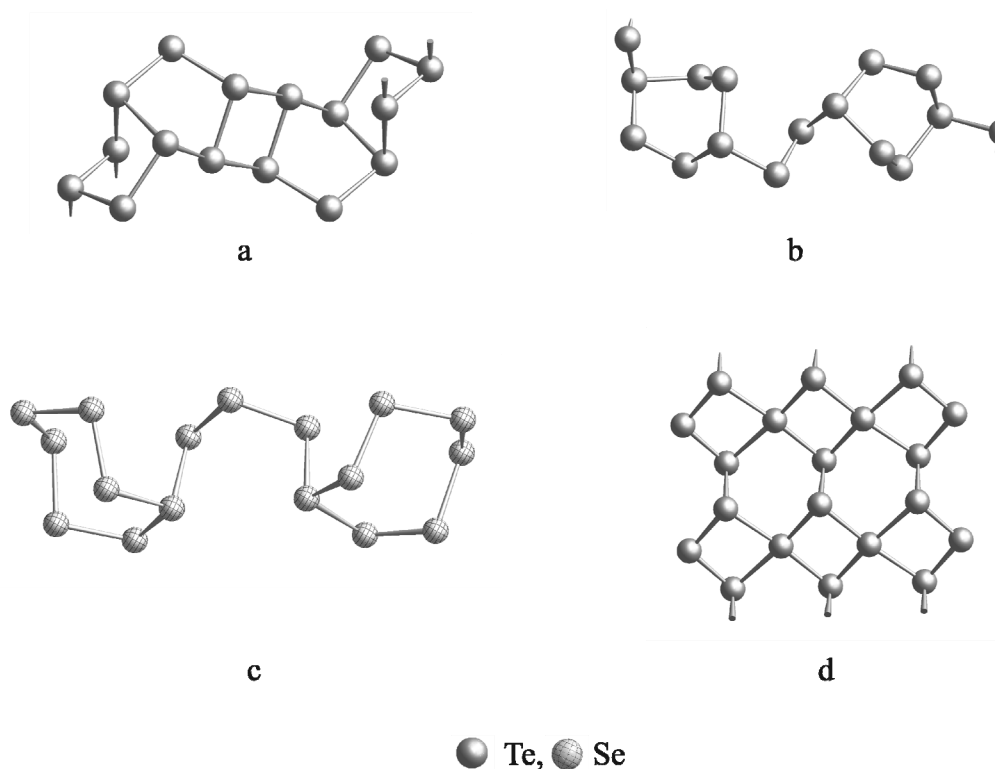


Figure 1.5: The structures of the homoatomic polycations: (a) the association of the Te_8^{2+} ions into an undulated chain (b) polymeric chain of Te_8^{2+} (c) Se_{17}^{2+} , and (d) the infinite folded band of Te_{10}^{2+} .

Te_{10}^{2+} was also reported as a polymer. The structure of $(\text{Te}_4)(\text{Te}_{10})[\text{Bi}_4\text{Cl}_{16}]$ contains two different polymeric cations, i.e. Te_4^{2+} and Te_{10}^{2+} [67]. The structure of the Te_{10}^{2+} polycation is similar to Te_7^{2+} (Figure 1.4c) and consists of two tetra-coordinated, six tri-coordinated and two di-coordinated tellurium atoms. The two tetra-coordinated Te atoms are

members of two adjacent planar four-membered rings and the six tricoordinated centers link the planar Te_{10}^{2+} units forming an infinite folded band (Figure 1.5d).

The largest discrete homoatomic polycation is Se_{17}^{2+} , which was synthesized by the oxidation of elemental selenium with WCl_6 through CVT [68]. The electron-precise structure of Se_{17}^{2+} is similar to S_{19}^{2+} and consists of two seven-membered rings, which are linked by a three-membered selenium chain (Figure 1.5c).

1.2.2. Heteroatomic Polycations from High-Temperature Synthesis

In addition to homoatomic, a number of heteroatomic polycations were obtained through the higher temperature routes. *Beck* et al. synthesized a small number of mixed polycations of groups 15 and 16, while *Ruck* et al. focused on the incorporation of transition metals and post transition elements into the bismuth polycations and managed to prepare a couple of novel heteroatomic clusters. A most recent review published by *Braunschweig* et al. emphasizes on the ability of bismuth species to build mixed clusters with transition metals [69], generating a wide variety of structures containing transition metal–bismuth bonds [70].

A series of mixed polycations $(\text{Bi}_4E_4)^{4+}$ were obtained from acidic $\text{NaCl}/\text{AlCl}_3$ melts ($E = \text{S}, \text{Se}, \text{Te}$). These mixed polycations reveal crystallographic S_4 symmetry, which is slightly distorted from a regular cube, whose corners are occupied alternately by Bi and E atoms (Figure 1.6c) [71].

${}^1[\text{Sb}_2\text{Te}_2]^+$ is a polymeric heteroatomic polycation, which forms strands made up of stacked Sb_2Te_2 -rings. These rings are connected with their neighbors alternating via two, three, or four covalent bonds. Mostly Sb-Te bonds are present, in smaller number Sb-Sb bonds, while Te-Te bonds are not observed (Figure 1.6d) [72].

The mixed chalcogen polycations $(\text{Se}_4\text{Te}_3)^{2+}$ and ${}^\infty[\text{Se}_{4.85}\text{Te}_{3.15}]^{2+}$ were obtained by reacting $\text{Te}_6[\text{WOCl}_4]_2$ with selenium, or Se/Te mixtures with WOCl_4 [73]. The $(\text{Se}_4\text{Te}_3)^{2+}$ polycation is almost similar to polymeric ${}^1[\text{Te}_7^{2+}]$, built by four-membered planar Te_2Se_2 rings connected via three atomic Se–Te–Se bridges in the 1,3 positions of the rings (Figure 1.6f). The polymeric cation ${}^\infty[\text{Se}_{4.85}\text{Te}_{3.15}]^{2+}$ consists of five-membered rings that are connected in the 1,3-positions by three-atomic bridges.

The heteroatomic arsenic/sulfur polycation $(\text{As}_3\text{S}_5)^+$ was synthesized by treating As, S, and AsCl_3 in AlCl_3 melts at $80\text{ }^\circ\text{C}$ to get yellow crystals of $(\text{As}_3\text{S}_5)[\text{AlCl}_4]$ [74]. The polycation $(\text{As}_3\text{S}_5)^+$ has C_s molecular symmetry (Figure 1.6e). The structure of the eight-atomic cage can be derived from an As_3S tetrahedron with four edges capped by sulfur atoms.

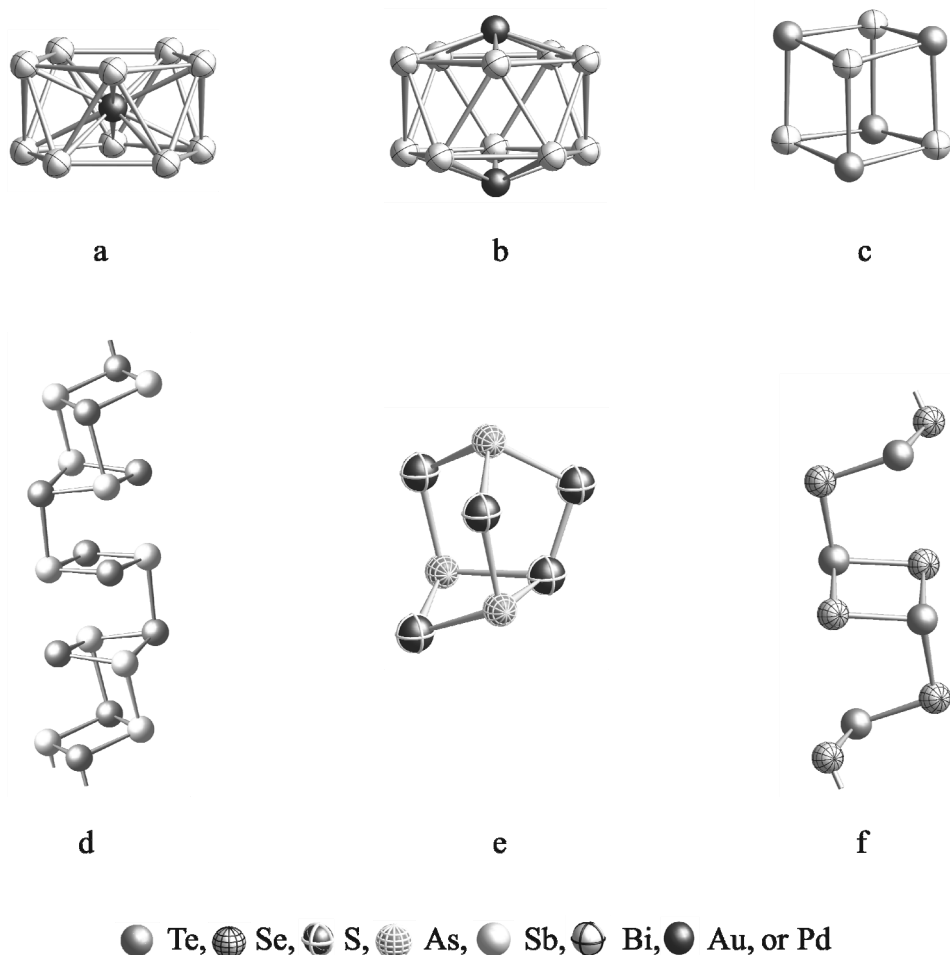


Figure 1.6: The structures of the heteroatomic polycations (a) $(\text{Pd}@\text{Bi}_{10})^{4+}$ (b) $(\text{Bi}_{10}\text{Au}_2)^{6+}$ (c) $(\text{Bi}_4\text{Te}_4)^{4+}$ (d) the polymeric strand of ${}^1_\infty[\text{Sb}_2\text{Te}_2]^+$ (e) $(\text{As}_3\text{S}_5)^+$, and (f) ${}^1_\infty[\text{Se}_4\text{Te}_3]^{2+}$.

The Zintl–Klemm concept is easily applicable to above mentioned heteroatomic $(\text{Bi}_4\text{E}_4)^{4+}$, ${}^1_\infty[\text{Sb}_2\text{Te}_2]^+$, and $(\text{As}_3\text{S}_5)^+$ polycations. Each group 15 element has three bonds, which is consistent with neutrality for a group 15 element, while with three bonds E , as an element of group 16, behaves as a pseudo-element of group 15 with a positive charge. Therefore, they belong to the electron-precise species.

The heteroatomic $(\text{Bi}_8\text{Si}_2)^{3+}$ was found in the semiconducting compounds $\text{Bi}_{14}\text{Si}_2\text{MI}_{12}$ ($M = \text{Rh}, \text{Ir}$) [51a]. The polycation reveals a square-antiprism of bismuth atoms of which square faces are capped by two silicon atoms.

The stuffed polycation $(\text{Pd}@\text{Bi}_{10})^{4+}$ was discovered in $\text{Bi}_{14}\text{PdBr}_{16}$ and $\text{Bi}_{16}\text{PdCl}_{22}$ [51b, 51c]. It consists of a pentagonal antiprism Bi_{10}^{4+} and an uncharged palladium atom at the centre (Figure 1.6a).

The isoelectronic and isostructural $(\text{Au}@\text{Bi}_{10})^{5+}$ is a part of the semiconducting compounds $\text{AuBi}_{14-\delta}\text{Sn}_{2+\delta}\text{X}_{21-\delta}$ ($\delta \approx 0.4$) [51e]. The capped polycation $(\text{Bi}_{10}\text{Au}_2)^{6+}$, a heteroicosahedron with Au^+ cations in 1,12-positions, was found as the central part of the molecule $(\text{Bi}_{10}\text{Au}_2)[\text{SbBi}_3\text{Br}_9]_2$ (Figure 1.6b) [51d]. The heteroatomic cluster cation $(\text{Bi}_{10}\text{Au}_2)^{6+}$ was also reported in a series of compounds $(\text{Bi}_{10}\text{Au}_2)[\text{EBi}_3\text{X}_9]_2$ ($E = \text{As}, \text{Bi}; X = \text{Cl}, \text{Br}$) [51f]. Disregarding the 6s electrons, which do not contribute because of their stabilization by relativistic effects, the Bi_{10}^{4+} polyhedron with $10 \cdot 3 - 4 = 26$ electrons in the skeleton meets the expectations for an electron-precise *arachno*-cluster according to the Wade–Mingos classification ($2n + 6 = 26$ electrons for bonding within the cluster).

In the molten salt approach, the addition of an excess of a more acidic halogenide is the obvious way to increase the yield and to get good quality crystals. These salts may provide effective, alternative route to sub-valent compounds. This is exemplified by the improved synthesis of Bi_6Cl_7 from Bi and BiCl_3 in SbCl_3 melts [50c]. Likewise, GaCl_3 melts can be used to synthesize Bi_5^{3+} polycations through synproportionations [75]. Thus different Lewis acids are available, which can effectively enhance the number of possibilities of polycation and cluster synthesis using this scheme. Alternatively, a stronger oxidizing agent might be expected to be required in systems where the synproportionation fails. Although, the higher temperature route is comparatively successful and provided a large number of novel polycations, there are yet some problems associated with it, e.g. (i) contamination with solid by-products, especially in the case of peritectically forming compounds, (ii) long annealing time, (iii) kinetic hindrance of solid-solid reactions, and (iv) the risk of product decomposition in case of thermally unstable compounds.

1.3. Synthesis in Organic Solvents

Kloo and co-workers introduced a new room temperature route in 1995 using Ga/GaX_3 -benzene media ($X = \text{Cl}, \text{Br}$) [26]. The use of benzene as solvent in the synthesis of clusters is useful in many aspects, since the solvent is inexpensive, easy to handle, and can be used at room temperature without specially designed glassware or other dedicated laboratory

equipment. Likewise, the isolation of solid polycationic compounds from the benzene solutions is conveniently performed by extraction with heptane or mesitylene. Moreover, gallium(III) halogenides have some unique properties, which make them ideal candidates as reagents for the synthesis of main group polycations and transition metal clusters, e.g. high solubility (up to 50 mol % in benzene), Lewis acidity, and the reducing ability of Ga/GaX₃-benzene mixtures. Taking into account these characteristics, three different procedures were applied to synthesize polycations; (i) by synproportionation of Bi and BiX₃ in GaX₃-benzene solutions to synthesize bismuth polycations in both chloride and bromide media, (ii) by reduction of the post-transition metal halogenides with a mixture of Ga/GaX₃ in benzene, and (iii) by oxidation of the post-transition metals with GaX₃ in benzene. *Kloo* et al. synthesized and isolated successfully some homoatomic polycations of antimony, bismuth, and tellurium.

Besides the synthesis of known polycations like Te₄²⁺ [16a, 16b], Bi₅³⁺ [16c], and Bi₈²⁺ [16b, 16c] by this room temperature method, for the first time an antimony polycation Sb₈²⁺, was obtained [10b, 16b]. All these polycations were isolated as salts of halogenido-gallates(III). The polycation Sb₈²⁺ has square-antiprismatic *D*_{4d} symmetry, which is analogous to the previously known Bi₈²⁺ cation (Figure 1.3d).

Considering the toxicity of benzene in the above mentioned procedure, later *Kloo* and co-workers used an alternative approach. Here benzene was replaced by dichloromethane to achieve the same goals. Dichloromethane had also been used earlier for the synthesis and crystallization of some mixed nitrogen/sulfur polycations, e.g. (SN)⁺, (SNS)⁺, or (S₄N₅)⁺ [76a–76c]. To synthesize bismuth clusters, *Kloo* and co-workers performed a two-step reaction, first to react Ga and GaCl₃ in order to get a crystalline adduct, which was subsequently treated with BiCl₃ in dichloromethane. Within a couple of weeks, they obtained a red/orange powder of Bi₅[GaCl₄]₃. Attempts to get single crystals were not successful. Moreover, the low reaction rate in dichloromethane is believed to be an effect of the significantly lower concentration of gallium metal in this solvent [76d].

The synthesis of main group polycations using GaX₃-benzene solutions facilitated to isolate good quality single-crystals in some cases, e.g. for the novel antimony polycation. On the other hand, this route cannot avoid some demerits, e.g. the use of toxic and cancer causing benzene [77], limitations in temperature (reactions could only be performed in the liquid range of the solvent), and general problems with controlled crystallization [16b, 16c].

1.4. Synthesis in Ionic Liquids

RTIL have opened new opportunities in the field of material synthesis and have provided new soft and low-temperature routes to inorganic solids that are usually prepared by high-temperature reactions. RTIL have distinct physical properties such as high thermal stability, wide liquid range, negligible vapor pressure, good ionic conductivity, and high solubility of both organic and inorganic substances [78, 79]. The inherent thermal stability of RTIL permits access to low and moderate temperatures at which kinetically stabilized phases can be obtained. The use of a soft-chemical approach is common in organic synthesis [78], catalysis [80], polymer science [79], nanotechnology [81], and in the synthesis of clathrates [82], and zeolites [83]. However, the application of this technique to prepare polycationic cluster compounds was relatively unexplored. Recently, *Ruck et al.*, *Kanatzidis et al.*, and *Feldmann et al.* expanded effectively the span of this approach and synthesized a couple of new polycations of groups 15 and 16 [17–23]. The key factors of this new synthetic route are: (i) very high solubility of the elements (e.g. Bi, Te, Sb, Se, Ga, In) and their halogenides allow reactions under mild conditions involving one-pot synthesis; (ii) low-temperature synthesis eliminates the risk of product decomposition; (iii) easier reproducibility of the products; (iv) controllable parameters, such as solvent acidity, oxidizing/reducing agent, or halide acceptor, allow modifying the synthesis with the objective to crystallize different compounds. It has been observed that synproportionation, oxidation, and reduction could be easily carried out in RTIL for clusters synthesis e.g. (i) by synproportionation Bi_5^{3+} [17], Te_4^{2+} [19], $\text{Te}_4^{1.78+}$ [84], and Te_8^{2+} [85] polycations were obtained; (ii) by oxidation of elemental tellurium with WOCl_4 , Te_6^{2+} was prepared [19], and (iii) by reduction of BiCl_3 with indium metal Bi_9^{5+} was synthesized [84].

1.4.1. Homoatomic Polycations from Ionic Liquids

In addition to the synthesis of some known homoatomic polycations like Te_4^{2+} , Te_6^{2+} , Te_8^{2+} , Bi_5^{3+} , and Bi_9^{5+} by this method, a partially reduced square-planar $\text{Te}_4^{1.78+}$ polycation was also isolated. The $\text{Te}_4^{1.78+}$ polycation was found in $\text{Te}_4[\text{Bi}_{0.74}\text{Cl}_4]$, synthesized by treating Te, TeCl_4 , and BiCl_3 at room temperature in the Lewis-acidic IL [bmim]Cl/ AlCl_3 (mole ratio = 1 : 2, [bmim]⁺: 1-*n*-butyl-3-methylimidazolium). The incommensurately modulated composite structure of $\text{Te}_4[\text{Bi}_{0.74}\text{Cl}_4]$ consists of stacks of Te_4 rings and chloridobismuthate strands. The

$\text{Te}_4^{1.78+}$ polycation is a four-membered ring in a slightly distorted square-planar conformation and is similar to Te_4^{2+} [14b, 86].

1.4.2. Heteroatomic Polycations from Ionic Liquids

Up to now, a small number of new heteroatomic polycations were also synthesized by means of this soft and sustainable chemical approach. Single crystals of $(\text{Sb}_7\text{S}_8\text{Br}_2)[\text{AlCl}_4]_3$ were obtained by reacting elemental sulfur and antimony in the Lewis-acidic IL $[\text{emim}]\text{Br}/\text{AlCl}_3$ (molar ratio = 1 : 11, $[\text{emim}]^+$: 1-ethyl-3-methylimidazolium) at 165 °C [21]. The heteroatomic polycation $(\text{Sb}_7\text{S}_8\text{Br}_2)^{3+}$ adopts a double-cubane structure, in which two distorted cubic clusters share one corner (the Sb atom). The other corners are alternately occupied with Sb and S atoms. Two Sb sites have terminal Sb–Br bonds projecting out of the cluster structure (Figure 1.7a). The red crystals of $(\text{Sb}_7\text{S}_8\text{Br}_2)[\text{AlCl}_4]_3$ exhibit nonlinear optical (NLO) properties, including difference-frequency generation (DFG) and second harmonic generation (SHG).

The two isostructural heteroatomic polymeric cations ${}_{\infty}^2[\text{A}_2\text{Te}_2\text{Br}]^+$ ($A = \text{Bi}, \text{Sb}$) were synthesized by reacting tellurium with bismuth or antimony in the less Lewis-acidic IL $[\text{emim}]\text{Br}/\text{AlCl}_3$ with molar ratio = 1 : 4.8 [22]. The structures of the semiconducting compounds $[\text{Bi}_2\text{Te}_2\text{Br}][\text{AlCl}_4]$ and $[\text{Sb}_2\text{Te}_2\text{Br}][\text{AlCl}_4]$ contain infinite ${}_{\infty}^2[\text{A}_2\text{Te}_2\text{Br}]^+$ chains, which consists of $[\text{ATe}]_2$ rhombic units that are connected via bromide ions. The A atoms are five fold-coordinated by three tellurium atoms and two bridging bromide atoms to form distorted square-pyramidal conformation (Figure 1.7d).

The first cationic heterocubane $(\text{Bi}_3\text{GaS}_5)^{2+}$ was prepared by the reaction of elemental Bi, S, BiCl_3 , and GaCl_3 in $[\text{bmim}]\text{Cl}$ at 150 °C. The red transparent crystals of $(\text{Bi}_3\text{GaS}_5)_2[\text{Ga}_3\text{Cl}_{10}]_2[\text{GaCl}_4]_2 \cdot \text{S}_8$ were obtained within 10 days [23]. The $(\text{Bi}_3\text{GaS}_5)^{2+}$ polycation is a distorted heterocubane (Figure 1.7c), which has localized bonds.

The first mixed antimony/selenium polycation $(\text{Sb}_{10}\text{Se}_{10})^{2+}$ was obtained by reacting antimony, selenium and selenium tetrachloride at room temperature in the Lewis-acidic IL $[\text{bmim}]\text{Cl}/\text{AlCl}_3$ (molar ratio = 1 : 2) [87]. In $(\text{Sb}_{10}\text{Se}_{10})[\text{AlCl}_4]_2$, the centrosymmetric polycyclic cation consists of two realgar-like $[\text{Sb}_4\text{Se}_4]^+$ cages, which are connected through

three-bonded selenium atoms with the central $[\text{Sb}_2\text{Se}_2]$ ring (Figure 1.7b). $(\text{Sb}_{10}\text{Se}_{10})^{2+}$ represents an electron-precise structure according to the Zintl concept.

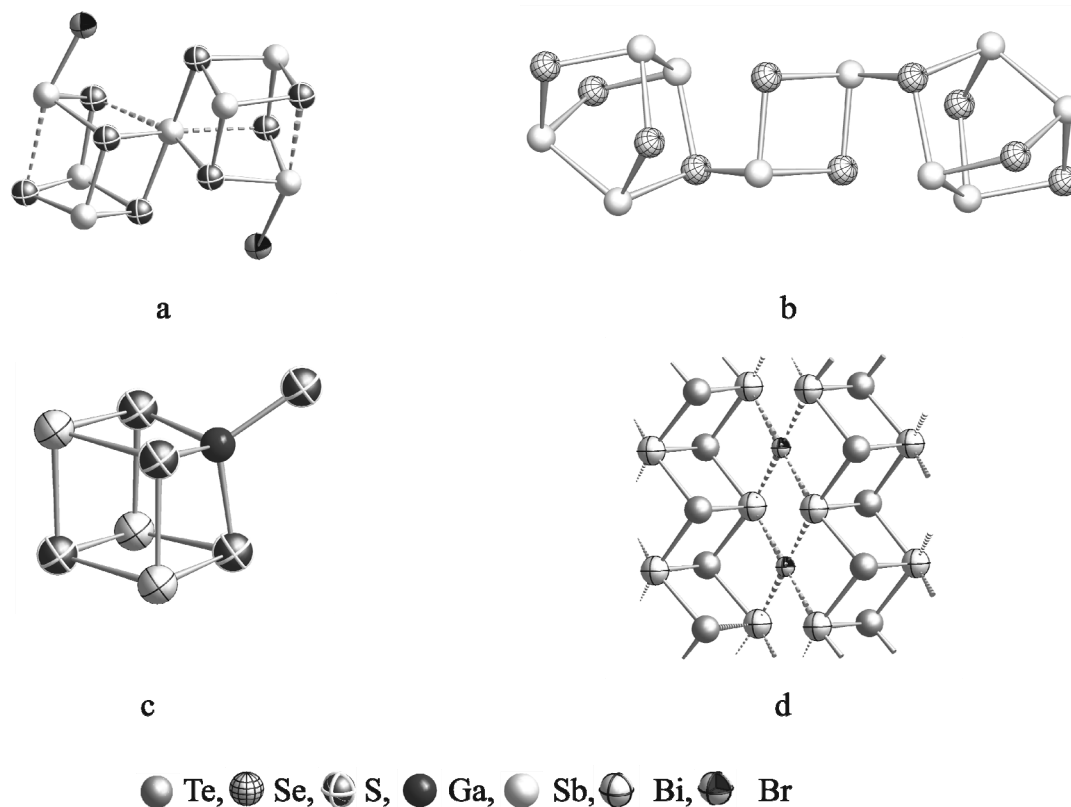


Figure 1.7: The structures of the heteroatomic polycations (a) $(\text{Sb}_7\text{S}_8\text{Br}_2)^{3+}$ (b) $(\text{Sb}_{10}\text{Se}_{10})^{2+}$ (c) $(\text{Bi}_3\text{GaS}_5)^{2+}$, and (d) an infinite layer of ${}_{\infty}^2[\text{Bi}_2\text{Te}_2\text{Br}]^+$.

The IL based low-temperature synthesis facilitated the isolation of a number of known and new main group sub-valent compounds in high yield. This stimulated the investigation of the physical properties. Recently, *Sun* and co-workers studied the photoluminescence (PL) properties of $\text{Bi}_5[\text{AlCl}_4]_3$ crystals, synthesized from IL [88a]. $\text{Bi}_5[\text{AlCl}_4]_3$ exhibits extremely broad near-infrared (NIR) PL with a full width at the half maximum (FWHM) of > 510 nm and an effective PL lifetime of $4.1 \mu\text{s}$ at 1160 nm. They also investigated Raman and absorption spectra of the IL containing subvalent bismuth, which confirmed the coexistence of Bi_5^{3+} and Bi^+ in the solution. The Bi_5^{3+} and Bi^+ emitters, stabilized by the Lewis-acidic IL, demonstrated ultrabroad NIR photoluminescence with a lifetime of around $1 \mu\text{s}$ [88b]. Additionally, this innovative facile route has proved that essentially all polycation syntheses previously performed in molten AlCl_3 can be made in IL at room temperature.

Table 1.1 A list of selected homo- and heteroatomic polycations of groups 15 and 16, synthesized by different routes.

Polycations	Inorganic solvents	Higher temperature synthesis	Organic solvents	Ionic liquids
O_2^+		[5]		
S_4^{2+}	[32]	-	-	-
S_8^{2+}	[37]	-	-	-
S_{19}^{2+}	[41]	-	-	-
Se_4^{2+}	[31]	[58]	-	-
Se_8^{2+}	[38]	[39, 66]	-	-
Se_{10}^{2+}	[40]	[58]	-	-
Se_{17}^{2+}	-	[68]	-	-
Te_4^{2+}	[33]	[14b]	[16a, 16b]	[19]
$Te_4^{1.78+}$	-	-	-	[84]
Te_6^{4+}	[35]	-	-	-
Te_6^{2+}	-	[59a, 60]	-	[19]
Te_7^{2+}	[36]	[61]	-	-
Te_8^{2+}	-	[62–64]	-	[85]
Te_8^{4+}	-	[65]	-	-
Te_{10}^{2+}	-	[67]	-	-
N_5^+	[10a]	-	-	-
Bi_5^{3+}	[42]	[14a, 15, 50]	[16c, 76d]	[17]
Bi_5^+	-	[53]	-	-
Bi_6^{2+}	-	[53, 54]	-	-
Bi_8^{2+}	-	[14a, 50]	[16b, 16c]	-
Bi_9^{5+}	-	[6, 7, 50c, 56, 57]	-	[84]
Sb_8^{2+}	-	-	[10b]	-
$(Te_2Se_2)^{2+}$, $(Te_3Se)^{2+}$, and $(S_3Se)^{2+}$	[43]	-	-	-
$(Te_3S_3)^{2+}$ and $(Te_xSe_{6-x})^{2+}$	[44]	-	-	-
$(Se_4Te_3)^{2+}$	-	[73]	-	-
$(Te_2Se_6)^{2+}$	[45]	-	-	-
$(Te_4S_4)^{2+}$	[46]	-	-	-
$(Te_2Se_8)^{2+}$	[45, 47]	-	-	-
$(As_3Se_4)^+$ and $(As_3S_4)^+$	[48a]	-	-	-
$(S_4N_4)^{2+}$ and $(S_4N_5)^+$	[48b, 76c]	-	-	-
$(S_5N_5)^+$ and $(S_6N_4)^{2+}$	[48c, 48d]	-	-	-
$(SN)^+$ or $(SNS)^+$	-	-	[48e, 76a, 76b]	-
$(As_3S_5)^+$	-	[74]	-	-
$[Sb_2Te_2]_n^+$	-	[72]	-	-
$(Bi_4Te_4)^{4+}$, $(Bi_4Se_4)^{4+}$, and $(Bi_4S_4)^{4+}$	-	[71]	-	-
$(Bi_8Si_2)^{3+}$	-	[51a]	-	-
$(Pd@Bi_{10})^{4+}$ and $(Au@Bi_{10})^{5+}$	-	[51b, 51c, 51e]	-	-
$(Bi_{10}Au_2)^{6+}$	-	[51d, 51f]	-	-
$(Sb_7S_8Br_2)^{3+}$	-	-	-	[21]
$[Bi_2Te_2Br]_n^+$ and $[Sb_2Te_2Br]_n^+$	-	-	-	[22]
$(Bi_3GaS_5)^{2+}$	-	-	-	[23]
$(Sb_{10}Se_{10})^{2+}$	-	-	-	[87]

1.5. Polynuclear Transition Metal Complexes in Ionic Liquids

Ionic liquids (IL) are being applied extensively as convenient solvents for organic and inorganic synthesis [78, 89], for crystal engineering of coordination compounds [90–96], for liquid–liquid extraction [97], for electrodeposition [98], for spectroscopic studies [88], as electrolyte in photovoltaic devices (solar cells) [99] and as a constituent in hybrid materials [100]. Moreover, transition metal containing IL are regarded as potential materials that combine the properties of IL with additional inherent magnetic, optical, or catalytic properties that depend on the incorporated metal ion [101–105]. A significant and distinctive feature of IL is the tunability of their chemical and physical properties by selecting an appropriate combination of cation and anion.

There are several classical routes available to synthesize polynuclear transition metal compounds. Mostly, they had been synthesized employing either higher temperature reactions (crystallization from melt or CVT) [51, 70, 106] or by treating the precursors in some organic solvents (non-polar, e.g. ether or benzene, or polar, e.g. dichloromethane or acetonitrile) [107–109] or inorganic solvents (e.g. water or aqueous HCl) [110].

In the late 1980's, *Hussey* and co-workers introduced RTIL for stabilizing both monomeric and polymeric chlorido complexes of transition metals [111]. In many cases, RTIL proved to be superior to conventional molecular solvents such as water or acetonitrile, because the solvation and solvolysis pathways that are often available to these complexes in molecular solvents are absent in RTIL. Moreover, they also managed to investigate the spectroscopic and electrochemical properties of some of the transition metal chloride clusters [112–114]. Later, *Hughbanks* et al. reported a novel procedure, using RTIL to isolate the centered hexanuclear zirconium halogenide cluster compounds and studied their spectroscopic, electrochemical, and structural properties [115–118]. Following the same procedure, *Köckerling* et al. and *Saito* et al. synthesized some new centered hexanuclear zirconium halogenide clusters and trinuclear rhenium halogenide clusters respectively [119, 120]. *Mudring* and co-workers synthesized a number of new salt-like structures from IL, containing lanthanides in the anionic network and investigated their structural and physical properties [93–96]. *Dyson* et al. used IL as reagent and solvent to prepare several new organometallics. They also studied catalytic properties of transition metal carbonyl clusters in IL [121–122]. *Nockemann* and co-workers obtained some polynuclear metal complexes from

task specific or functionalized IL [123, 124]. With respect to the number of metal atoms present in the structure, metal clusters or complexes are categorised and discussed.

Table 1.2 List of abbreviations for different ionic liquids.

Ionic Liquid	Abbreviation
betainium bis(trifluoromethyl)sulfonylimide	[Hbet][Tf ₂ N]
1-carboxymethyl-3-methylimidazolium bis(trifluoromethyl)sulfonylimide	[Hbetmim][Tf ₂ N]
<i>N</i> -carboxymethyl- <i>N</i> -methylmorpholinium bis(trifluoromethyl)sulfonylimide	[Hbetmmor][Tf ₂ N]
<i>N</i> -carboxymethyl- <i>N</i> -methylpyrrolidinium bis(trifluoromethyl)sulfonylimide	[Hbetmpyr][Tf ₂ N]
<i>N</i> -butylpyridinium oxopentafluoridomolybdate	[bpy]MoOF ₅
1-ethyl-3-methylimidazolium tetrabromidoaluminate	[emim]Br/AlBr ₃
1-butyl-1-methylpyrrolidinium trifluoromethanesulfonate	[bmpyr][OTf]
1-propyl-3-methylimidazolium bis(trifluoromethyl)sulfonylimide	[C ₃ mim][Tf ₂ N]
1-butyl-3-methylpyrrolidinium bis(trifluoromethyl)sulfonylimide	[C ₄ mpyr][Tf ₂ N]

1.5.1. Binuclear Complexes

Nockemann and co-workers developed carboxyl-functionalized IL that are able to dissolve considerable amounts of a wide range of metal oxides, including rare-earth oxides. Such IL are of particular interest for applications in the nuclear fuel cycle, namely, for the extraction of uranium from ores and for the processing of spent nuclear fuel rods [123–126]. *Nockemann* et al. reported different metal complexes formed upon dissolution of corresponding metal oxides and hydroxides in different IL, functionalized with a carboxyl group, e.g. [Hbet][Tf₂N], [Hbetmim][Tf₂N], [Hbetmmor][Tf₂N] and [Hbetmpyr][Tf₂N]. X-ray diffraction studies on single crystals of the metal complexes revealed a rich structural variety with strong dependence on the cationic core attached to the carboxylate groups. The task specific betainium IL produced a number of polynuclear complexes. All these complexes were incorporated with zwitterionic carboxylate ligands and [Tf₂N][−] counterions. Besides, the structural determination of single crystals of the complexes crystallized from these IL, the measurement of absorption and luminescence spectra of the metal complexes were also carried out. Task specific IL were used to synthesize different binuclear complexes, e.g. [(UO₂)₂(bet)₆(H₂O)₂][Tf₂N]₄, [Cu₂(betmmor)₄][Tf₂N]₄, [Eu₂(betmmor)₆(H₂O)₂][Tf₂N]₆, [Cu₂(betmpyr)₄(H₂O)₂][Tf₂N]₄, [Eu₂(bet)₈(H₂O)₄][Tf₂N]₆, [Cu₂(betmim)₄(H₂O)₂][Tf₂N]₄·H₂O, [Cd₂(betpy)₂(H₂O)₂][Tf₂N]₂, [Eu₂(bet)₈(H₂O)₂][Tf₂N]₆·2H₂O, or [Y₂(bet)₆(H₂O)₄][Tf₂N]₆ [123, 124].

The crystal structure of binuclear complex [(UO₂)₂(bet)₆(H₂O)₂][Tf₂N]₄ consists of the binuclear complex cation [(UO₂)₂(bet)₆]⁴⁺ with six coordinating betaine zwitterions and two

water molecules, surrounded by four non-coordinating bistriflimide $[\text{Tf}_2\text{N}]^-$ counterions (Figure 1.8).

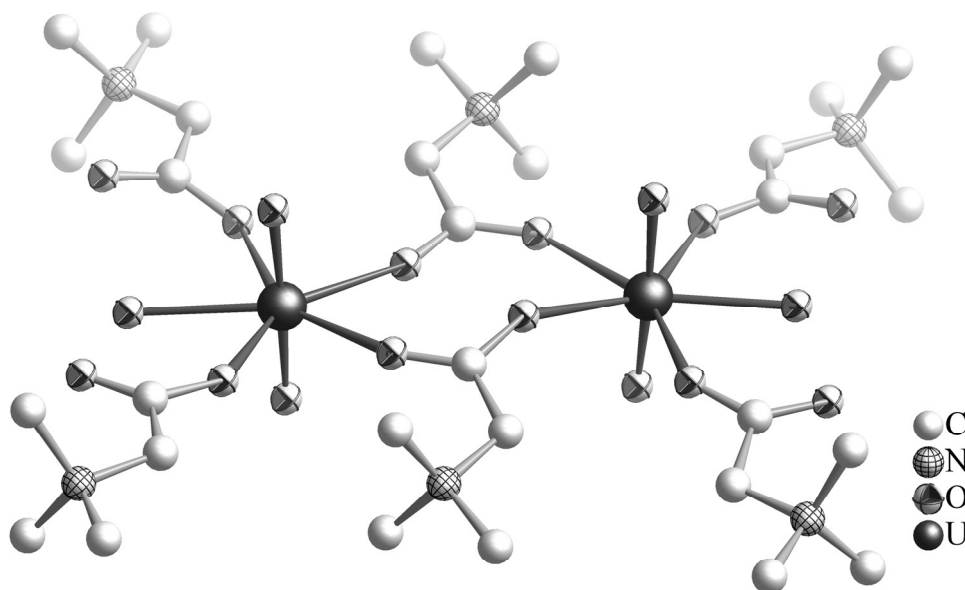


Figure 1.8: The binuclear $[(\text{UO}_2)_2(\text{bet})_6(\text{H}_2\text{O})_2]^{4+}$ complex cation. Hydrogen atoms are omitted for clarity as in the following Figures.

Two of the carboxyl functionalized betaine zwitterions are μ_2 -bridging. The other four betaine zwitterions exhibit monodentate coordination to each of the two uranyl cations in the asymmetric unit. Four of the coordinating betaine ligands and one water molecule form slightly distorted pentagonal bipyramidal oxygen coordination around each of the uranium(VI) atoms [124a]. Spectroscopic studies revealed that the uranyl complex was decomposed in aqueous solution, while in acetonitrile and in the IL $[\text{Hbet}][\text{Tf}_2\text{N}]$, the carboxylate groups remained coordinated.

The structure of the $[\text{Cu}_2(\text{betmim})_4(\text{H}_2\text{O})_2][\text{Tf}_2\text{N}]_4 \cdot \text{H}_2\text{O}$ complex also exhibits a dimeric core, consisting of four μ_2 -bridging *N*-carboxymethyl-*N*-methylimidazolium ligands and two water molecules (Figures 1.9). The surrounding anion network of four $[\text{Tf}_2\text{N}]^-$ ions prefer hydrogen bonding with the acidic protons of imidazolium cations rather than with the coordinated water molecules. Both copper(II) ions show a distorted square-pyramidal coordination by oxygen atoms [124b].

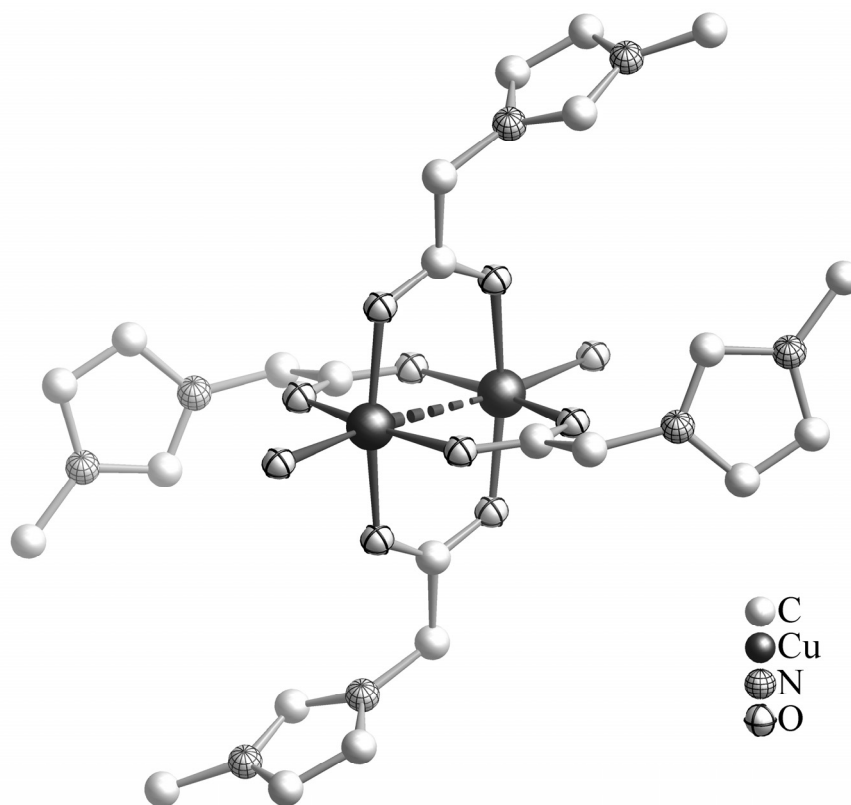


Figure 1.9: The binuclear $[\text{Cu}_2(\text{betmim})_4(\text{H}_2\text{O})_2]^{4+}$ complex cation.

Recently, *Hagiwara* et al. reported the binuclear molybdenum complex $[\text{bpy}]_2[\text{Mo}_2\text{O}_4\text{F}_6]$. It was obtained in an attempt to crystallize the low-melting salt bpyMoOF_5 , but single crystals of $[\text{bpy}]_2[\text{Mo}_2\text{O}_4\text{F}_6]$ resulted from the hydrolysis of bpyMoOF_5 with some traces of water during the crystal growth [127].

1.5.2. Trinuclear Complexes

Saito et al. synthesized a trinuclear rhenium sulfide cluster from Lewis basic IL by treating $\text{Re}_3\text{S}_7\text{Cl}_7$ with a 1:1 mixture of emimBr and AlBr_3 at 70 °C for 2 days followed by refluxing in acetonitrile to get a viscous solution. After cooling and filtration, diethyl ether was layered and a black solid was obtained, which was recrystallized from acetonitrile/diethyl ether to get good quality single crystals of $[\text{emim}]_3[\text{Re}_3(\mu_3\text{-S})(\mu\text{-S})_3\text{Br}_9]\text{Br}$ [120]. The structure of the cluster anion comprises an almost equilateral triangle of rhenium atoms with one $\mu_3\text{-S}^{2-}$, three $\mu\text{-S}^{2-}$, and nine terminal Br^- ligands (Figure 1.10). The cation network is composed of three emim^+ ions. This synthetic procedure has revealed that the IL $\text{emimBr}/\text{AlBr}_3$ has the ability to

remove one of the S atoms in the $\mu\text{-S}_2^{2-}$ ligands of the precursor complex $[\text{Re}_3(\mu_3\text{-S})(\mu\text{-S}_2)_3\text{Cl}_6]\text{Cl}$, to exchange Cl^- for Br^- , and to coordinate extra bromido ligands to the Re_3S_4 core.

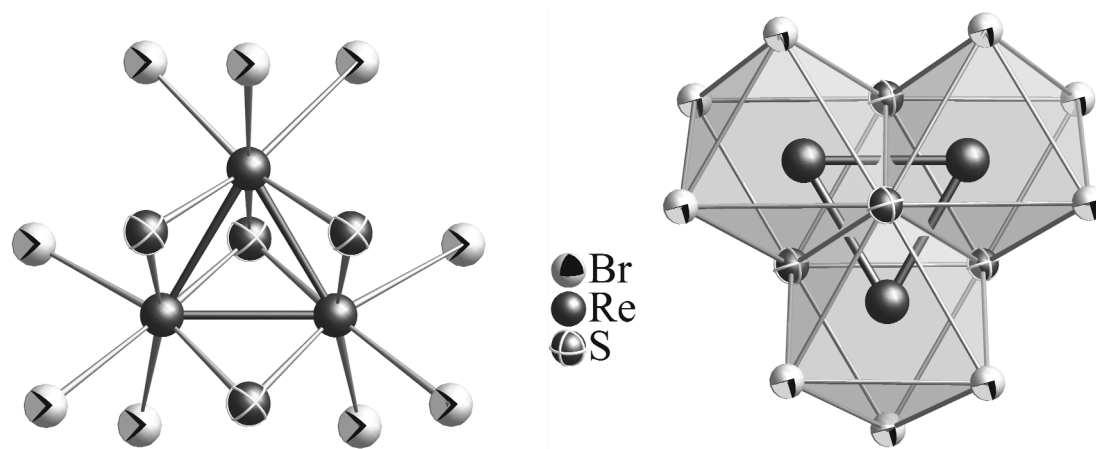


Figure 1.10: Left: The $[\text{Re}_3(\mu_3\text{-S})(\mu\text{-S})_3\text{Br}_9]^{2-}$ cluster anion, Right: Polyhedra representation emphasizing the edge-sharing of coordination octahedra.

Nockemann and co-workers demonstrated the preparation of the trinuclear cobalt complex $[\text{Co}_3(\text{bet})_8(\text{Hbet})_2(\text{H}_2\text{O})_2][\text{Tf}_2\text{N}]_{10}[\text{Hbet}]_2$ from the task specific IL $[\text{Hbet}][\text{Tf}_2\text{N}]$ [123a]. The synthesis was accomplished by reacting $\text{Co}(\text{OH})_2$ with $[\text{Hbet}][\text{Tf}_2\text{N}]$ in the presence of water. The crystal structure of $[\text{Co}_3(\text{bet})_8(\text{Hbet})_2(\text{H}_2\text{O})_2][\text{Tf}_2\text{N}]_{10}[\text{Hbet}]_2$ contains discrete trimeric $[\text{Co}_3(\text{bet})_8(\text{Hbet})_2(\text{H}_2\text{O})_2]^{8+}$ units, eight non-coordinating $[\text{Tf}_2\text{N}]^-$ anions as counter ions and two additional $[\text{Hbet}][\text{Tf}_2\text{N}]$ ion pairs as “solvent” molecules in the crystal structure (Figure 1.11).

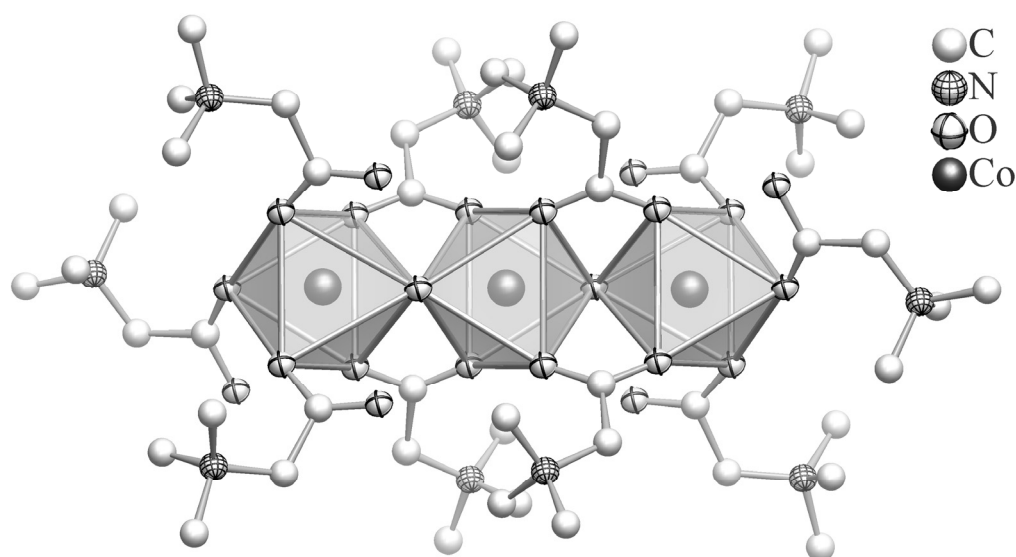


Figure 1.11: The trimeric $[\text{Co}_3(\text{bet})_8(\text{Hbet})_2(\text{H}_2\text{O})_2]^{8+}$ complex cation, highlighting the corner-sharing $[\text{CoO}_6]$ octahedra.

The three cobalt(II) atoms of the trimeric $[\text{Co}_3(\text{bet})_8(\text{Hbet})_2(\text{H}_2\text{O})_2]^{8+}$ units are connected by four μ_2 -bridging carboxylate groups of the betaine ligands and two bridging water molecules. The octahedral oxygen coordination of each cobalt atom is slightly distorted (Figure 1.11).

1.5.3. Tetranuclear Complexes

The first tetranuclear cobalt complex $[\{\mu_2\text{-HCC}(\text{CH}_2)_3\text{N}=\text{C}(\text{H})\text{N}(\mu_2\text{-CCH}(\text{CH}_2)_3\text{CH}=\text{CH})\}\{\text{Co}_2(\text{CO})_6\}_2]\text{BPh}_4$ was reported by *Dyson* and co-workers [128]. The synthesis was performed, employing 1,3-dialkyne-functionalized imidazolium IL derivatives, e.g. 1,3-dipentynylimidazolium tetraphenylborate, was treated with $\text{Co}_2(\text{CO})_8$ in dichloromethane.

In the structure of the tetranuclear complex, the 1,3-dialkyne arms adopt a trans conformation. The Co–Co distances are found to be shorter than in the parent $\text{Co}_2(\text{CO})_8$ complex. The Co atoms are bridged by alkyne ligands (Figure 1.12). The three different kinds of C–H... π interactions were observed in the structure. In addition, one of the H atoms in the CH_2 group is also involved in a C–H... π interactions with the phenyl ring of the counterion.

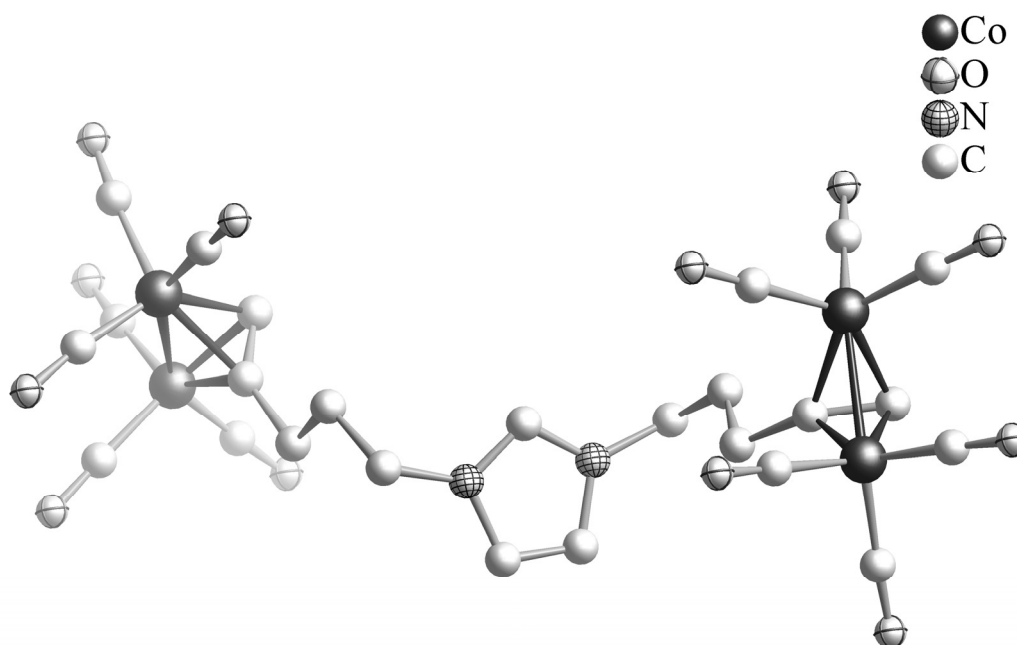


Figure 1.12: The tetranuclear $[\{\mu_2\text{-HCC}(\text{CH}_2)_3\text{N}=\text{C}(\text{H})\text{N}(\mu_2\text{-CCH}(\text{CH}_2)_3\text{CH}=\text{CH})\}\{\text{Co}_2(\text{CO})_6\}_2]^{4+}$ complex cation.

Nockemann et al. synthesized two tetranuclear complexes, $[\text{Mn}_4(\text{bet})_{10}(\text{H}_2\text{O})_4][\text{Tf}_2\text{N}]_8$ and $[\text{Zn}_4(\text{bet})_{10}(\text{H}_2\text{O})_2][\text{Tf}_2\text{N}]_8$, by applying the task specific IL $[\text{Hbet}][\text{Tf}_2\text{N}]$ [123a]. The synthesis was performed by reacting the corresponding metal oxides with $[\text{Hbet}][\text{Tf}_2\text{N}]$ in the presence of water.

The crystal structure of the tetranuclear manganese complex $[\text{Mn}_4(\text{bet})_{10}(\text{H}_2\text{O})_4][\text{Tf}_2\text{N}]_8$ consists of discrete tetrameric $[\text{Mn}_4(\text{bet})_{10}(\text{H}_2\text{O})_4(\text{Tf}_2\text{N})]^{7+}$ units and seven non-coordinating $[\text{Tf}_2\text{N}]^-$ counterions. The four manganese(II) atoms which differ in their coordination, are connected by bridging carboxylate groups of the betaine ligands. The oxygen coordination environment of the manganese atoms Mn2 and Mn4 can be described as strongly distorted octahedra, while Mn1 and Mn3 are found in distorted square based pyramidal coordination by five oxygen atoms. In addition to the bridging carboxylate groups of the ligands, water molecules complete the octahedral surrounding of Mn2 and Mn4 (Figure 1.13).

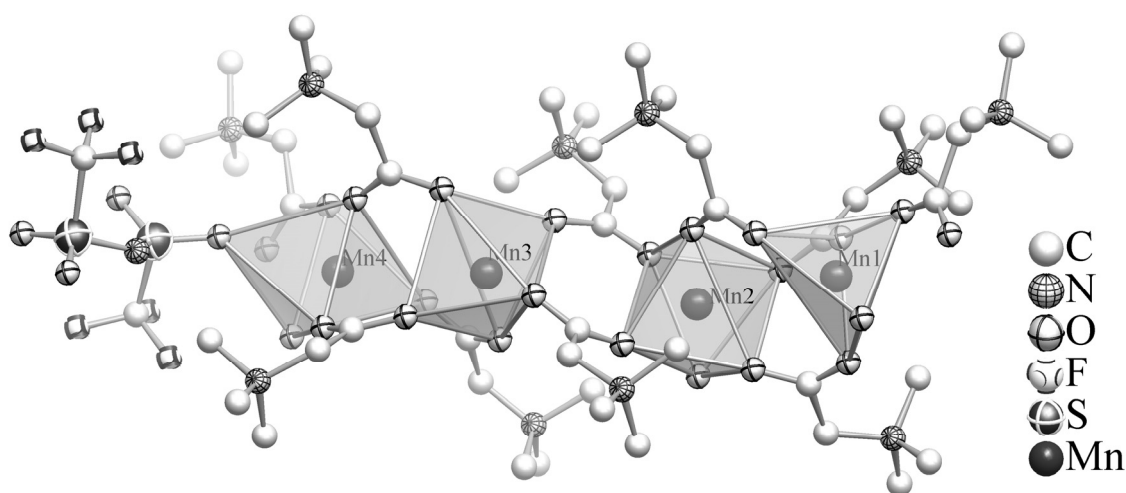


Figure 1.13: The tetranuclear $[\text{Mn}_4(\text{bet})_{10}(\text{H}_2\text{O})_4(\text{Tf}_2\text{N})]^{7+}$ complex cation.

In the tetrameric zinc complex $[\text{Zn}_4(\text{bet})_{10}(\text{H}_2\text{O})_2][\text{Tf}_2\text{N}]_8$, the discrete tetrameric cation $[\text{Zn}_4(\text{bet})_{10}(\text{H}_2\text{O})_2]^{8+}$ is surrounded by eight non-coordinating $[\text{Tf}_2\text{N}]^-$ anions (Figure 1.14). The zinc(II) atoms are connected by bridging carboxylate groups of the betaine ligands. The crystal structure shows two independent zinc (Zn1 and Zn2) atoms which exhibit square pyramidal coordination. Zn1 is coordinated by five carboxylate groups that are in μ -bridging to the adjacent zinc atoms Zn2 and Zn1', respectively. Zn2 is surrounded by one monodentate betaine ligand, three betaine ligands that are μ -bridging to Zn1 and one water molecule.

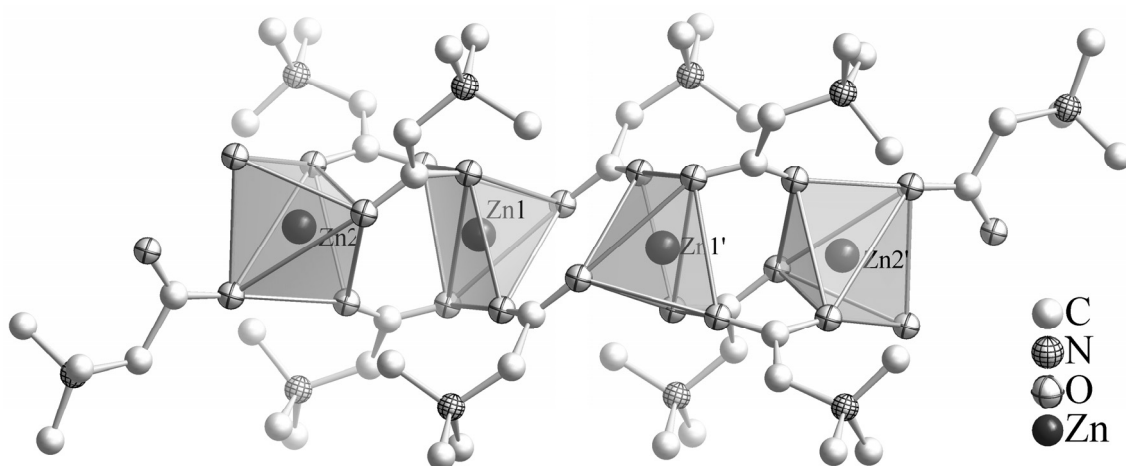


Figure 1.14: The tetranuclear $[\text{Zn}_4(\text{bet})_{10}(\text{H}_2\text{O})_2]^{8+}$ complex cation.

1.5.4. Pentanuclear Complexes

Nockemann and co-workers continued their efforts to build even higher nuclearity metal complexes and were successful to isolate two pentanuclear complexes, $[\text{Ni}_5(\text{bet})_{12}(\text{H}_2\text{O})_6][\text{Tf}_2\text{N}]_{10}$ and $[(\text{Pb}_4\text{O})\text{Pb}(\text{OH})(\text{bet})_8(\text{Tf}_2\text{N})_3][\text{Tf}_2\text{N}]_4 \cdot \text{MeOH}$, by applying the same synthetic strategy of reacting metal oxides with $[\text{Hbet}][\text{Tf}_2\text{N}]$ in the presence of water or methanol [123a].

The crystal structure of the pentanuclear complex $[\text{Ni}_5(\text{bet})_{12}(\text{H}_2\text{O})_6][\text{Tf}_2\text{N}]_{10}$ consists of discrete pentameric $[\text{Ni}_5(\text{bet})_{12}(\text{H}_2\text{O})_6]^{10+}$ units and non-coordinating $[\text{Tf}_2\text{N}]^-$ anions as counterions (Figure 1.15).

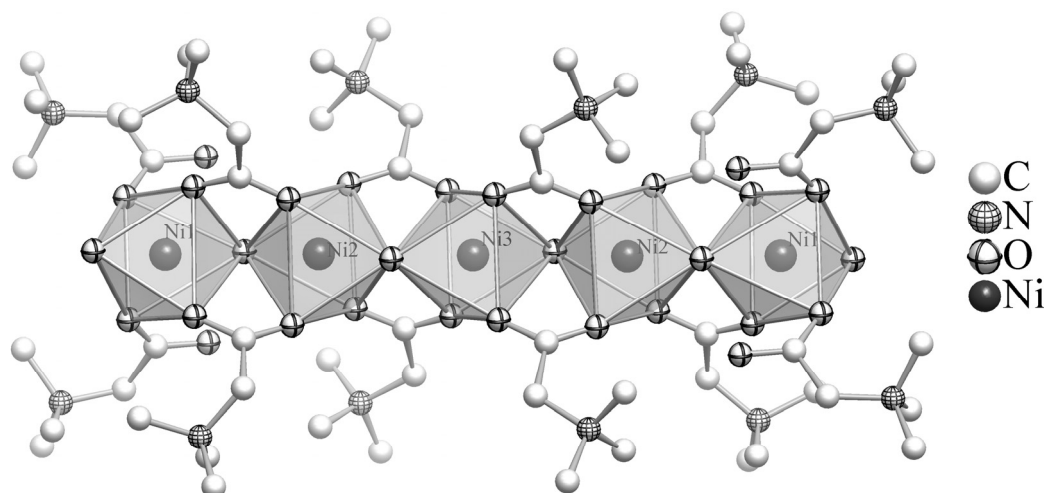


Figure 1.15: The pentanuclear $[\text{Ni}_5(\text{bet})_{12}(\text{H}_2\text{O})_6]^{10+}$ complex cation, the chain of corner-sharing $[\text{NiO}_6]$ octahedra is prominent.

The three symmetrically independent nickel(II) atoms of the pentameric $[\text{Ni}_5(\text{bet})_{12}(\text{H}_2\text{O})_6]^{10+}$ unit are connected by eight μ_2 -bridging carboxylate groups of the betaine ligands and four bridging water molecules. Each Ni atom is coordinated by oxygen atoms of four betaine ligands and two water molecules to give slightly distorted octahedral coordination polyhedron. The terminal betaine ligands and water molecules are coordinated to Ni1 atoms in a monodentate fashion (Figure 1.15).

The pentanuclear lead complex $[(\text{Pb}_4\text{O})\text{Pb}(\text{OH})(\text{bet})_8(\text{Tf}_2\text{N})_3][\text{Tf}_2\text{N}]_4\cdot\text{MeOH}$ contains an oxo-hydroxo cluster inside the discrete pentameric $[(\text{Pb}_4\text{O})\text{Pb}(\text{OH})(\text{bet})_8(\text{Tf}_2\text{N})_3]^{4+}$ unit. The cation is surrounded by four non-coordinating $[\text{Tf}_2\text{N}]^-$ counter ions and one methanol molecule. The cationic unit $[(\text{Pb}_4\text{O})\text{Pb}(\text{OH})(\text{bet})_8(\text{Tf}_2\text{N})_3]^{4+}$ is composed of an oxo-centered $[\text{OPb}_4]^{6+}$ tetrahedron, which is connected to an additional lead atom through a μ_3 -bridging hydroxide and chelating-bridging carboxylate groups of betaine ligands. The $[\text{Pb}_4(\mu_4\text{-O})\text{Pb}(\mu_3\text{-OH})]^{7+}$ moiety is surrounded by eight betaine ligands and two coordinating $[\text{Tf}_2\text{N}]^-$ anions (Figure 1.16). The $\mu_4\text{-O}$ atom tetrahedrally bridges Pb2, Pb3, Pb4, and Pb5 atoms while the $(\mu_3\text{-OH})$ -ligand bridges Pb1, Pb2, and Pb3 in a pyramidal shape (Figure 1.16).

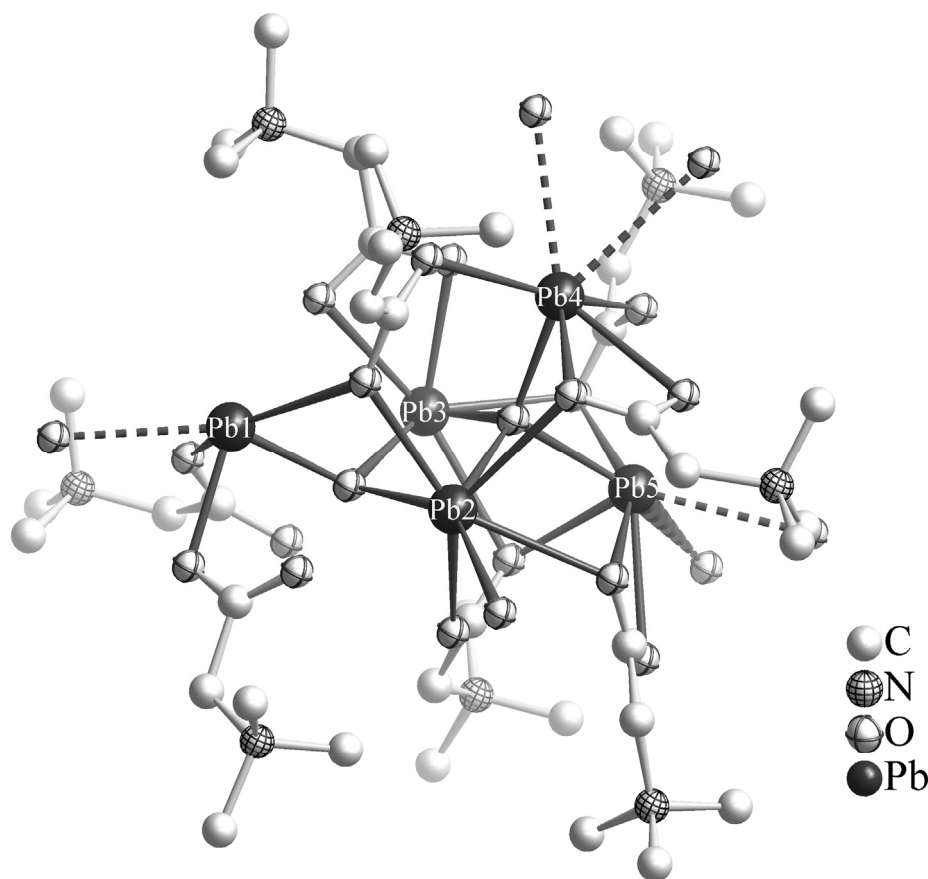


Figure 1.16: The pentanuclear $[(\text{Pb}_4\text{O})\text{Pb}(\text{OH})(\text{bet})_8(\text{Tf}_2\text{N})_3]^{4+}$ complex cation.

1.5.5. Hexanuclear and High-Nuclearity Complexes

Hughbanks and co-workers introduced a new synthetic scheme, using room-temperature Lewis-basic IL to isolate centered hexanuclear zirconium halogenide cluster compounds and studied their spectroscopic, electrochemical, and structural properties [115–118]. Room-temperature chloridoaluminate molten salts, mixtures of emimCl/AlCl₃ were used as solvents to excise and isolate centered hexanuclear zirconium halogenide clusters from their solid-state precursors, e.g. Zr₆Br₁₄F, Li₂Zr₆Cl₁₅Mn, or Rb₅Zr₆Cl₁₈B. Compounds that include the cation of the IL, such as [emim]₄[(Zr₆C)Cl₁₈], [emim]₄[(Zr₆Fe)Cl₁₈], [emim]₅[(Zr₆Mn)Cl₁₈]·1.5CH₃CN, [emim]₅[(Zr₆Mn)Cl₁₈]·C₆H₅CH₃·2CH₃CN or [emim]₅[(Zr₆B)Cl₁₈]·C₆H₅CH₃·2CH₃CN, were isolated in good yield. The molecular cluster anions consist of octahedral (Zr₆Z) (Z = Fe, Mn, B, Be or C) units with the 12 edges bridged by chloride ligands (denoted as *inner* ligands Clⁱ). Six terminal chloride ions occupy the apical positions (*outer* chlorides Cl^a) (Figure 1.17) [129].

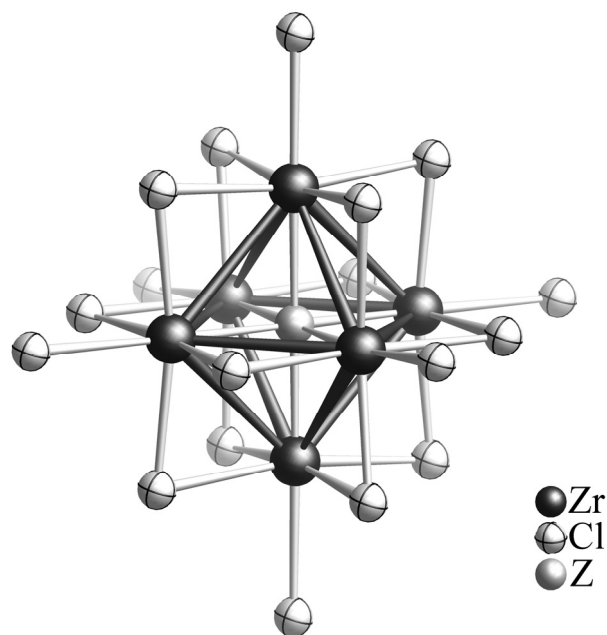


Figure 1.17: A typical heptanuclear cluster anion [(Zr₆Z)Cl₁₈]ⁿ⁻ (Z = Fe, Mn, Be or B and n = 4–5).

They proposed that in basic molten salts, the chloride nucleophilicity is sufficient, which could serve as a reagent for excising these centered clusters from highly cross-linked solid-state compounds. They were also successful to carry out exchange of halogenides in the basic molten salts. This approach was found to be effective for several compounds that resist dissolution in acetonitrile or are unstable in aqueous solution. Later, *Köckerling* et al.

followed the same route and isolated cluster phases $[\text{emim}]_4[(\text{Zr}_6\text{Fe})\text{Br}_{18}]$ and $[\text{emim}]_4[(\text{Zr}_6\text{Be})\text{Br}_{18}]$ from their solid-state precursors $\text{Na}_4[(\text{Zr}_6\text{Be})\text{Cl}_{16}]$ and $\text{K}[(\text{Zr}_6\text{Fe})\text{Cl}_{15}]$ by dissolving in Lewis basic $\text{emimBr}/\text{AlBr}_3$. In the bromide based IL, a complete exchange of all the outer and inner chlorides by bromide took place [119].

Mudring and co-workers isolated a number of new salt-like structures from IL, containing lanthanides in the anion network. Besides mononuclear complexes [93, 95], they also synthesized an octanuclear europium cluster compound $[\text{bmpyr}]_6[\text{Eu}_8(\mu_4\text{-O})(\mu_3\text{-OH})_{12}(\mu_2\text{-OTf})_{14}(\mu\text{-OTf})_2] \cdot (\text{HOTf})_{1.5}$ from the IL $[\text{bmpyr}][\text{OTf}]$. The structural characterization revealed an Eu_8 cluster unit, which is centered by an oxide anion [96]. Moreover, they also prepared some low melting IL, e.g. $[\text{C}_3\text{mim}][\text{Eu}(\text{Tf}_2\text{N})_4]$ (melting point = 81.0 °C), $[\text{C}_4\text{mim}][\text{Eu}(\text{Tf}_2\text{N})_4]$ (melting point = 67.9 °C), and $[\text{C}_4\text{mpyr}]_2[\text{Eu}(\text{Tf}_2\text{N})_5]$ (melting point = 92.1 °C). The dimeric europium units of the composition $[\text{Eu}_2(\text{Tf}_2\text{N})_8]^{2-}$ were confirmed in the first two substances through crystallographic studies. These low melting IL possess excellent photophysical properties (high lifetimes at high europium(III) concentration, small linewidth, and high color purity), which might render them particularly valuable for various optical applications [94a].

IL with polyoxometallate (POM) anions are also known. The first POM-based IL was reported by *Giannelis* et al [130]. The synthesis was performed by combining a partially deprotonated heteropolyacid $[\text{H}_{3-x}\text{PW}_{12}\text{O}_{40}]^{x-}$ with quaternary ammonium ions $(\text{CH}_3)(\text{C}_{18}\text{H}_{37})\text{N}^+[(\text{CH}_2\text{CH}_2\text{O})_n\text{H}][(\text{CH}_2\text{CH}_2\text{O})_m\text{H}]$ ($m + n = 15$). This new family of materials was characterized by electrochemical and thermal analysis. The fluid character and proton transport properties under anhydrous conditions make these IL possible candidates for fuel cell and catalytic applications. Later, *Dietz* et al. carried out further investigations for the preparation and preliminary characterization of the other members of this family of aprotic, POM-based IL, and described their potential as organic-inorganic hybrid materials [131]. *Hou* et al. and many other promoted this class of materials by adding IL to the list that exhibited excellent catalytic performance in organic synthesis [132–136].

Shan et al. synthesized several new inorganic IL [137] consisting of an inorganic polyoxometalate anion with the Keggin structure and sodium cations, e.g. $\text{Na}_{13}[\text{Ln}(\text{TiW}_{11}\text{O}_{39})_2] \cdot x\text{H}_2\text{O}$ ($\text{Ln} = \text{La}, \text{Ce}, \text{Pr}, \text{Sm}, \text{Gd}, \text{Dy}, \text{Er}, \text{Tm}, \text{or Yb}, x = 27.1\text{--}43.7$), $\text{Na}_5[\text{MTiW}_{11}\text{O}_{39}] \cdot x\text{H}_2\text{O}$ and $\text{Na}_6[\text{MTiW}_{11}\text{O}_{39}] \cdot x\text{H}_2\text{O}$ ($M = \text{Cr}, \text{Mn}, \text{Fe}, \text{or Zn}, x = 27.2\text{--}30.2$).

These inorganic IL were characterized by NMR, IR spectroscopy and by elemental analysis. Moreover, their physicochemical properties were also investigated. It was concluded that these IL are almost immiscible with water below room temperature, but the solubility of the IL increases sharply with an increase in temperature.

Table 1.3 A list of selected homo- and heteropolynuclear transition metal complexes and clusters synthesized from IL.

Complexes	Nuclearity	References
$[(\text{UO}_2)_2(\text{bet})_6(\text{H}_2\text{O})_2][\text{Tf}_2\text{N}]_4$	2	[124a]
$[\text{Cu}_2(\text{betmmor})_4][\text{Tf}_2\text{N}]_4$	2	[124b]
$[\text{Eu}_2(\text{betmmor})_6(\text{H}_2\text{O})_2][\text{Tf}_2\text{N}]_6$	2	[124b]
$[\text{Cu}_2(\text{betmpyr})_4(\text{H}_2\text{O})_2][\text{Tf}_2\text{N}]_4$	2	[124b]
$[\text{Cu}_2(\text{betmim})_4(\text{H}_2\text{O})_2][\text{Tf}_2\text{N}]_4 \cdot \text{H}_2\text{O}$	2	[124b]
$[\text{Cd}_2(\text{betPy})_2(\text{H}_2\text{O})_2][\text{Tf}_2\text{N}]_2$	2	[124b]
$[\text{Eu}_2(\text{bet})_8(\text{H}_2\text{O})_4][\text{Tf}_2\text{N}]_6$	2	[123b]
$[\text{Eu}_2(\text{bet})_8(\text{H}_2\text{O})_2][\text{Tf}_2\text{N}]_6 \cdot 2\text{H}_2\text{O}$	2	[123b]
$[\text{Y}_2(\text{bet})_6(\text{H}_2\text{O})_4][\text{Tf}_2\text{N}]_6$	2	[123b]
$[\text{bpy}]_2[\text{Mo}_2\text{O}_4\text{F}_6]$	2	[127]
$[\text{emim}]_3[\text{Re}_3(\mu_3\text{-S})(\mu\text{-S})_3\text{Br}_9]\text{Br}$	3	[120]
$[\text{Co}_3(\text{bet})_8(\text{Hbet})_2(\text{H}_2\text{O})_2][\text{Tf}_2\text{N}]_{10}[\text{Hbet}]_2$	3	[123a]
$[\{\mu_2\text{-HCC}(\text{CH}_2)_3\text{N}=\text{C}(\text{H})\text{N}(\mu_2\text{-CCH}(\text{CH}_2)_3\text{-CH}=\text{CH})\} \{\text{Co}_2(\text{CO})_6\}_2]\text{BPh}_4$	4	[128]
$[\text{Mn}_4(\text{bet})_{10}(\text{H}_2\text{O})_4][\text{Tf}_2\text{N}]_8$	4	[123a]
$[\text{Zn}_4(\text{bet})_{10}(\text{H}_2\text{O})_2][\text{Tf}_2\text{N}]_8$	4	[123a]
$[\text{Ni}_5(\text{bet})_{12}(\text{H}_2\text{O})_6][\text{Tf}_2\text{N}]_{10}$	5	[123a]
$[(\text{Pb}_4\text{O})\text{Pb}(\text{OH})(\text{bet})_8(\text{Tf}_2\text{N})_3][\text{Tf}_2\text{N}]_4 \cdot \text{MeOH}$	5	[123a]
$[\text{emim}]_4[(\text{Zr}_6\text{C})\text{Cl}_{18}]$	6	[118b]
$[\text{emim}]_5[(\text{Zr}_6\text{B})\text{Cl}_{18}] \cdot \text{C}_6\text{H}_5\text{CH}_3 \cdot 2\text{CH}_3\text{CN}$	6	[116]
$[\text{emim}]_4[(\text{Zr}_6\text{Fe})\text{Cl}_{18}]$	7	[115]
$[\text{emim}]_5[(\text{Zr}_6\text{Mn})\text{Cl}_{18}] \cdot 1.5\text{CH}_3\text{CN}$	7	[115]
$[\text{emim}]_5[(\text{Zr}_6\text{Mn})\text{Cl}_{18}] \cdot \text{C}_6\text{H}_5\text{CH}_3 \cdot 2\text{CH}_3\text{CN}$	7	[118b]
$[\text{emim}]_4[(\text{Zr}_6\text{Fe})\text{Br}_{18}]$	7	[119]
$[\text{emim}]_4[(\text{Zr}_6\text{Be})\text{Br}_{18}]$	7	[119]
$[\text{bmpyr}]_6[\text{Eu}_8(\mu_4\text{-O})(\mu_3\text{-OH})_{12}(\mu_2\text{-OTf})_{14}(\mu\text{-OTf})_2] \cdot (\text{HOTf})_{1.5}$	8	[96]

2. Experimental

2.1. Synthesis

Because of the high moisture sensitivity of the anhydrous metal halides used in this work, all manipulations were performed under dry argon (99.999 %) atmosphere in standard Schlenk tubes. The manufacturers and purities of the respective starting materials are summarized in Table 2.1. TeCl_4 was synthesized from the elements [138]. Bi was treated with hydrogen at 220 °C prior to use in synthesis. BiCl_3 and AlCl_3 were sublimated three times. I_2 was sublimated twice over BaO. Organic reagents were distilled before use. The Lewis acidic IL $[\text{BMIM}]\text{Cl}/\text{AlCl}_3$ were prepared in different compositions according to a literature procedure [139].

Table 2.1 Starting materials for the synthesis.

Substance	Purity, Supplier
1-methylimidazole	99 %, Merck
1-chlorobutane	98.5 %, Merck
AlCl_3	98 %, Fluka
Bi	chemical pure, Riedel de Haën
BiCl_3	99.999 %, Alfa Aesar
Cl_2	99.8 %, Air Liquide
I_2	99.5 %, Grüssing
In	99.999 %, Aldrich
Mo	99.95 %, Aldrich
MoCl_5	99.6 %, ABCR
Sb	99.999 %, ABCR
Se	99 %, Aldrich
SeCl_4	99.8 %, ABCR
Sn	99.999 %, Aldrich
Te	99.999 %, Aldrich
WOCl_4	98 %, Aldrich
WCl_6	99.9 %, ABCR

2.2. X-Ray Crystallography

The powder diffraction patterns were measured using a STOE STADI P powder diffractometer, equipped with a position sensitive detector covering 90° in 2θ and using $\text{Cu-K}\alpha_1$ radiation. The sample were sealed in 0.3 mm glass capillaries and kept spinning during the data collection at 293(2) K. Because of the high moisture and air sensitivity of the isolated substances, crystals were selected in an argon filled glove box and sealed in glass capillaries of 0.2 mm diameter. Intensity data of the single-crystals were recorded using an imaging plate diffraction system (IPDS I or IPDS II, both Stoe & Cie., Darmstadt, Mo- $K\alpha$ radiation,

graphite monochromator) or a Bruker Kappa CCD diffractometer with graphite-monochromatized Mo- $K\alpha$ radiation at 293(2) K and at 150(2) K. The raw data were corrected for background, polarization, and the Lorentz factor. The microscopic descriptions of the crystal shapes, which were later used in the numerical absorption corrections [140], were optimized using sets of symmetrically equivalent reflections [141]. The structures were solved with direct methods and refined using SHELXL-97 [142]. Graphics of the structure were developed using the program Diamond 3.2g [143]. The incommensurate modulated structures of $\text{Te}_4[\text{Bi}_{0.74}\text{Cl}_4]$ was solved with the Charge Flipping algorithm [144] and refined with the JANA2006 program package [145].

2.3. Magnetic Susceptibility Measurements

The magnetic susceptibility measurements were performed with a SQUID magnetometer (MPMS-XL7, Quantum Design) between 1.8 K and 400 K in four different magnetic fields between 0.20 and 70 kOe.

2.4. Raman spectroscopy

Raman spectra were recorded using Raman spectrometer (Renishaw RM-2000) equipped with He-Ne-laser (632.8 nm). A resolution of 4.0 cm^{-1} was used. The single crystals were selected in an argon filled glove box and sealed in glass capillaries of 0.2 mm diameter.

2.5. Quantum chemical calculations

Electronic structures of $(\text{Sb}_{10}\text{Se}_{10})[\text{AlCl}_4]_2$ and $\text{Te}_4[\text{Bi}_{0.74}\text{Cl}_4]$ were investigated on *ab initio* level of theory (DFT) utilizing the TB-LMTO-ASA [146] program. Brillouin zone integrations were performed for $(\text{Sb}_{10}\text{Se}_{10})[\text{AlCl}_4]_2$ and $\text{Te}_4[\text{Bi}_{0.74}\text{Cl}_4]$ by a tetrahedron method using eight irreducible k -points. Scalar relativistic wave equation was solved. The Barth-Hedin exchange potential [147a] was employed for local density approximation (LDA) calculations, and Perdew-Wang 91 functional was utilized for generalized gradient field (GGA) calculations [147b, 147c]. Default SCF convergence criteria of 10^{-6} were employed. Band structures and density of states plots were visualized by means of Gnuplot program package [148]. Molecular calculation were performed in the framework of DFT using Amsterdam Density Functional (ADF) software [149], employing QZ4P basis set and BP86

functional [150]. Relativistic effects were treated with ZORA formalism [151]. The starting geometry was taken from the experimental crystal structure data. The integration and convergence criteria were increased up to 10^{-8} and 10^{-6} respectively.

Chemical bonding was characterized by topological analysis of electron localizability indicator (ELI, λ) [152], that was performed in the DGrid 4.6 program package [153] using the ELI-D representation according to [152]. Formal atomic charges were calculated via integration of electron density (ρ) in basins according to the QTAIM [154]. The visualization of results was performed in the Paraview program package [155].

The ELI-D allows for real space interpretation of chemical bonding, its gradient field can be computed from the results of the converged quantum chemical calculations. Its maxima are attractors, which mark out different bonding features, such as atomic electron shells, lone electron pairs or covalent bonds. Topological analysis of the ELI-D field is performed by a procedure similar to QTAIM, and the space is divided into basins that correspond to the respective attractors. The integration of the basin population yields an electron count for the particular bonding feature. The ELI-based oxidation numbers (ELIBON [156a]) are ideologically analogous to QTAIM formal atomic charges and, for a given atom, constitute all monosynaptic [156b] basin populations (core electrons, valence shells, lone pairs) plus the respective share of the atom in basins with higher synapticity [156b] (pair-wise and multicenter bonds).

ELIBON can be more accurately estimated on the basis of the polarity of the current bond. The bond polarity index p [156c] for a two-center bond is the ratio between difference and sum of ELI-D bond basin populations attributed to each atom by QTAIM partitioning of ELI-D bond basin. It equals zero for a non-polar bond and unity for an ideal ionic bond. The concept of ELIBON in its current form is not defined to partition the ELI-D basin population for bonds with both significant covalent and ionic contributions. There are only two options: If the bond is regarded as non-polar, then the respective ELI-D basin population is equally distributed between all the contributing atoms upon calculation of ELIBON. If the polarity index confirms high polarity of the bond, all respective electrons are attributed to one constituent.

3. Synthesis and Characterization of Polycationic Bismuth Cluster Compounds

3.1. Synthesis of $\text{Bi}_5[\text{AlCl}_4]_3$

Stoichiometric amounts of Bi and BiCl_3 (total mass = 288 mg) were added to the Lewis acidic IL $[\text{bmim}]\text{Cl}/\text{AlCl}_3$ (molar ratio = 1:2, volume \approx 1.5 mL) at 298 K, which immediately turned into a dark brown solution. The reaction mixture was left for stirring overnight at room temperature then filtered to separate unreacted material. After three days, dark brown cubic-shaped crystals were obtained. The excess IL was decanted in an argon filled glove box and single crystals were separated. The crystals of the compound were washed twice with dry dichloromethane to remove any traces of IL. Yield: 68 %.

3.2. Synthesis of Bi_6Cl_7

The same procedure was used as described for $\text{Bi}_5[\text{AlCl}_4]_3$, starting from In and BiCl_3 (total mass = 284 mg). After two days, black needle-shaped crystals were obtained. Yield: 63 %. The bromide analogue Bi_6Br_7 was also synthesized from Bi and BiBr_3 using the same methodology.

3.3. Results and Discussion

BiCl_3 and bismuth reacted immediately in the Lewis acidic IL $[\text{bmim}]\text{Cl}/\text{AlCl}_3$ at room temperature. Within minutes after mixing, the solution turned dark brown. It is indispensable to use Lewis acidic ionic solvents for metal cluster synthesis, because excess AlCl_3 picks up the free chloride ions from the solution to form tetrachloroaluminate ions, and these anions stabilize the polycations. Consequently, in case of neutral or basic IL no color change was observed. Probably the high viscosity of the reaction medium and excess Lewis acid AlCl_3 facilitated the isolation of dark-red crystals of $\text{Bi}_5[\text{AlCl}_4]_3$ only in three days. The addition of some polar organic co-solvents like acetonitrile, dichloromethane and tetrahydrofuran did not speed up crystallization. Besides the color of the solution and the precipitation of crystals, Raman spectra (Figure 3.1) indicate the presence of bismuth polycations in the IL as well. The Raman spectrum of bismuth polycations in solution suffered from strong fluorescence and

only three bands with weak intensities were identified in the characteristic range up to 400 cm^{-1} . The band at 134 cm^{-1} matches the most intensive mode $\nu_1(A_1')$ of the Bi_5^{3+} polycation [27]. The bands at 183 cm^{-1} and 345 cm^{-1} , which have also been observed in melts of $\text{Bi}_5[\text{AlCl}_4]_3/\text{NaAlCl}_4$ at 180 $^\circ\text{C}$ [42], can be attributed to $\nu_3(F_2)$ and $\nu_1(A_1)$ modes of the tetrahedral AlCl_4^- anions.

For comparison the Raman spectrum of a $\text{Bi}_5[\text{AlCl}_4]_3$ crystal grown from the IL was also recorded. The spectrum nicely matches with the previously reported results of Gillespie [42].

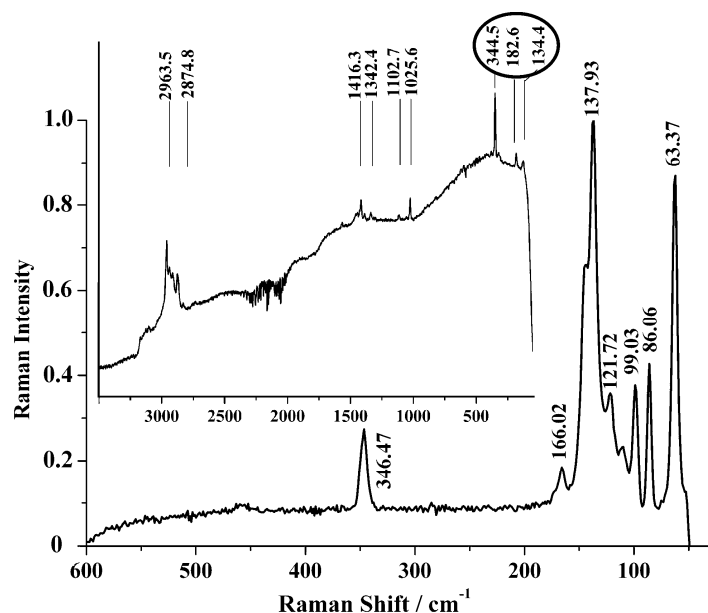


Figure 3.1: Raman spectra of single crystals of $\text{Bi}_5[\text{AlCl}_4]_3$, and of bismuth polycations (predominantly Bi_5^{3+}) in the IL (inset).

The representation of the Raman- and infrared-active normal vibrations for the trigonal bipyramid Bi_5^{3+} having D_{3h} symmetry is: $\Gamma_{\text{vib}} = 2A_1' + A_2'' + 2E' + 2E''$. Of these only A_1' , E' and E'' modes are Raman active. In the spectrum of crystalline $\text{Bi}_5[\text{AlCl}_4]_3$ the Raman bands (relative intensity in parentheses) for Bi_5^{3+} polycation are found at 63 cm^{-1} (0.9), 99 cm^{-1} (0.41), 122 cm^{-1} (0.35) and 138 cm^{-1} (1) for the Raman active $\nu_4(E')$, $\nu_6(E'')$, $\nu_2(A_1')$, and $\nu_1(A_1')$ vibrational modes. The bands at 86 cm^{-1} (0.43) and at 110 cm^{-1} (0.2) are attributed to lattice modes. Bands for AlCl_4^- anions are found at 166 cm^{-1} (0.18) and 346 cm^{-1} (0.3). In order to check whether the $\text{Bi}_5[\text{AlCl}_4]_3$ crystals grown from IL differ from those obtained by high-temperature melt reactions, X-ray diffraction at room temperature was performed on the powder (Figure 3.2) and a single-crystal. The unit cell dimensions ($a = 1187.1(2)$ pm, $c = 3012.0(3)$ pm) as well as the atomic parameters correspond within the accuracy of the

experiments with those determined by *Krebs* on a crystal grown by the high-temperature route [50a].

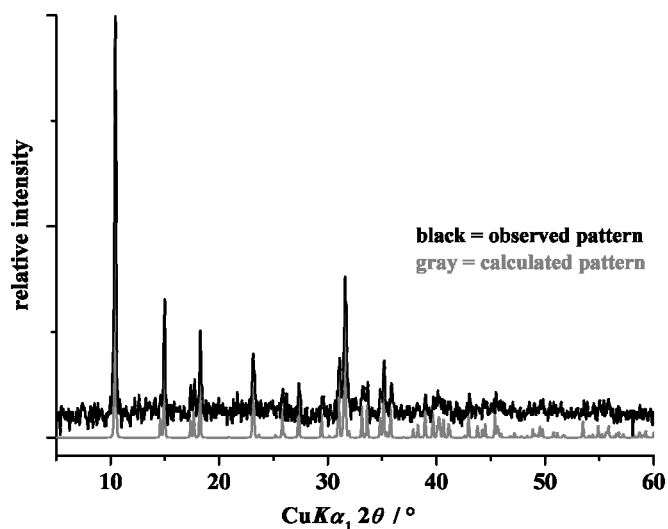


Figure 3.2: Powder diffraction pattern of $\text{Bi}_5[\text{AlCl}_4]_3$ crystals grown from an IL.

The rhombohedral crystal structure of $\text{Bi}_5[\text{AlCl}_4]_3$ is built from Bi_5^{3+} trigonal bipyramids and AlCl_4^- tetrahedra (Figure 3.3). The essential interatomic distances (in pm) are $d(\text{Bi1}-\text{Bi2}) = 301.2(1)$, $d(\text{Bi1}-\text{Bi1}) = 332.7(2)$, $d(\text{Al}-\text{Cl1}) = 214.4(5)$, and $d(\text{Al}-\text{Cl2}) = 214.5(6)$. The results of the structure determinations are summarized in Tables 3.1 and 3.2.

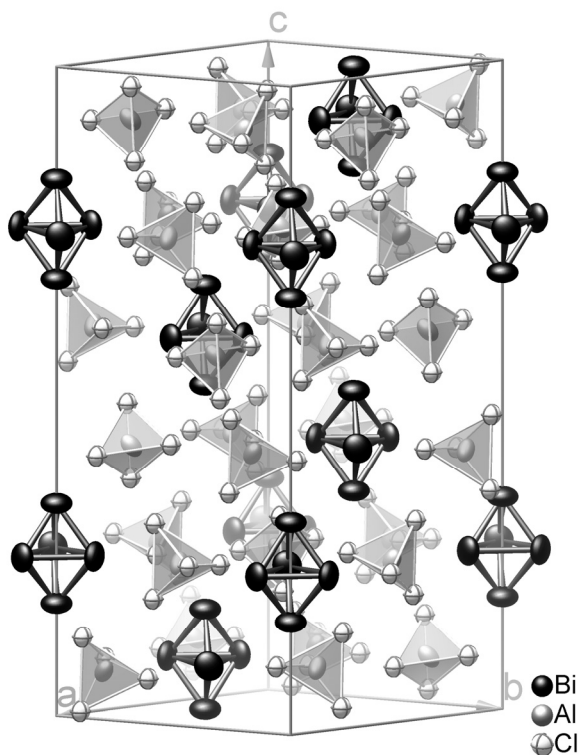


Figure 3.3: Rhombohedral structure of $\text{Bi}_5[\text{AlCl}_4]_3$, determined from a crystal grown from an IL. Ellipsoids represent 70 % probability at 293(2) K.

Bi_6Cl_7 was previously synthesized by *Corbett* and co-workers by reacting bismuth metal with molten BiCl_3 or with mixtures of BiCl_3 and KCl at temperatures above $250\text{ }^\circ\text{C}$ [7]. The severe problems associated with slow equilibria and concomitant metal contaminations of the final product experienced in the former synthetic route are only partially relieved by adding KCl . Later, *Beck* et al. applied two alterations to *Corbett's* methods to minimize these problems [50c]. In the first method, a reaction between Bi and BiCl_3 (1:2) was performed using a temperature gradient of $265\text{--}240\text{ }^\circ\text{C}$ for one week to get crystals of Bi_6Cl_7 . In the second method, Bi_6Cl_7 was conveniently synthesized from a melt of Bi , BiCl_3 , and SbCl_3 (2:1:4), keeping the temperature at $300\text{ }^\circ\text{C}$ for several days to get well-shaped single crystals. In contrast to these higher temperature methods, we developed a facile room-temperature route to synthesize Bi_6Cl_7 in only two days with relatively high yield. The crystal structure, which shows no noteworthy difference to the previously published structure solutions [7b, 50c], consists of distorted, tricapped trigonal prism Bi_9^{5+} polycations and chloridobismuthate(III) anions (Figure 3.4).

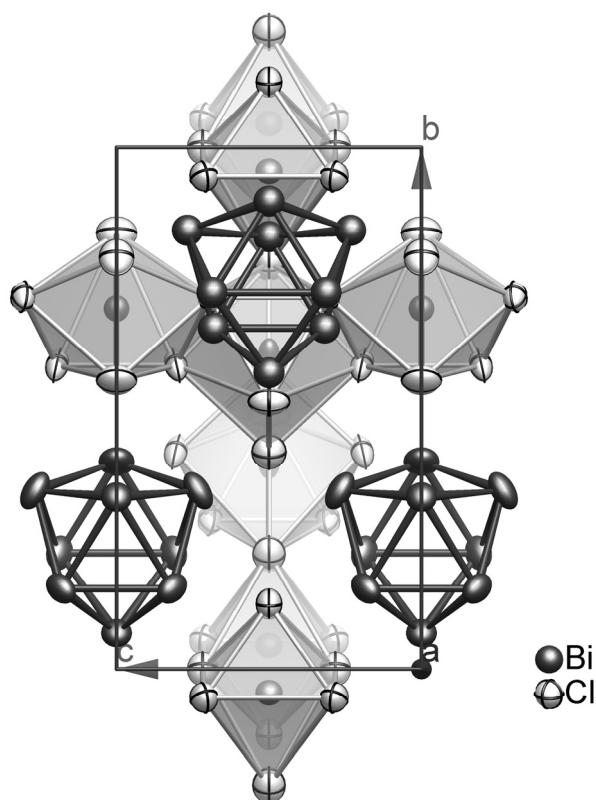


Figure 3.4: Orthonormal structure of Bi_6Cl_7 , determined from a crystal grown from an IL. Ellipsoids represent 80 % probability at $293(2)\text{ K}$.

The selected interatomic distances (in pm) are $d(\text{Bi}8\text{--Bi}9) = 308.2(2)$, $d(\text{Bi}1\text{--Bi}4) = 308.7(2)$, $d(\text{Bi}5\text{--Bi}9) = 311.2(3)$, $d(\text{Bi}2\text{--Bi}4) = 312.1(2)$, $d(\text{Bi}2\text{--Bi}9) = 312.9(1)$, $d(\text{Bi}1\text{--Bi}9)$

= 314.7(2), $d(\text{Bi1-Bi5}) = 317.2(4)$, $d(\text{Bi2-Bi2}') = 320.7(2)$, $d(\text{Bi2-Bi8}) = 321.5(3)$, $d(\text{Bi1-Bi1}') = 327.9(2)$, $d(\text{Bi3-Cl8}) = 258.9(4)$, $d(\text{Bi3-Cl3}) = 261.5(6)$, $d(\text{Bi3-Cl11}) = 290.2(3)$, $d(\text{Bi6-Cl6}) = 266.2(3)$, $d(\text{Bi6-Cl10}) = 278.9(4)$, $d(\text{Bi6-Cl12}) = 291.5(6)$, $d(\text{Bi6-Cl111}) = 292.2(5)$, $d(\text{Bi6-Cl17}) = 296.1(6)$, $d(\text{Bi7-Cl14}) = 259.9(3)$, $d(\text{Bi7-Cl15}) = 261.5(6)$, $d(\text{Bi7-Cl19}) = 278.5(2)$, and $d(\text{Bi7-Cl10}) = 308.9(3)$. The results of the structure determinations are summarized in Tables 3.2 and 3.3.

Table 3.1 Wyckoff positions, coordinates and equivalent isotropic displacement parameters for $\text{Bi}_5[\text{AlCl}_4]_3$. U_{eq} is one third of the trace of the orthogonalized U_{ij} tensor.

atom	W. p.	x	y	z	$U_{\text{eq}}/\text{pm}^2$
Bi1	4 <i>f</i>	0.16179(8)	0	1/4	600(3)
Bi2	2 <i>e</i>	0	0	0.32705(4)	705(5)
Al	4 <i>f</i>	0.5220(5)	1/4	1/2	368(15)
Cl1	4 <i>f</i>	0.4197(5)	0.0081(6)	0.3075(1)	469(10)
Cl2	2 <i>e</i>	0.7124(4)	0.1662(5)	0.2421(3)	563(17)

Table 3.2 Crystallographic data and details of the structure determination for $\text{Bi}_5[\text{AlCl}_4]_3$ and Bi_6Cl_7 .

Sum formula	$\text{Bi}_5[\text{AlCl}_4]_3$	Bi_6Cl_7
Crystal system	rhombohedral	orthorhombic
Space group	$R\bar{3}c$	$Pnmm$
Temperature (K)	293(2)	293(2)
a, b, c (pm)	1187.1(2), 1187.1(2), 3012.0(3)	2309.1(3), 1507.2(2), 877.4(3)
V (10^6pm^3)	3675.9(9)	3053.3(4)
Formula units per cell	6	8
Calculated density ($\text{g}\cdot\text{cm}^{-3}$)	4.21	6.58
Measurement device	imaging plate diffractometer (IPDS-I, Stoe)	
Radiation	graphite-monochromated Mo- $K\alpha$ radiation ($\lambda = 71.073 \text{pm}$)	
Range of indices	$-13 \leq h, k \leq 13, -34 \leq l \leq 34$	$-18 \leq h, k \leq 18, -14 \leq l \leq 14$
2θ range ($^\circ$)	$4.0 \leq 2\theta \leq 47$	$4.5 \leq 2\theta \leq 50$
$\mu(\text{Mo-}K\alpha)$ (mm^{-1})	37.4	68.5
Transmission(max, min)	0.11, 0.03	0.57, 0.021
Measured reflections	10389	13621
Unique reflections	638	3046
Reflections with $F_o > 4\sigma(F_o)$	465	2613
$R(\text{int}), R(\sigma)$	0.134, 0.041	0.041, 0.033
No. of parameters	33	139
Twin fractions	reverse-obverse twin with domain ratio of 0.91(2):0.09(2)	—
$R_I [F_o > 4\sigma(F_o)]$	0.042	0.032
R_I (all F_o)	0.071	0.041
wR_2 (all F_o^2)	0.077	0.036
Goodness of fit	1.09	1.15
$\Delta\rho(\text{max, min})$ ($\text{e}\cdot 10^{-6} \text{pm}^{-3}$)	+1.19, -0.99	+2.64, -1.92

Table 3.3 Wyckoff positions, coordinates and equivalent isotropic displacement parameters for Bi₆Cl₇. U_{eq} is one third of the trace of the orthogonalized U_{ij} tensor.

atom	W. p.	x	y	z	$U_{\text{eq}}/\text{pm}^2$
Bi1	8 <i>h</i>	0.04603(2)	0.22224(4)	0.1845(1)	359(3)
Bi2	8 <i>h</i>	0.20034(3)	0.15241(1)	0.1820(1)	347(5)
Bi3	4 <i>g</i>	0.41010(2)	0.45443(6)	0	251(1)
Bi4	4 <i>g</i>	0.4183(1)	0.0079(2)	0	325(1)
Bi5	4 <i>g</i>	0.7121(3)	0.1660(2)	0	442(2)
Bi6	4 <i>g</i>	0.41367(4)	0.1011 (1)	0	380(3)
Bi7	4 <i>g</i>	0.85712(6)	0.30734(2)	0	238(2)
Bi8	4 <i>g</i>	0.23836(7)	0.3295(1)	0	321(1)
Bi9	8 <i>h</i>	0.15261(6)	0.34210(2)	0.2673(1)	389(1)
Cl1	4 <i>e</i>	0	0	0.280(1)	33(2)
Cl2	4 <i>g</i>	0.5447(4)	0.0815(3)	0	36(1)
Cl3	4 <i>g</i>	0.6068(3)	0.3736(5)	0	31(1)
Cl4	4 <i>g</i>	0.7635(5)	0.2079(4)	0	38(1)
Cl5	4 <i>g</i>	0.7890(5)	0.4452(6)	0	41(1)
Cl6	4 <i>g</i>	0.3131(2)	0.0130(6)	0	37(1)
Cl7	8 <i>h</i>	0.3379 (3)	0.2139(4)	0.1921(5)	29(1)
Cl8	8 <i>h</i>	0.3321(3)	0.4435(6)	0.2129(6)	33(2)
Cl9	4 <i>g</i>	0.9321(3)	0.1620(3)	0	38(2)
Cl10	8 <i>h</i>	0.4421(3)	0.0823(4)	0.3046(6)	32(1)
Cl11	4 <i>g</i>	0.4636(4)	0.2787(4)	0	38(2)

4. Synthesis and Characterization of Polycationic Tellurium Cluster Compounds

4.1. Synthesis of $[\text{Mo}_2\text{Te}_{12}]\text{I}_6$

The starting materials were added together in the Lewis acidic IL $[\text{bmim}]\text{Cl}/\text{AlCl}_3$ (molar ratio = 1:1.3, volume = 1.5 mL) having molar ratio of Mo:Te:I = 1:6:3 (total mass = 355 mg). The reaction mixture was left for stirring overnight at room temperature. After three days, black, cube-shaped crystals were obtained. Yield: 35 %. The energy-dispersive X-ray (EDX) analysis of a single crystal gave the atomic ratio Mo:Te:I = 10:55:35 (expected = 10:60:30). EDX is only a semiquantitative technique, which sometimes cannot give exact estimation for two closely related elements.

4.2. Synthesis of $\text{Te}_4[\text{AlCl}_4]_2$

The stoichiometric amount of Te and TeCl_4 (total mass = 260 mg) were added to the Lewis acidic IL $[\text{bmim}]\text{Cl}/\text{AlCl}_3$ (molar ratio = 1:1.3, volume = 1.5 mL). The reaction mixture was left for stirring overnight at room temperature then filtered to separate unreacted material. Addition of a small amount of anhydrous NaCl into the dark violet filtrate led to the precipitation of violet, column-like crystals in two days. Yield: 66 %. EDX: Te:Al:Cl = 27:15:58 (expected = 29:14:57).

4.3. Synthesis of $\text{Te}_4[\text{Bi}_6\text{Cl}_{20}]$

The synproportionation of Te and TeCl_4 was carried out in the presence of BiCl_3 (molar ratio = 3.5:0.5:6, total mass = 275 mg) in the Lewis acidic IL $[\text{bmim}]\text{Cl}/\text{AlCl}_3$ (molar ratio = 1:1.3, volume = 1.5 mL). The same procedure was applied as described for $\text{Te}_4[\text{AlCl}_4]_2$ to isolate black crystals in only two days. Yield: 54 %.

4.4. Synthesis of $\text{Te}_6[\text{WOCl}_4]_2$

The same procedure was used as described for $\text{Te}_4[\text{AlCl}_4]_2$, starting from Te and WOCl_4 (total mass = 288 mg). After three days, black, irregular shaped crystals were obtained. Yield: 39 %.

4.5. Synthesis of $\text{Te}_8[\text{Bi}_4\text{Cl}_{14}]$

The same procedure was used as described for $\text{Te}_4[\text{Bi}_6\text{Cl}_{20}]$ but the molar ratio of the reactants was taken according to $\text{Te}_8[\text{Bi}_4\text{Cl}_{14}]$ (total mass = 285 mg). After two days, black, irregular shaped crystals were obtained. Yield: 63 %.

4.6. Results and Discussion

$[\text{Mo}_2\text{Te}_{12}]\text{I}_6$ is homeotypic to $[\text{Mo}_2\text{Te}_{12}]\text{Br}_6$ containing a heteropolycationic $[\text{Mo}_2\text{Te}_{12}]^{6+}$ cluster. $[\text{Mo}_2\text{Te}_{12}]\text{Br}_6$ was synthesized by *Beck* through CVT [157]. He used a temperature gradient of 340 °C to 270 °C to get single-crystals of $[\text{Mo}_2\text{Te}_{12}]\text{Br}_6$ within four weeks. Despite many attempts, the CVT synthesis of the analogous iodide failed [158]. In our studies, $[\text{Mo}_2\text{Te}_{12}]\text{I}_6$ was obtained by reacting Mo, Te and I_2 in the Lewis acidic IL $[\text{bmim}]\text{Cl}/\text{AlCl}_3$ at room temperature to give a dark solution within minutes. After overnight stirring and a crystallization period of only three days, single-crystals could be isolated with a yield of 35 %.

The monoclinic cell (space group $P2_1/n$) contains four formula units. The cationic complex $[\text{Mo}_2\text{Te}_{12}]^{6+}$ has a pair of molybdenum atoms, which are connected by two bridging $\eta^2\text{-Te}_2^{2-}$ groups (Figure 4.1a). In addition, each molybdenum atom is coordinated by a terminal polycationic Te_4^{2+} ligand in η^4 mode. As a result, both molybdenum atoms are in square-antiprismatic environment.

The point symmetry of the $[\text{Mo}_2\text{Te}_{12}]^{6+}$ complex in both compounds, i.e. in monoclinic $[\text{Mo}_2\text{Te}_{12}]\text{I}_6$ and in triclinic $[\text{Mo}_2\text{Te}_{12}]\text{Br}_6$, is close to D_{2h} (mmm), although the site symmetry of the cluster is C_i in the bromide and C_s in the iodide. Moreover, there is only one independent complex present in the unit cell of $[\text{Mo}_2\text{Te}_{12}]\text{I}_6$ whereas two independent complexes are found in $[\text{Mo}_2\text{Te}_{12}]\text{Br}_6$.

The distances between molybdenum and tellurium atoms of the Te_2^{2-} groups are slightly shorter (272.35(4) pm to 274.41(4) pm) than those between molybdenum and tellurium atoms of the Te_4^{2+} rings (278.99(5) pm to 285.38(4) pm). The Te_4^{2+} rings show significant distortion (distances: 276.12(5) pm to 286.85(4) pm, angles: 87.19(1) ° to 92.61(1) °) from D_{4h} to

butterfly conformation with dihedral angles 5.3° and 5.9° (Table 4.3). The results of the structure determinations are summarized in Tables 4.1 to 4.3.

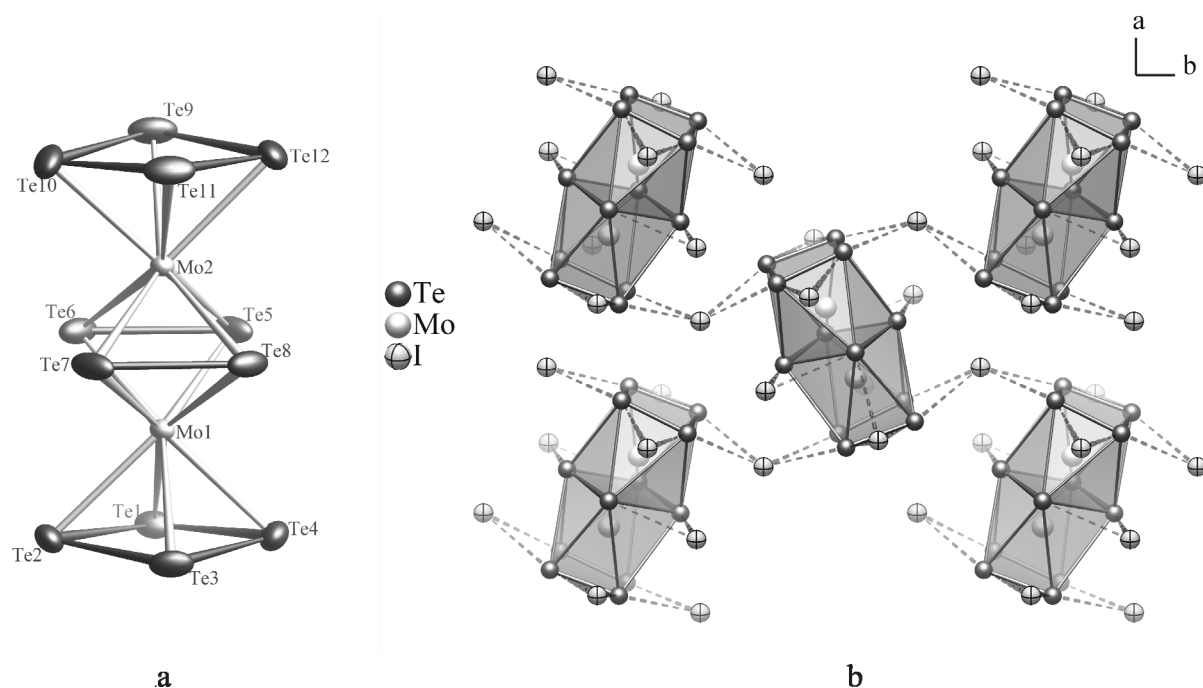


Figure 4.1: (a) $[\text{Mo}_2\text{Te}_{12}]^{6+}$ complex cation, the ellipsoids represent 90 % probability at 150(2) K, (b) Section of the crystal structure of $[\text{Mo}_2\text{Te}_{12}]\text{I}_6$.

The complexes $[(\text{Mo}^{3+})_2(\text{Te}_2^{2-})_2(\text{Te}_4^{2+})_2]^{6+}$ are surrounded by iodide ions, which connect them into layers (Figure 4.1b). The shortest distance between an iodide ion and an atom of the Te_4^{2+} rings is 302.20(4) pm. After refinement of the structure model of $[\text{Mo}_2\text{Te}_{12}]\text{I}_6$, we found a residual electron density of $+5.08 \text{ e} \cdot 10^{-6} \text{ pm}^{-3}$, which can be interpreted as a second orientation of the Te_4^{2+} rings with weight of a few percents. This disorder could not be refined neither in a split atom model nor in a twin model. Slow cooling of the crystals did not lead to ordering.

$[\text{Mo}_2\text{Te}_{12}]\text{I}_6$ is paramagnetic with Weiss temperature $\theta = +5.8 \text{ K}$ (Figure 4.2). An analysis based on the Curie-Weiss law gives a paramagnetic effective moment of $3.53 \mu_{\text{B}}$ per molybdenum atom, which is slightly lower than the spin-only value of $3.87 \mu_{\text{B}}$ for a d^3 configuration. In low fields some traces of ferromagnetism are found but these are very weak and most probably due to minor impurity phases.

The absence of intramolecular coupling of the magnetic cations in $[\text{Mo}_2\text{Te}_{12}]\text{I}_6$ is astonishing, since the short distance of 297.16(5) pm between the molybdenum(III) atoms suggests a chemical bond. In the present case the complex is a diradical with seventeen electrons per central atom. The electron counting scheme adds up the three valence electrons of a molybdenum(III) atom, six electrons of the π -system of the Te_4^{2+} ring, and four electrons (two lone-pairs) of each Te_2^{2-} group ($3 + 6 + 4 \cdot 2 = 17$).

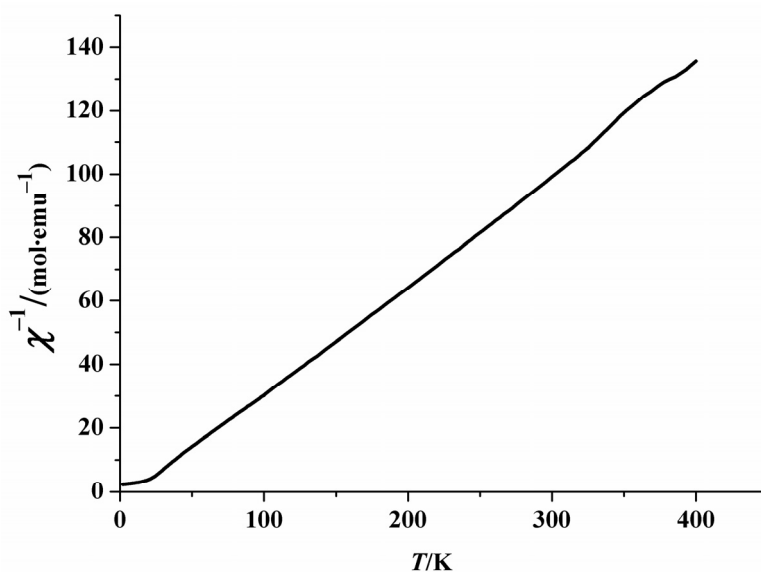


Figure 4.2: Temperature dependence of reciprocal molar susceptibility for $[\text{Mo}_2\text{Te}_{12}]\text{I}_6$ in a magnetic field of $H = 35$ kOe.

In contrast, the closely related *catena*-compound $\text{MoTe}_4\text{Br} = [(\text{Mo}^{3+})_2(\text{Te}_2^{2-})_2(\text{Te}_2\text{Br}^-)_2]$ with a Mo–Mo bond length of 300.5(2) pm shows only weak, nearly temperature-independent paramagnetism with a magnetic moment of $0.4 \mu_{\text{B}}$ at 310 K, indicating a strong coupling and an eighteen electron situation [157].

$\text{Te}_4[\text{AlCl}_4]_2$ was reported by *Corbett* and co-workers through synproportionation at 250 °C [14b]. Contrary to higher temperature method, we obtained $\text{Te}_4[\text{AlCl}_4]_2$ by reacting Te and TeCl_4 in the Lewis acidic IL $[\text{bmim}]\text{Cl}/\text{AlCl}_3$ at room temperature. Addition of a small amount of anhydrous NaCl is helpful for getting single crystals in two days (66 % yield). The orthorhombic compound contains planar Te_4^{2+} polycations and tetrahedral AlCl_4^- anions (Figure 4.3). The atomic coordinates agree within three standard deviations with those published earlier (Table 4.4) [14b].

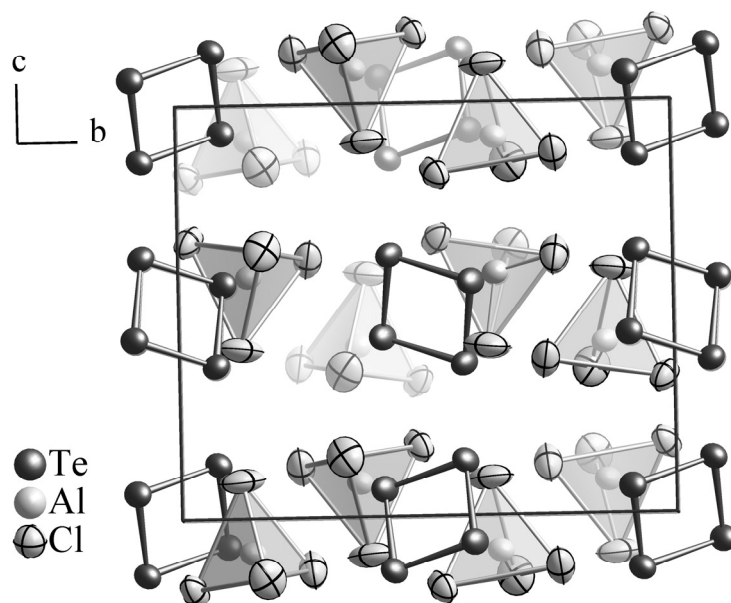


Figure 4.3: Crystal structure of $\text{Te}_4[\text{AlCl}_4]_2$. The ellipsoids represent 80 % probability at 293(2) K.

Crystals of $\text{Te}_6[\text{WOCl}_4]_2$ was synthesized previously within two weeks using CVT in the temperature gradient of 230 °C to 210 °C [59a]. We carried out the oxidation of elemental tellurium with WOCl_4 in IL at room temperature. Addition of anhydrous NaCl to the dark colored filtrate resulted in precipitation of black crystals in three days (yield: 39 %). The crystal structure consists of boat shaped Te_6^{2+} polycations and one-dimensional chains of square-pyramidal $[\text{WOCl}_4]^-$ anions (Figure 4.4). The atomic coordinates agree within six standard deviations with those published by *Beck* (Table 4.7) [59a].

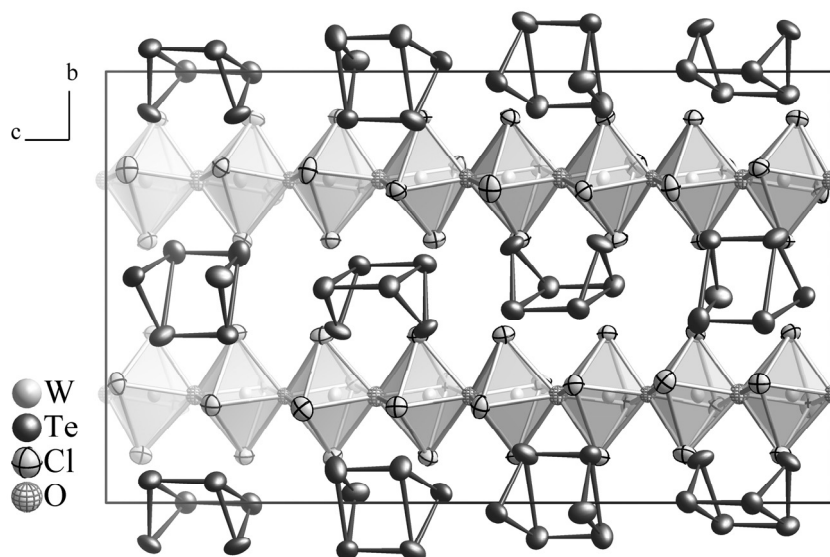


Figure 4.4: Crystal structure of $\text{Te}_6[\text{WOCl}_4]_2$. The ellipsoids represent 80 % probability at 293(2) K.

Crystals of $\text{Te}_4[\text{Bi}_6\text{Cl}_{20}]$ were formerly isolated by *Beck* et al. using a temperature gradient of 170 °C to 90 °C for several days to get single crystals in 40 % yield [59b] We carried out the synproportionation of elemental Te with Te(IV) in the presence of BiCl_3 in IL at room temperature. Addition of anhydrous NaCl to the dark colored filtrate resulted in the precipitation of black crystals in only two days (yield: 54 %). The unit cell consists of discrete Te_4^{2+} polycations and polymeric chloridobismuthate $[\text{Bi}_6\text{Cl}_{20}]^{2-}$ anions (Figure 4.5). The crystal structure shows no noteworthy difference to the previously published structure solution (Table 4.8 to 4.10) [59b].

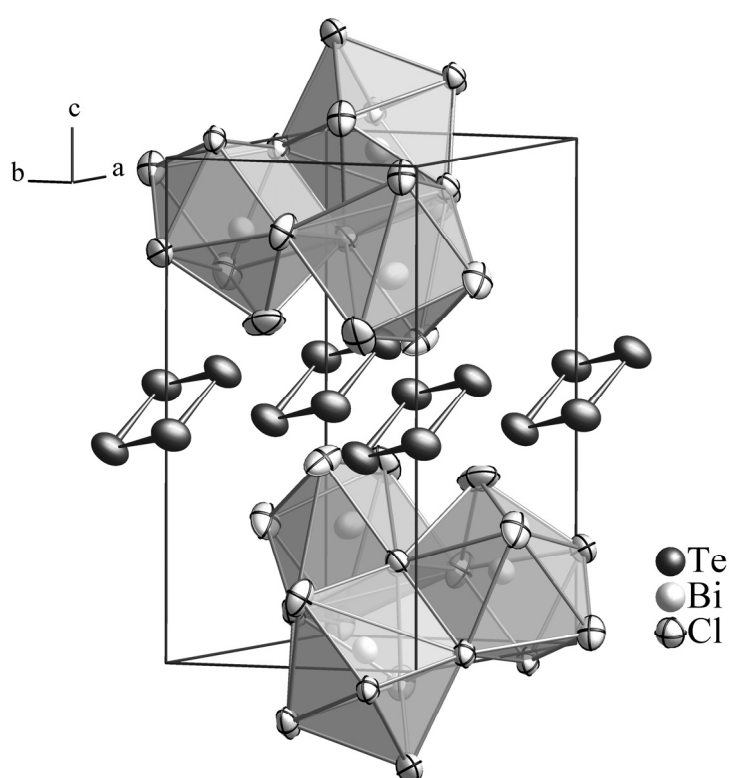


Figure 4.5: Crystal structure of $\text{Te}_4[\text{Bi}_6\text{Cl}_{20}]$. The ellipsoids represent 80 % probability at 293(2) K.

$\text{Te}_8[\text{Bi}_4\text{Cl}_{14}]$ was also synthesized by *Beck* et al. using a temperature gradient of 160 °C to 90 °C in two days with 30 % yield [64a] Contrary to higher temperature method, we obtained $\text{Te}_8[\text{Bi}_4\text{Cl}_{14}]$ by reacting Te, TeCl_4 , and BiCl_3 in the Lewis acidic IL $[\text{bmim}]\text{Cl}/\text{AlCl}_3$ at room temperature (63 % yield). The orthorhombic unit cell contains one-dimensional infinite chain of $[\text{Te}_8]^{2+}$ polycations and two-dimensional polymeric chloridobismuthate(III) anions (Figure 4.6). The crystal structure shows no noteworthy difference to the previously published structure solution (Table 4.8 and 4.11) [64a].

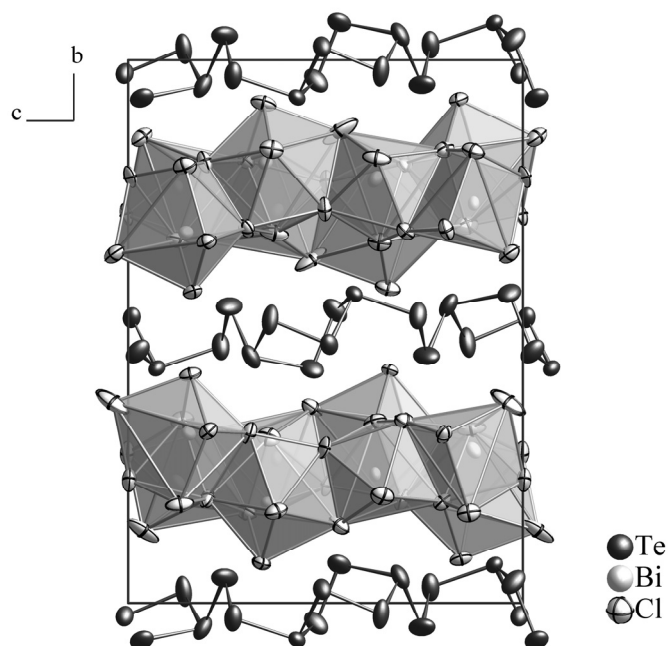


Figure 4.6: Crystal structure of $\text{Te}_8[\text{Bi}_4\text{Cl}_{14}]$. The ellipsoids represent 80 % probability at 293(2) K.

Table 4.1 Coordinates and equivalent isotropic displacement parameters for $[\text{Mo}_2\text{Te}_{12}]\text{I}_6$ at 150(2) K. All atoms occupy Wyckoff positions $4e$. U_{eq} is defined as one third of the trace of the orthogonalized U_{ij} tensor.

atom	x	y	z	$U_{\text{eq}} / \text{pm}^2$
Te1	0.31709(3)	0.37043(2)	0.17595(2)	131.6(6)
Te2	0.36271(3)	0.38843(2)	0.35915(2)	146.1(6)
Te3	0.27428(3)	0.54712(2)	0.32742(2)	155.6(6)
Te4	0.20828(3)	0.52383(2)	0.14798(2)	155.9(6)
Te5	-0.02771(3)	0.34316(2)	0.10664(2)	155.7(6)
Te6	0.07955(3)	0.24667(2)	0.24851(2)	145.1(6)
Te7	0.03788(3)	0.41154(2)	0.39261(2)	164.7(6)
Te8	-0.07073(3)	0.50746(2)	0.25047(2)	160.4(6)
Te9	-0.26539(3)	0.20622(2)	0.17358(2)	176.9(6)
Te10	-0.19369(3)	0.23018(2)	0.35450(2)	207.7(7)
Te11	-0.30688(3)	0.38207(2)	0.32504(2)	188.6(7)
Te12	-0.35434(3)	0.36452(2)	0.14525(2)	188.0(6)
Mo1	0.12620(3)	0.41140(2)	0.25141(2)	73.4(6)
Mo2	-0.11637(3)	0.34246(2)	0.24880(2)	71.9(6)
I1	0.42135(3)	0.20062(2)	0.28829(2)	171.5(6)
I2	0.36168(3)	0.43821(2)	0.53966(2)	227.0(7)
I3	0.16105(3)	0.44977(2)	-0.04292(2)	235.9(7)
I4	-0.33000(3)	0.29032(2)	-0.04388(2)	191.8(6)
I5	-0.07943(3)	0.05472(2)	0.29289(2)	172.1(6)
I6	-0.14299(4)	0.32255(2)	0.53245(2)	282.7(8)

Table 4.2 Crystallographic data and details of the structure determinations for [Mo₂Te₁₂]I₆, Te₄[AlCl₄]₂, and Te₆[WOCl₄]₂.

Compound	[Mo ₂ Te ₁₂]I ₆	Te ₄ [AlCl ₄] ₂	Te ₆ [WOCl ₄] ₂
Crystal system	monoclinic	orthorhombic	monoclinic
Space group	<i>P2₁/n</i>	<i>Pbca</i>	<i>P2₁/c</i>
Temperature (K)	150(2)	293(2)	293(2)
<i>a</i> , <i>b</i> , <i>c</i> (pm), <i>β</i> (°)	1138.92(2), 1628.13(2), 1611.05(2), 105.88(1)	1072.1(1), 1412.8(1), 1183.2(2), 90	917.07(8), 1631.9(2), 3077.5(3), 117.008(7)
<i>V</i> (10 ⁶ pm ³)	2873.42(7)	1792.1(4)	4103.4(7)
Formula units per cell	4	4	8
Calculated density (g·cm ⁻³)	5.74	3.14	4.69
Measurement device	CCD Kappa (Bruker)	imaging plate diffractometer (IPDS-I, Stoe)	
Radiation	graphite-monochromated Mo- <i>Kα</i> radiation (<i>λ</i> = 71.073 pm)		
Measurement range	-17 ≤ <i>h</i> ≤ 17 -27 ≤ <i>k</i> ≤ 26 -27 ≤ <i>l</i> ≤ 26	-11 ≤ <i>h</i> ≤ 11 -14 ≤ <i>k</i> ≤ 14 -12 ≤ <i>l</i> ≤ 12	-9 ≤ <i>h</i> ≤ 9 -18 ≤ <i>k</i> ≤ 18 -34 ≤ <i>l</i> ≤ 34
<i>μ</i> (Mo- <i>Kα</i>) (mm ⁻¹)	19.3	7.7	20.6
Measured reflections	72507	8267	23195
Unique reflections <i>F_o</i> > 4σ(<i>F_o</i>)	13529, 9970	1106, 868	5789, 3911
<i>R</i> (int), <i>R</i> (σ)	0.041, 0.039	0.079, 0.038	0.086, 0.066
<i>R_I</i> [<i>F_o</i> > 4σ(<i>F_o</i>)]	0.035	0.033	0.063
<i>R_I</i> (all <i>F_o</i>)	0.060	0.050	0.103
<i>wR₂</i> (all <i>F_o</i> ²)	0.060	0.066	0.070
No. of parameters	182	64	305
Goodness of fit	1.27	1.20	1.27
Δρ(max, min) (e·10 ⁻⁶ pm ⁻³)	+5.08, -4.31	+0.86, -0.76	+1.33, -1.23

Table 4.3 Selected interatomic distances (pm) in [Mo₂Te₁₂]I₆.

atoms	distance	atoms	distance
Te1– Te2	286.85(4)	Te7– Te8	276.81(4)
	Te4	Mo1	272.73(4)
	Mo1	Mo2	273.71(4)
Te2– Te3	276.93(4)	Te8– Mo1	273.10(4)
	Mo1	Mo2	273.49(4)
	I2	Te9– Te10	283.07(5)
Te3– Te4	280.66(4)	Te12	276.12(5)
	Mo1	Mo2	285.38(4)
Te4– Mo1	280.24(4)	Te10– Te11	276.91(5)
Te5– Te6	276.71(4)	Mo2	279.97(5)
	Mo1	I6	314.77(5)
	Mo2	Te11– Te12	281.18(5)
Te6– Mo1	273.22(4)	Mo2	284.43(5)
	Mo2	Te12– Mo2	278.99(5)
		Mo1– Mo2	297.16(5)

Table 4.4 Coordinates and equivalent isotropic displacement parameters for $\text{Te}_4[\text{AlCl}_4]_2$ at 293(2) K. All atoms occupy Wyckoff positions 8c. U_{eq} is defined as one third of the trace of the orthogonalized U_{ij} tensor.

atom	x	y	z	$U_{\text{eq}}/\text{pm}^2$
Te1	0.01047(6)	0.07424(4)	0.36773(4)	578(2)
Te2	0.39219(6)	0.40979(4)	0.43419(5)	600(2)
Al	0.3885(3)	0.3590(2)	0.0846(2)	490(7)
Cl1	0.3823(4)	0.1221(3)	0.4090(2)	1037(11)
Cl2	0.0701(3)	0.3304(2)	0.3535(3)	861(9)
Cl3	0.3128(2)	0.4785(2)	0.1715(2)	663(7)
Cl4	0.2755(3)	0.2391(2)	0.1256(2)	782(7)

Table 4.5 Selected interatomic distances (in pm) in $\text{Te}_4(\text{AlCl}_4)_2$.

atoms	distances	atoms	distances
Te1– Te2 ⁱ	266.56(8)	Al1– Cl1	209.6(3)
	Te2	Cl2	211.9(4)
		Cl3	213.8(3)
		Cl4	213.9(4)

Table 4.6 Selected interatomic distances (in pm) in $\text{Te}_6[\text{WOCl}_4]_2$.

atoms	distances	atoms	distances
W1– O1	173(1)	W4– O4	170(1)
	O2	O1	212(1)
	Cl1	Cl13	233.0(5)
	Cl2	Cl14	238.4(5)
	Cl3	Cl15	238.0(5)
	Cl4	Cl16	233.0(5)
W2– O2	173(1)	Te1– Te2	270.2(2)
	O3	Te6	269.7(2)
	Cl5	Te2– Te3	272.9(2)
	Cl6	Te3– Te4	270.6(2)
	Cl7	Te4– Te5	270.4(2)
	Cl8	Te5– Te6	273.4(2)
W3– O3	171(1)	Te7– Te8	270.3(2)
	O4	Te12	270.1(2)
	Cl9	Te8– Te9	273.2(2)
	Cl10	Te9– Te10	270.4(2)
	Cl11	Te11	321.4(2)
	Cl12	Te10– Te11	270.9(2)
		Te11– Te12	273.5(2)

Table 4.7 Coordinates and equivalent isotropic displacement parameters for $\text{Te}_6[\text{WOCl}_4]_2$ at 293(2) K. All atoms occupy Wyckoff positions 4e. U_{eq} is defined as one third of the trace of the orthogonalized U_{ij} tensor.

atom	x	y	z	U_{eq}/pm^2
W1	0.53225(9)	0.25128(5)	0.93373(2)	219(2)
W2	0.50167(9)	0.25213(5)	0.05432(2)	228(2)
W3	0.54404(9)	0.25070(5)	0.18493(3)	227(2)
W4	0.52395(9)	0.24840(5)	0.30749(2)	219(2)
Te1	0.0241(2)	0.60064(9)	0.31925(6)	454(4)
Te2	0.7653(2)	0.50199(9)	0.30013(5)	431(4)
Te3	0.7755(2)	0.49912(9)	0.39012(5)	449(4)
Te4	0.0381(2)	0.59618(9)	0.44054(5)	466(4)
Te5	0.1631(2)	0.44656(9)	0.43946(6)	477(4)
Te6	0.1540(2)	0.45059(6)	0.34943(6)	491(4)
Te7	0.8179(2)	0.47672(9)	0.03812(5)	479(4)
Te8	0.9965(2)	0.6132(1)	0.07737(6)	512(4)
Te9	0.0068(2)	0.61062(9)	0.16747(5)	454(4)
Te10	0.8173(2)	0.4775(1)	0.15634(6)	501(4)
Te11	0.1254(2)	0.4229(1)	0.18337(6)	560(5)
Te12	0.1225(2)	0.4187(1)	0.09414(5)	496(4)
Cl1	0.5828(7)	0.1110(3)	-0.0477(2)	367(12)
Cl2	0.8083(6)	0.2771(3)	-0.0153(2)	339(12)
Cl3	0.4787(6)	0.3922(3)	-0.0661(2)	350(12)
Cl4	0.2476(6)	0.2241(3)	0.8999(2)	353(12)
Cl5	0.5460(7)	0.1110(3)	0.0696(2)	394(13)
Cl6	0.7853(6)	0.2775(3)	0.0996(2)	313(12)
Cl7	0.4479(6)	0.3931(3)	0.0567(2)	321(12)
Cl8	0.2230(6)	0.2286(4)	0.0289(2)	416(14)
Cl9	0.6118(7)	0.1121(3)	0.2022(2)	397(13)
Cl10	0.8228(6)	0.2817(3)	0.2300(2)	388(13)
Cl11	0.4913(6)	0.3931(3)	0.1878(2)	348(12)
Cl12	0.2632(6)	0.2231(3)	0.1582(2)	325(12)
Cl13	0.5608(7)	0.1079(3)	0.3220(2)	418(13)
Cl14	0.8093(6)	0.2733(3)	0.3555(2)	344(13)
Cl15	0.4720(6)	0.3909(3)	0.3095(2)	313(12)
Cl16	0.2429(6)	0.2305(3)	0.2783(2)	389(14)
O1	0.532(2)	0.2502(7)	0.8775(4)	27(3)
O2	0.503(1)	0.2525(7)	-0.0017(4)	25(3)
O3	0.528(2)	0.2533(8)	0.1275(4)	30(3)
O4	0.534(1)	0.2523(7)	0.2538(4)	19(3)

Table 4.8 Crystallographic data and details of the structure determinations for $\text{Te}_4[\text{Bi}_6\text{Cl}_{20}]$, and $\text{Te}_8[\text{Bi}_4\text{Cl}_{14}]$.

Compound	$\text{Te}_4[\text{Bi}_6\text{Cl}_{20}]$	$\text{Te}_8[\text{Bi}_4\text{Cl}_{14}]$
Crystal system	triclinic	orthorhombic
Space group	$P\bar{1}$	$P2_12_12_1$
Temperature (K)	293(2)	293(2)
a, b, c (pm)	739.9(1), 876.6(2), 1391.7(3)	879.9(1), 2268.3(1), 1641.2(1)
α, β, γ ($^\circ$)	87.79(2), 83.06(2), 87.93(2)	90, 90, 90
V (10^6 pm^3)	894.9	3272.8
Formula units per cell	1	4
Calculated density ($\text{g}\cdot\text{cm}^{-3}$)	5.74	4.77
Measurement device	imaging plate diffractometer (IPDS-I, Stoe)	
Radiation	graphite-monochromated Mo- $K\alpha$ radiation ($\lambda = 71.073 \text{ pm}$)	
Measurement range	$-7 \leq h \leq 7$ $-9 \leq k \leq 9$ $-15 \leq l \leq 15$	$-9 \leq h \leq 9$ $-25 \leq k \leq 25$ $-18 \leq l \leq 18$
$\mu(\text{Mo-}K\alpha)$ (mm^{-1})	34.1	29.6
Measured reflections	7244	27070
Unique reflections $F_o > 4\sigma(F_o)$	2516	4831
$R(\text{int}), R(\sigma)$	0.051, 0.042	0.040, 0.032
$R_I [F_o > 4\sigma(F_o)]$	0.056	0.037
R_I (all F_o)	0.071	0.043
wR_2 (all F_o^2)	0.082	0.060
No. of parameters	137	236
Goodness of fit	1.21	1.13
$\Delta\rho(\text{max, min})$ ($\text{e}\cdot 10^{-6} \text{ pm}^{-3}$)	+2.66, -2.78	+1.31, -1.91

Table 4.9 Coordinates and equivalent isotropic displacement parameters for $\text{Te}_4[\text{Bi}_6\text{Cl}_{20}]$ at 293(2) K. All atoms occupy Wyckoff positions $4i$. U_{eq} is defined as one third of the trace of the orthogonalized U_{ij} tensor.

atom	x	y	z	U_{eq}/pm^2
Te1	0.1005(2)	0.8363(1)	0.57200(8)	481(5)
Te2	0.1752(3)	0.1309(2)	0.5367(1)	462(5)
Bi1	0.4253(2)	0.9733(1)	0.8331(1)	290(3)
Bi2	0.6043(2)	0.4808(1)	0.7406(1)	345(3)
Bi3	0.0932(1)	0.2642(1)	0.0327(1)	282(3)
Cl1	0.2392(9)	-0.0399(5)	0.0229(4)	258(3)
Cl2	-0.0872(1)	0.4560(6)	0.8959(4)	334(5)
Cl3	0.277(1)	0.7108(6)	0.8425(5)	371(2)
Cl4	0.304(10)	-0.2027(7)	0.2680(5)	410(2)
Cl5	0.2147(9)	0.2127(6)	0.2004(4)	310(1)
Cl6	0.1388(1)	0.1158(7)	0.8019(4)	372(2)
Cl7	0.4099(9)	0.3217(6)	-0.0410(5)	345(1)
Cl8	0.8441(3)	0.5271(6)	0.5986(4)	410(2)
Cl9	0.3581(2)	0.4594(7)	0.6360(6)	506(2)
Cl10	0.4703(4)	-0.0898(9)	0.6483(5)	544(2)

Table 4.10 Selected interatomic distances (in pm) in $\text{Te}_4[\text{Bi}_6\text{Cl}_{20}]$.

atoms	distances	atoms	distances
Te1– Te2	266.8(3)	Bi3– C11	284.2(5)
Bi1– C11	282.7(5)	C12	267.8(6)
	C13	C13	306.8(7)
	C14	C15	261.8(6)
	C15	C17	249.7(6)
	C16	C110	290.5(6)
	C110		263.0(6)
Bi2– C14	251.1(6)		
	C18		252.3(6)
	C19		248.5(7)

Table 4.11 Coordinates and equivalent isotropic displacement parameters for $\text{Te}_8[\text{Bi}_4\text{Cl}_{14}]$ at 293(2) K. All atoms occupy Wyckoff positions 4a. U_{eq} is defined as one third of the trace of the orthogonalized U_{ij} tensor.

atom	x	y	z	U_{eq}/pm^2
Te1	0.1310(2)	−0.0474(1)	−0.1888(1)	348(4)
Te2	−0.1199(1)	0.0209(1)	−0.1404(1)	391(4)
Te3	−0.1552(1)	−0.0247(1)	0.0089(1)	290(3)
Te4	0.0017(1)	0.0688(1)	0.0726(1)	244(3)
Te5	0.2963(1)	0.0378(1)	0.0240(1)	371(4)
Te6	0.2557(2)	−0.0698(1)	−0.0346(1)	378(4)
Te7	−0.0357(1)	0.0285(1)	0.2342(1)	364(4)
Te8	0.1936(2)	−0.0453(1)	0.2558(1)	472(4)
Bi1	0.0826(1)	0.73561(3)	0.12503(4)	191(2)
Bi2	−0.3877(1)	0.81779(3)	0.1458(1)	200(2)
Bi3	−0.5821(1)	0.68933(3)	0.3473(1)	195(2)
Bi4	−0.0576(1)	0.78004(3)	0.3745(1)	230(2)
Cl1	0.0069(6)	0.7848(2)	−0.0045(3)	397(1)
Cl2	0.1461(5)	0.6423(2)	0.0344(4)	346(2)
Cl3	−0.1818(4)	0.6959(2)	0.1437(4)	336(1)
Cl4	−0.4172(5)	0.8096(2)	0.3000(3)	274(1)
Cl5	−0.6275(5)	0.5798(2)	0.3427(3)	271(1)
Cl6	−0.6743(5)	0.8325(2)	0.1254(4)	321(2)
Cl7	−0.5604(5)	0.6879(2)	0.1940(3)	297(1)
Cl8	−0.3820(6)	0.9273(2)	0.1628(3)	306(1)
Cl9	−0.2994(4)	0.6645(2)	0.3631(4)	308(1)
Cl10	0.0079(7)	0.7251(3)	0.5025(3)	465(1)
Cl11	0.2041(5)	0.8196(2)	0.3701(4)	403(1)
Cl12	−0.1395(7)	0.8683(3)	0.4624(6)	531(12)
Cl13	0.0973(4)	0.6847(2)	0.2967(3)	243(11)
Cl14	−0.0578(5)	0.8345(2)	0.1992(3)	281(1)

Table 4.12 Selected interatomic distances (in pm) in $\text{Te}_8[\text{Bi}_4\text{Cl}_{14}]$.

atoms		distances	atoms		distances
Te1–	Te2	281.0(2)	Bi3–	Cl8	251.7(5)
	Te6	280.3(2)		Cl7	252.4(5)
	Te8	276.0(2)		Cl9	256.0(4)
Te2–	Te3	267.7(2)	Cl13	293.8(4)	
Te3–	Te4	273.7(2)	Cl10	323.5(5)	
Te4–	Te5	279.9(2)	Cl12	342.3(5)	
	Te7	282.4(2)	Cl11	352.2(4)	
Te5–	Te6	264.8(2)	Cl14	318.6(5)	
Te7–	Te8	264.5(2)	Bi4–	Cl4	345.6(6)
Bi1–	Cl1	249.2(5)		Cl9	337.9(5)
	Cl2	264.7(5)	Cl10	250.5(6)	
	Cl3	251.8(4)	Cl11	247.3(4)	
	Cl6	306.5(4)	Cl12	257.6(6)	
	Cl7	350.7(4)	Cl13	285.6(5)	
	Cl13	304.8(5)	Cl14	313.1(5)	
	Cl14	283.6(5)			
Bi2–	Cl4	255.4(5)			
	Cl5	249.5(5)			
	Cl6	256.3(4)			
	Cl7	340.8(5)			
	Cl11	341.3(5)			
	Cl12	310.6(4)			
	Cl14	305.8(5)			

5. Synthesis and Characterization of Sn[SnCl][W₃Cl₁₃]

5.1. Synthesis of Sn[SnCl][W₃Cl₁₃]

Stoichiometric amounts of Sn and WCl₆ (total mass = 285 mg) were added to the Lewis acidic IL [bmim]Cl/AlCl₃ (molar ratio = 1:1.3, volume = 1.5 mL). The reaction mixture was left for stirring overnight at room temperature. After two days, dark brown, column-like crystals were obtained. Yield: 43 %.

5.2. Results and Discussion

Reacting elemental Sn and WCl₆ in Lewis acidic IL [bmim]Cl/AlCl₃ at room temperature gives a dark brown solution within minutes. After overnight stirring, single-crystals of a new cluster compound Sn[SnCl][W₃Cl₁₃] were obtained in only two days with a good yield of 43 %. Contrary to solid state synthesis (240 °C to 500 °C, 6 to 7 days) of A₃[W₃Cl₁₃] (A = Li, Na, K) cluster compounds by *Messerle* et al. and *Meyer* et al. [159, 160], we have established a soft and convenient room temperature route. In this synthetic scheme, we have utilized first time Sn as a reducing agent to convert WCl₆ into a trinuclear [W₃Cl₁₃]³⁻ cluster in IL media. The resulting Sn²⁺ cations are included in the product.

The symmetry of the diffraction pattern of Sn[SnCl][W₃Cl₁₃] is hexagonal. Wilson plot and (E^2-1) statistics clearly support an acentric structure. The only systematic reflection condition is $00l$ with $l = 2n$. The structure solution neatly succeeded in the polar space group $P6_3$, and the results confirmed the absence of any further symmetry elements. Although the coordinates seemed to be reasonable, non positive definite tensors of displacement, $wR_2 = 28$ %, $R_1(F_o > 4\sigma(F_o)) = 12$ %, and residual electron densities of +8.4 to -4.8 e/(10⁶ pm³) were clear indicators for a crystallographic problem. Refinement in the monoclinic space group $P2_1$ applying a threefold twinning along [001] did not solve the issue. The correct solution was found based on the observation that the data set merges quite well in the higher Laue class $6/mmm$. Refinement as a merohedral twin with mirror plane ($\bar{1}10$) as twin law (volume fraction of the second individual 44.7(1) %) gave $wR_2 = 3.6$ %, $R_1(F_o > 4\sigma(F_o)) = 1.9$ %, and residual electron densities of +0.58 to -0.72 e/(10⁶ pm³). Remarkably, the alternative twin law, a two-fold axis along [110], led to $wR_2 = 6.4$ % and $R_1(F_o > 4\sigma(F_o)) = 2.9$ %.

Such sensitivity to the preservation or the reversal of the polar axis (Flack parameter $x = -0.01(1)$) must be the result of rather large differences of the Bijvoet pairs [161]. In fact, huge deviations from Friedel's law were found for the intensities of the reflections $00l$ (Table 5.1). Most striking is that the intensity of the reflection 004 is 175 % of the intensity of $00\bar{4}$. Since the reflections $00l$ are the Fourier transform of the projection of the structure onto the c axis, the enormous polarity that is visible in the X-ray diffraction experiment can be rationalized by analyzing the distribution of the atoms according to their z parameters. In Figure 5.1, the relative scattering powers (atomic form factor f at $\theta = 0$, i.e. atomic number Z) from the layers of atoms as a function of the z parameter is shown. The tungsten atoms are a dominating factor in scattering. Relative to them the scattering power of the other atoms is distributed unequally. This clearly non-centrosymmetric sequence along z in combination with the anomalous dispersion of the heavy atom tungsten ($\Delta f' = -0.849$, $\Delta f'' = +6.8722$) gives rise to the observed Bijvoet differences of the $00l$ reflections.

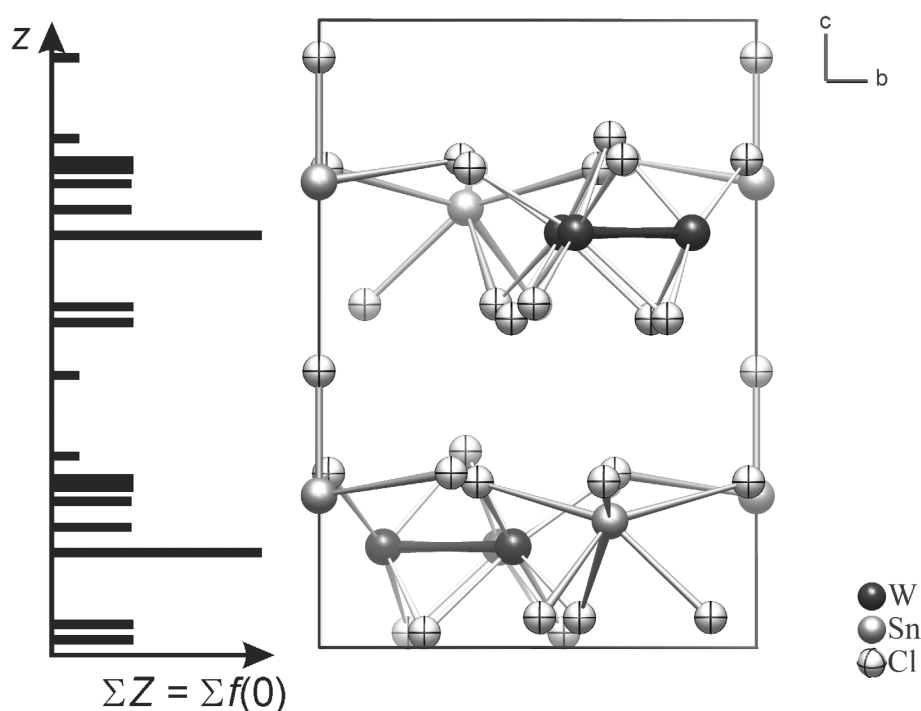


Figure 5.1: Projection of the unit cell of $\text{Sn}[\text{SnCl}][\text{W}_3\text{Cl}_{13}]$ along $[100]$ demonstrating the layer motif as well as the polarity of the structure. The histogram indicates the relative X-ray scattering power of the atomic layers along z .

With respect to the extended sum formula $\text{Sn}[\text{SnCl}][\text{W}_3\text{Cl}_{13}]$, the structure can be subdivided into a $[\text{W}_3\text{Cl}_{13}]^{3-}$ cluster anion, a Sn^{2+} cation, and a $[\text{SnCl}]^+$ cation. The crystallographic point group of the $[\text{W}_3(\mu_3\text{-Cl})(\mu\text{-Cl})_3\text{Cl}_9]^{3-}$ cluster anions is C_3 , but pseudo-

symmetry C_{3v} is observed within double standard deviation. The bonding W–W distance of 272.18(6) pm is in excellent agreement with those in $\text{Na}_3[\text{W}_3\text{Cl}_{13}]$ (273.7(1) pm) [160]. W atoms are additionally connected by one $\mu_3\text{-Cl}^-$ and three $\mu\text{-Cl}^-$ ligands. Each W atom is further coordinated by three terminal Cl^- ions. Irrespective of the connectivity, the W–Cl distances are very similar (238.4(3) to 247.6(3) pm). Consequently, the W atom is in a slightly distorted octahedral environment (Figure 5.2). Comparable isolated groups $[\text{Bi}_3\text{Br}_{13}]^{4-}$ (without metal-metal bonds) [56e] as well as interconnected clusters $[\text{Nb}_3\text{Cl}_{13}]^{n-}$ [162] have been described previously.

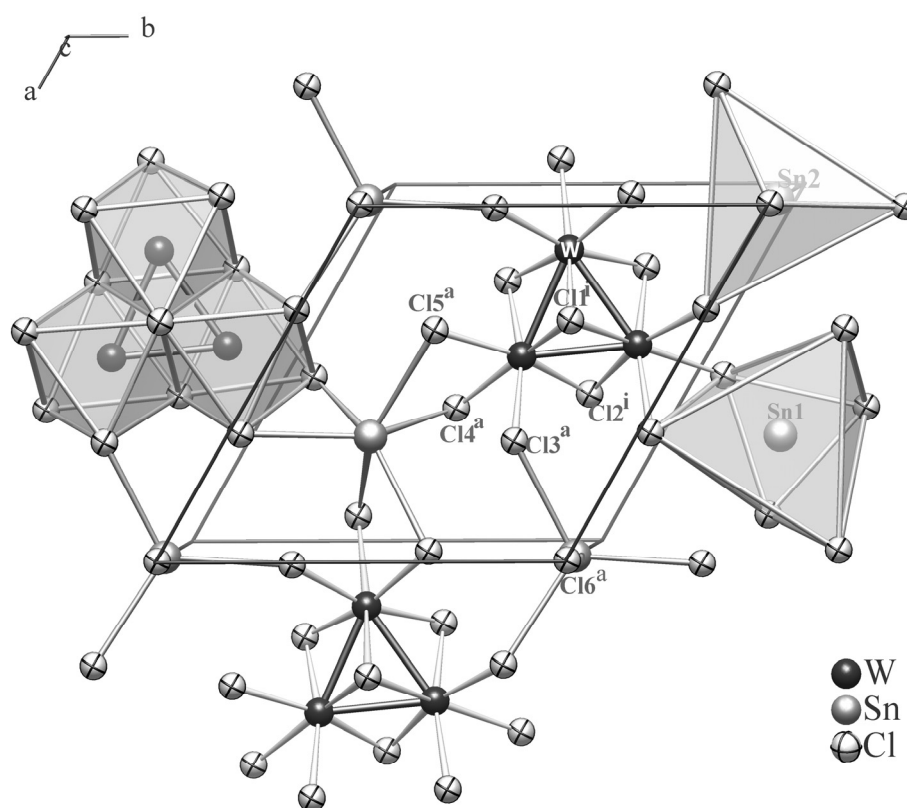


Figure 5.2: One layer in the crystal structure of $\text{Sn}[\text{SnCl}][\text{W}_3\text{Cl}_{13}]$. The second layer is obtained by 6_3 screw rotation along the c axis.

The trinuclear $[\text{W}_3\text{Cl}_{13}]^{3-}$ cluster anions are encircled by Sn^{2+} cations, which link them into a two-dimensional network parallel to (001). The cation Sn1 is in distorted trigonal-antiprismatic coordination by six Cl^- anions with three short (269.0(3) pm) and three long distances (307.7(4) pm). The lone-pair of the Sn^{2+} cation might be directed towards the center of the wide triangular face that is formed by Cl5 atoms ($\text{Cl}\cdots\text{Cl}$: 517 pm).

Sn2 is in trigonal pyramidal coordination, which is fairly common for Sn^{2+} complexes [163]. If the virtual position of the lone-pair is taken into account a ψ -bipyramid results. Remarkably the Cl6 anion is only bonded to this cation (Figure 5.1 and 5.2), which is highlighted in the formulation as a $[\text{Sn}^{\text{II}}\text{Cl}]^+$ group. Furthermore, the distance of 236.1(5) pm could be taken as a reference for the length of a $\text{Sn}^{\text{II}}\text{-Cl}$ single-bond. In accordance, *Breese* and *O'Keeffe* list a bond-valence parameter $R(\text{Sn}^{\text{II}}\text{-Cl}) = 236$ pm [164]. However, considering bond lengths, it must be emphasized that Sn2 and Cl6 atoms are displaced from the 6_3 axis by about 34 and 23 pm, respectively. In the presented structure model the disorder is approximated by enlarged displacement parameters U_{11} and U_{12} . Alternatively, split positions Sn2' with $x = 0.0000(8)$, $y = 0.0355(5)$, and Cl6' with $x = 0.025(3)$, $y = 0.021(4)$ can be used. The longest distance between these split positions is 242.4(6) pm. Bond valence sums calculated with this standard length are $\Sigma \nu = 2.00$ for Sn1 and $\Sigma \nu = 1.83$ for Sn2. The results of the structure determinations are summarized in Tables 5.1 to 5.4.

Table 5.1 Bijvoet differences $\Delta = 2 [F_c^2(hkl) - F_c^2(\overline{hkl})] / [F_c^2(hkl) + F_c^2(\overline{hkl})]$ for $\text{Sn}[\text{SnCl}][\text{W}_3\text{Cl}_{13}]$.

h	k	l	$F_c^2(hkl)$	$F_c^2(\overline{hkl})$	Δ	$F_o^2(hkl)$	$F_o^2(\overline{hkl})$
0	0	4	613	350	54.6 %	621(8)	336(7)
0	0	6	520	463	11.6 %	547(7)	451(6)
0	0	8	1296	1269	2.2 %	1317(8)	1345(11)
0	0	10	662	614	7.5 %	663(6)	630(6)
0	0	12	220	181	19.4 %	220(5)	181(3)

Table 5.2 Wyckoff positions, coordinates, and equivalent displacement parameters for the atoms in $\text{Sn}[\text{SnCl}][\text{W}_3\text{Cl}_{13}]$. U_{eq} (in pm^2) is defined as one third of the trace of the orthogonalized tensor U_{ij} .

atom	position	x	y	z	U_{eq}
W	$6c$	0.55686(5)	0.41171(5)	0.16074(4)	143(1)
Sn1	$2b$	1/3	2/3	0.2012(1)	279(4)
Sn2	$2a$	0	0	0.2419(1)	784(7)
Cl1	$2b$	2/3	1/3	0.3128(3)	139(9)
Cl2	$6c$	0.4411(4)	0.2014(4)	0.0237(2)	242(7)
Cl3	$6c$	0.3240(4)	0.3036(5)	0.2775(3)	292(8)
Cl4	$6c$	0.4040(4)	0.5062(4)	0.0473(2)	262(8)
Cl5	$6c$	0.6380(4)	0.6541(5)	0.2637(3)	280(8)
Cl6	$2a$	0	0	0.4402(4)	469(15)

Table 5.3 Selected interatomic distances (in pm) in Sn[SnCl][W₃Cl₁₃].

atoms	distances	atoms	distances
W– W	272.18(6)	Sn1– Cl4	269.0(3)
	C11 239.7(3)		Cl5 307.7(4)
	C12 239.4(3)	Sn2– Cl3	304.6(3)
	C13 238.4(3)		Cl6 236.1(5)
	C14 247.6(3)		
	C15 238.9(4)		

Table 5.4 Crystallographic data and details of the structure determination for Sn[SnCl][W₃Cl₁₃].

Sum formula	Sn ₂ W ₃ Cl ₁₄
Crystal system	hexagonal
Space group	<i>P</i> 6 ₃
Temperature (K)	293(2)
<i>a</i> , <i>c</i> (pm)	959.8(1), 1190.3(2)
<i>V</i> (10 ⁶ pm ³)	949.6(2)
Formula units per cell	2
Calculated density (g·cm ⁻³)	4.50
Measurement device	imaging plate diffractometer (IPDS-I, Stoe)
Radiation	graphite-monochromated Mo- <i>K</i> α radiation ($\lambda = 71.073$ pm)
Measurement range	$-10 \leq h, k \leq 10; -13 \leq l \leq 13$
μ (Mo- <i>K</i> α) (mm ⁻¹)	22.6
Measured reflections	7694
Unique reflections ($F_o > 4\sigma(F_o)$)	928, 909
<i>R</i> (int), <i>R</i> (σ)	0.060, 0.024
<i>R</i> _{<i>I</i>} [$F_o > 4\sigma(F_o)$]	0.019
<i>R</i> _{<i>I</i>} (all <i>F</i> _o)	0.020
<i>wR</i> ₂ (all <i>F</i> _o ²)	0.036
Twin fraction	0.447(1)
Flack parameter	-0.01(1)
Extinction parameter	0.0006(1)
No. of parameters, restraints	60, 1
Goodness of fit	1.18
$\Delta\rho$ (max, min) (e·10 ⁻⁶ pm ⁻³)	+0.58, -0.72

6. Synthesis and Characterization of Molybdenum Cluster Compounds

6.1. Synthesis of Bi[Mo₅Cl₁₃]Cl

Stoichiometric amounts of Bi, BiCl₃ and MoCl₅ (total mass = 275 mg) were added to the Lewis acidic IL [bmim]Cl/AlCl₃ (molar ratio = 1:1.3, volume = 1.5 mL). The dark blue reaction mixture was left for stirring overnight at room temperature then filtered to separate unreacted material. Addition of anhydrous NaCl helped to get black, cube-shaped crystals in only three days. Yield: 47 %.

6.2. Synthesis of BiCl[Mo₆Cl₁₄]

The same procedure was used as described for Bi[Mo₅Cl₁₃]Cl, starting from Bi and MoCl₅ (total mass = 290 mg), i.e. BiCl₃ was omitted in the synthesis. Addition of a small amount of anhydrous NaCl into the red filtrate led to the precipitation of light red crystals in only two days. Yield: 56 %.

6.3. Results and Discussion

Reacting elemental Bi, BiCl₃, and MoCl₅ in Lewis acidic IL [bmim]Cl/AlCl₃ at room temperature gave a dark blue solution within minutes. After overnight stirring, black, cube-shaped single-crystals of Bi[Mo₅Cl₁₃]Cl were obtained in only three days. Contrary to the multi-step synthesis of $A_2[Mo_5X_{13}]$ ($A = n\text{-Bu}_4\text{N}^+$, Ph_4As^+ ; $X = \text{Cl}, \text{Br}$) cluster compounds from K₃MoCl₆ or MoCl₂ in melts of Bi, BiCl₃, AlCl₃, and KCl at 306 °C by Schäfer et al. [165, 166] and Gray et al. [167], we have established a single-step, soft and convenient room temperature route. In this synthetic scheme, we have utilized elemental Bi as a reducing agent to convert MoCl₅ into a pentanuclear [Mo₅Cl₁₃]²⁻ cluster in IL media. The resulting bismuth(III) cations are included in the product.

The crystal structure of Bi[Mo₅Cl₁₃]Cl has been solved in the cubic centrosymmetric space group $Pn\bar{3}$ depending upon the observed reflections symmetry. All attempts to refine ordered structure models of lower symmetry, including multiple twinning, failed. The structure of Bi[Mo₅Cl₁₃]Cl (Figure 6.1) is a defect variant of the Pb[Mo₆Cl₁₄] type [168]. One of the molybdenum atoms of the Mo₆ cluster core is missing, resulting in a [Mo₅□Cl₁₃]²⁻

cluster and an isolated chloride ion. With respect to the high crystallographic symmetry, the vacancies are distributed statistically. The crystal of $\text{Bi}[\text{Mo}_5\text{Cl}_{13}]\text{Cl}$ proved to be an unbalanced merohedral twin. The results of the structure determinations are summarized in Tables 6.1 and 6.2. With respect to the magnetic properties of $\text{Bi}[\text{Mo}_5\text{Cl}_{13}]\text{Cl}$ (see below) a hypothetical alternative structure model, basing on the statistical missing of each sixth complete octahedron, is ruled out.

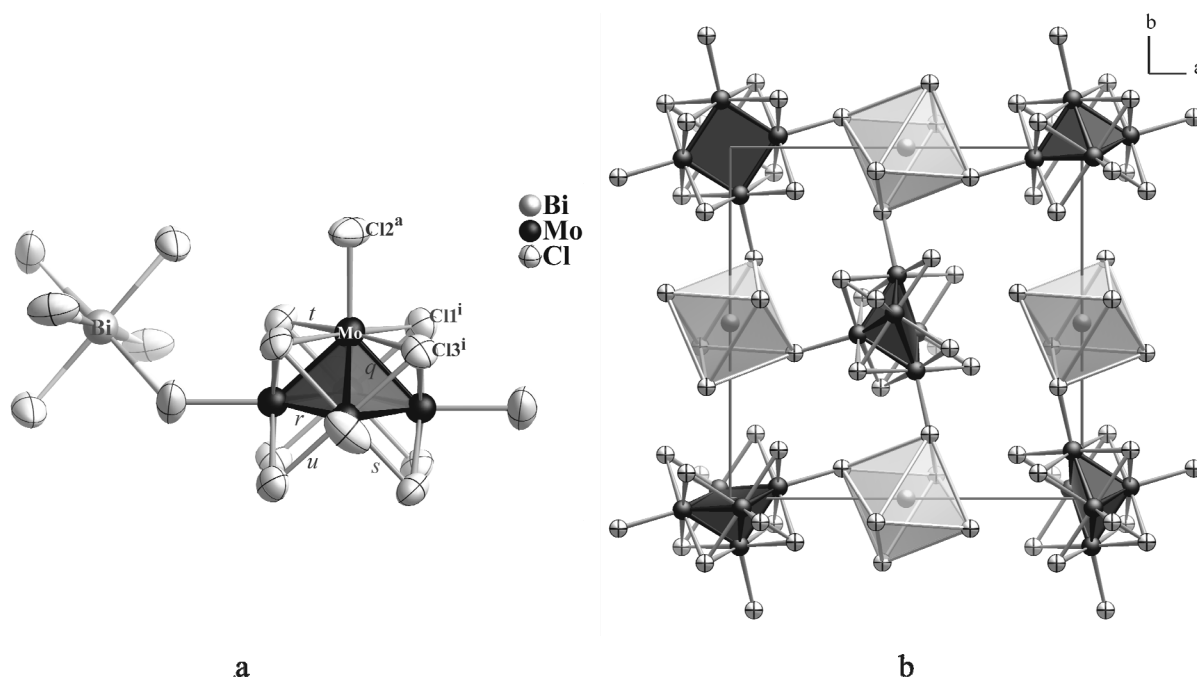


Figure 6.1: (a) A characteristic unit of $\text{Bi}[\text{Mo}_5\text{Cl}_{13}]\text{Cl}$, where each Mo atom is coordinated by four inner Cl^i and one apical Cl^a . The ellipsoids represent 90 % probability at 293(2) K. Distances (in pm): Mo–Mo(q) 258.9(1), Mo–Mo(r) 259.3(1), Mo–Cl3(s) 245.07(1), Mo–Cl3(t) 246.99(2), Mo–Cl3(u) 247.76(1), Mo–Cl2 250.84(1), Mo–Cl1 251.94(2), Bi–Cl2 274.1(1), (b) Section of the cubic crystal structure of $\text{Bi}[\text{Mo}_5\text{Cl}_{13}]\text{Cl}$ with an arbitrary choice of unoccupied molybdenum atom positions in the $[\text{Mo}_5\Box]$ cluster cores.

In the $[\text{Mo}_5\text{Cl}_{13}]^{2-}$ cluster anion, the molybdenum atoms form a square pyramid (Figure 6.1a), where each metal atom is coordinated by four Cl^i ligands and one Cl^a ligand (i = inner, a = apical, according to the notation of *Schäfer* and *Schnering* [129]). As a result, the Mo_5 core is surrounded by eight inner Cl^i ligands in the form of a cube. Out of these eight inner Cl^i , four are present as μ_3 -bridging ligands above the faces of the pyramid and the other four as μ -bridging ligands to the basal Mo atoms. As a consequence of the high crystallographic symmetry, a variation of the Mo– Cl^i distances [245.1(1) to 251.9(2) pm] correlated to the bonding mode of the chloride ion cannot be observed. The five apical Cl^a [Mo– Cl^a 250.8(1) pm] and the isolated chloride ion are also bonded to the bismuth cation. The average Mo–Mo bond length of 259 pm is somewhat shorter than those in the $[\text{Mo}_6\text{Cl}_8^i\text{Cl}_6^a]^{2-}$ cluster (Mo–Mo

= 262 pm) [106c] but are in good agreement with those in $A_2[\text{Mo}_5X_{13}]$ ($A = n\text{-Bu}_4\text{N}^+$, Ph_4As^+ ; $X = \text{Cl}, \text{Br}$; $\text{Mo-Mo} = 256.3(3)$ pm and $260.2(3)$ pm) [165]. Such a relative decrease in bond lengths has also been observed in the pentanuclear tungsten cluster compounds $[\text{PrN}]_2[\text{W}_5\text{I}_{13}]$ ($\text{W-W} = 264$ pm) [169], $(\text{W}_5\text{I}_8)\text{I}(\text{I}_3)_4$ and $(\text{W}_5\text{I}_8)\text{I}_2(\text{I}_3)_3$ ($\text{W-W} = 268$ pm) [170].

The bismuth cation is in a slightly distorted octahedral environment by six Cl^a ligands. The Bi-Cl distance is 274.1(1) pm, while the angles $\text{Cl}^a\text{-Bi-Cl}^a$ deviate by $\pm 3.09(4)^\circ$ from orthogonality. Such distorted coordination polyhedra are typical for bismuth(III) cations and have also been observed, for example, in the crystal structures of Tl_3BiCl_6 [171] and $(\text{C}_{12}\text{H}_{14}\text{N}_2)_3[\text{BiCl}_6]_2 \cdot 2\text{H}_2\text{O}$ [172].

$\text{Bi}[\text{Mo}_5\text{Cl}_{13}]\text{Cl}$ is paramagnetic and this behavior is in good agreement with those reported by *Gray* and co-workers for $(\text{Bu}_4\text{N})_n[\text{Mo}_5X_{13}]$ cluster compounds [167]. In the temperature range between 1.8 K and 400 K, the molar susceptibility of $\text{Bi}[\text{Mo}_5\text{Cl}_{13}]\text{Cl}$ follows a simple Curie law (Figure 6.2).

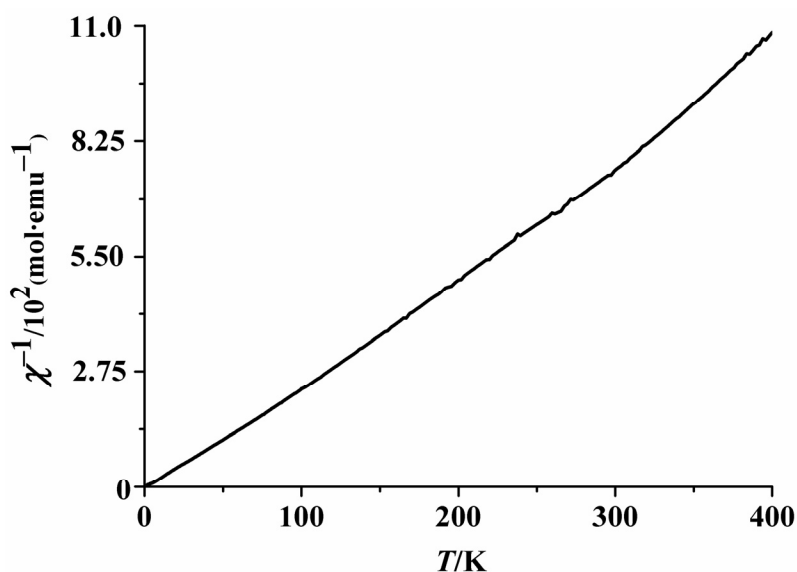


Figure 6.2: Temperature dependence of the reciprocal molar susceptibility of $\text{Bi}[\text{Mo}_5\text{Cl}_{13}]\text{Cl}$ in an external magnetic field of $H = 70$ kOe.

The experimental effective magnetic moment of $1.67 \mu_{\text{B}}$ suggests pure spin magnetism of an unpaired electron ($S = \frac{1}{2}$; $g \approx 2$) and is fairly close to the value of $1.70 \mu_{\text{B}}$ observed for $[\text{Bu}_4\text{N}]_2[\text{Mo}_5\text{Cl}_{13}]$ [167]. In fact the $[\text{Mo}_5\text{Cl}_{13}]^{2-}$ anion comprises the odd number of 19 electrons in molybdenum based cluster orbitals [173].

Crystals of the molybdenum richer cluster compound $[\text{BiCl}][\text{Mo}_6\text{Cl}_{14}]$ have previously been synthesized by *Beck* et al. within 10 days using a high temperature route (550 °C) [106c]. We performed the oxidation of elemental Bi with MoCl_5 in IL at room temperature. Addition of anhydrous NaCl to the red filtrate resulted in the precipitation of light red crystals in only two days.

The crystal structure, which shows no noteworthy difference to the previously published structure solution (Tables 6.2 to 6.4) [106c], consists of $[\text{Mo}_6\text{Cl}_8^i\text{Cl}_6^a]^{2-}$ units containing an almost regular octahedral Mo_6 cluster core. The clusters are bonded via Cl^a to $[\text{BiCl}]^{2+}$ dumbbells, which have a Bi–Cl bond length of only 249.7(2) pm (Figure 6.3).

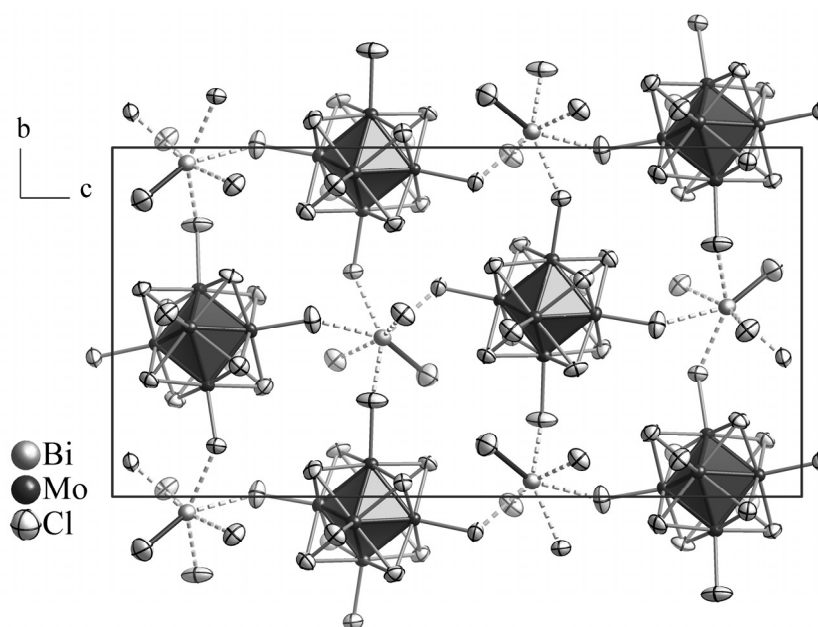


Figure 6.3: Section of monoclinic crystal structure of $\text{BiCl}[\text{Mo}_6\text{Cl}_{14}]$, containing an almost regular octahedral Mo_6 cluster core. $[\text{BiCl}]^{2+}$ dumbbells are represented as thick Bi–Cl bonds. The ellipsoids represent 90 % probability at 293(2) K.

Table 6.1 Wyckoff positions, coordinates and equivalent displacement parameters for the atoms in $\text{Bi}[\text{Mo}_5\text{Cl}_{13}]\text{Cl}$. The occupancy factor of the molybdenum atom is $5/6$. U_{eq} (in pm^2) is defined as one third of the trace of the orthogonalized tensor U_{ij} .

Atom	W.p.	<i>x</i>	<i>y</i>	<i>z</i>	U_{eq}
Bi	4 <i>c</i>	1/2	0	0	308(1)
Mo	24 <i>h</i>	0.13549(4)	0.03265(3)	−0.02650(4)	238(1)
Cl1	8 <i>e</i>	0.13779(8)	0.13779(8)	0.13779(8)	261(5)
Cl2	24 <i>h</i>	0.3178(1)	0.0856(1)	−0.0673(1)	402(3)
Cl3	24 <i>h</i>	0.18423(9)	−0.1244(1)	0.07223(9)	286(3)

Table 6.2 Crystallographic data and details of the structure determination for Bi[Mo₅Cl₁₃]Cl and [BiCl][Mo₆Cl₁₄].

Sum formula	BiMo ₅ Cl ₁₄	BiMo ₆ Cl ₁₅
Crystal system	cubic	monoclinic
Space group	$Pn\bar{3}$	$C2/c$
Temperature (K)	293(2)	293(2)
a, b, c (pm)	1291.6(3)	1267.6(1), 1304.3(1), 2573.8(3)
α, β, γ (°)	90, 90, 90	90, 91.782(8), 90
V (10 ⁶ pm ³)	2154.7(9)	4253.3(7)
Formula units per cell	4	8
Calculated density (g·cm ⁻³)	3.65	4.11
Measurement device	imaging plate diffractometer (IPDS-I, Stoe)	
Radiation	graphite-monochromated Mo- $K\alpha$ radiation ($\lambda = 71.073$ pm)	
Range of indices	$-14 \leq h, k, l \leq 14$	$-13 \leq h \leq 14, -14 \leq k \leq 14, -28 \leq l \leq 28$
2θ range (°)	$4.5 \leq 2\theta \leq 47.4$	$4.5 \leq 2\theta \leq 47.0$
μ (Mo- $K\alpha$) (mm ⁻¹)	12.7	13.5
Transmission(max, min)	0.455, 0.326	0.172, 0.051
Measured reflections	11600	11627
Unique reflections	537	3083
Reflections with $F_o > 4\sigma(F_o)$	475	2616
R (int), R (σ)	0.109, 0.025	0.049, 0.036
No. of parameters	34	200
Extinction coefficient	—	$8.8(3) \times 10^{-5}$
Twin fraction	0.028(1)	—
R_I [$F_o > 4\sigma(F_o)$]	0.034	0.026
R_I (all F_o)	0.044	0.037
wR_2 (all F_o^2)	0.021	0.026
Goodness of fit	1.26	1.05
$\Delta\rho$ (max, min) (e·10 ⁻⁶ pm ⁻³)	+0.40, -0.52	+0.64, -0.64

Table 6.3 Coordinates and displacement parameters for the atoms in [BiCl][Mo₆Cl₁₄]. All atoms reside on Wyckoff positions 8*f*. U_{eq} (in pm²) is defined as one third of the trace of the orthogonalized tensor U_{ij} .

Atom	x	y	z	U_{11}	U_{22}	U_{33}	U_{12}	U_{13}	U_{23}	U_{eq}
Bi	0.21246(2)	0.45547(2)	0.10824(1)	148(1)	155(1)	182(2)	10(1)	11(1)	7(1)	161.6(7)
Mo1	0.29521(4)	0.47725(3)	0.30002(2)	125(3)	142(3)	117(3)	13(2)	-4(2)	19(2)	128(1)
Mo2	0.30039(4)	0.32035(3)	0.36280(2)	108(3)	104(2)	142(3)	5(2)	-11(2)	2(2)	118(1)
Mo3	0.12695(4)	0.42801(3)	0.34961(2)	98(3)	126(2)	139(3)	-5(2)	-14(2)	-4(2)	121(1)
Mo4	0.40240(4)	0.48627(3)	0.38833(2)	99(3)	112(2)	144(3)	-10(2)	-12(2)	7(2)	119(1)
Mo5	0.23330(4)	0.43666(3)	0.43715(2)	122(3)	109(2)	113(3)	-7(2)	-10(2)	6(2)	115(1)
Mo6	0.23051(4)	0.59402(3)	0.37430(2)	132(3)	102(2)	146(3)	2(2)	-13(2)	0(2)	127(1)
Cl1	0.3362(1)	0.5074(1)	0.20991(7)	225(9)	399(9)	151(9)	50(7)	29(7)	29(7)	258(4)
Cl2	0.3671(1)	0.14576(9)	0.34918(7)	274(9)	129(7)	210(10)	9(6)	22(7)	10(6)	203(3)
Cl3	-0.0604(1)	0.3929(1)	0.32331(7)	128(9)	250(7)	240(10)	-22(6)	-16(7)	-58(7)	208(4)
Cl4	0.5823(1)	0.5234(1)	0.42138(7)	122(8)	264(8)	290(10)	3(6)	-10(7)	-77(7)	224(4)
Cl5	0.1851(1)	0.3999(1)	0.52677(6)	270(10)	202(7)	125(9)	-52(6)	6(7)	17(6)	200(3)
Cl6	0.1743(1)	0.7774(1)	0.37699(8)	230(10)	132(7)	520(10)	25(6)	-84(8)	-11(7)	293(4)
Cl7	0.3318(1)	0.59528(9)	0.45748(6)	197(9)	145(6)	174(9)	-41(6)	-10(7)	-31(6)	172(3)
Cl8	0.0740(1)	0.5405(1)	0.42119(6)	122(8)	177(6)	165(9)	24(6)	2(6)	-2(6)	155(3)
Cl9	0.3932(1)	0.6328(1)	0.32783(7)	185(9)	143(6)	290(10)	-41(6)	33(7)	65(6)	206(4)
Cl10	0.1384(1)	0.28002(9)	0.40904(6)	187(9)	150(7)	220(10)	-49(6)	0(7)	30(6)	185(3)
Cl11	0.3984(1)	0.33709(9)	0.44677(6)	153(9)	158(7)	185(9)	5(6)	-37(7)	40(6)	166(3)
Cl12	0.1302(1)	0.57727(9)	0.29095(6)	176(9)	197(7)	189(9)	42(6)	-54(7)	48(6)	188(3)
Cl13	0.4556(1)	0.3760(1)	0.31609(6)	125(9)	194(7)	210(10)	34(6)	31(7)	19(6)	176(3)
Cl14	0.1965(1)	0.3167(1)	0.28062(6)	200(10)	192(7)	190(10)	9(6)	-26(7)	-47(6)	192(4)

Table 6.4 Selected interatomic distances (in pm) in [BiCl][Mo₆Cl₁₄].

atoms	distances	atoms	distances
Bi–	C11 308.4 (2)	Mo3–	C13 249.2(2)
	C12 290.6(1)		C18 246.5(2)
	C13 277.4(2)		C110 246.4(2)
	C14 287.3(2)		C112 246.5(2)
	C15 283.3(2)		C114 247.7(2)
	C16 275.1(1)		Mo5 259.20(8)
	C115 249.7(2)		Mo6 260.08(7)
Mo1–	C11 242.5(2)	Mo4–	C14 245.7(2)
	C19 247.4(1)		C17 246.7(2)
	C112 247.0(2)		C19 246.6(2)
	C113 244.9(2)		C111 246.1(2)
	C114 248.2(1)		C113 246.2(2)
	Mo2 260.70(7)		Mo5 260.00(8)
	Mo3 260.00(8)		Mo6 260.85(7)
	Mo4 260.41(8)	Mo5–	C15 245.2(2)
	Mo6 259.70(8)		C17 246.5(1)
Mo2–	C12 245.8(1)		C18 245.6(1)
	C110 246.2(2)		C110 246.8(1)
	C111 246.9(2)		C111 246.9(2)
	C113 244.7(2)		Mo6 261.30(7)
	C114 245.7(2)	Mo6–	C16 249.7(1)
	Mo3 262.18(7)		C17 246.2(2)
	Mo4 259.51(6)		C18 245.6(2)
	Mo5 260.54(7)		C19 246.9(2)
			C112 246.9(2)

7. Synthesis and Characterization of $(\text{Sb}_{10}\text{Se}_{10})[\text{AlCl}_4]_2$

7.1. Synthesis of $(\text{Sb}_{10}\text{Se}_{10})[\text{AlCl}_4]_2$

The stoichiometric amounts of Sb, Se and SeCl_4 (total mass = 240 mg) were added to the Lewis acidic IL $[\text{bmim}]\text{Cl}/\text{AlCl}_3$ (molar ratio = 1:2, volume \approx 1.5 mL) which immediately turned into a dark brown solution. The reaction mixture was left for stirring overnight at room temperature then filtered to separate unreacted material. After four days, black block-shaped crystals were obtained. The excess IL was decanted in an argon filled glove box and single crystals were separated. The crystals of the compound were washed twice with dry dichloromethane to remove any traces of IL. Yield: 56 %.

7.2. Results and Discussion

Black air-sensitive block-shaped crystals of decaantimony-decaselenium-bis(tetrachloridoaluminate) $(\text{Sb}_{10}\text{Se}_{10})[\text{AlCl}_4]_2$, were obtained by reacting antimony, selenium, and selenium(IV) chloride in the Lewis acidic IL $[\text{bmim}]\text{Cl}/\text{AlCl}_3$ at room temperature. The use of SeCl_4 in a small amount is important to initiate the reaction at room-temperature by dissolving the elements; otherwise antimony remains mostly undissolved. X-ray diffraction on a single crystal has revealed a centrosymmetric triclinic cell (Table 7.1 and 7.4), which contains the finite heteronuclear polycation $(\text{Sb}_{10}\text{Se}_{10})^{2+}$ together with two tetrahedral $[\text{AlCl}_4]^-$ anions (Figure 7.1). The shape of the finite $(\text{Sb}_{10}\text{Se}_{10})^{2+}$ polycation is unprecedented. It can be regarded as a combination of two $[\text{Sb}_4\text{Se}_4]$ cages, which are connected through three-bonded selenium atoms with a central $[\text{Sb}_2\text{Se}_2]$ ring. The cages resemble realgar-type molecules, such as S_4N_4 , As_4S_4 , As_4Se_4 , or $(\text{Te}_4\text{S}_4)^{2+}$ [45, 174], that are named after the low-temperature modification of arsenic(II) sulfide, $\alpha\text{-As}_4\text{S}_4$ [174b].

The four selenium atoms in the $[\text{Sb}_4\text{Se}_4]$ cage are almost coplanar with ± 1.7 pm deviation from the mean plane through the center of the disphenoid formed by the four antimony atoms. The Sb–Sb distances of 287.54(4) pm and 288.03(3) pm correspond to typical Sb–Sb single-bond length described in literature [282.2(1) to 289.3(4) pm] [175]. The Sb–Se distances vary from 254.59(5) to 268.87(4) pm, which also match well with literature data (257.6 to 277.7 pm) [176]. In the $[\text{Sb}_4\text{Se}_4]$ cage, the Sb–Se–Sb, Se–Sb–Sb, and Se–Sb–Se bond angles have mean values of 103.8° , 99.1° , and 90.8° , which are fairly close to the

corresponding As–S–As, S–As–As, and S–As–S angles found in α -As₄S₄ (101.5°, 97.8°, and 92.8°) [174b]. The bridging four-membered [Sb₂Se₂] ring has Sb–Se bond lengths of 255.81(4) and 262.94(5) pm, while the bond angles are 88.96(2)° and 91.05(2)°.

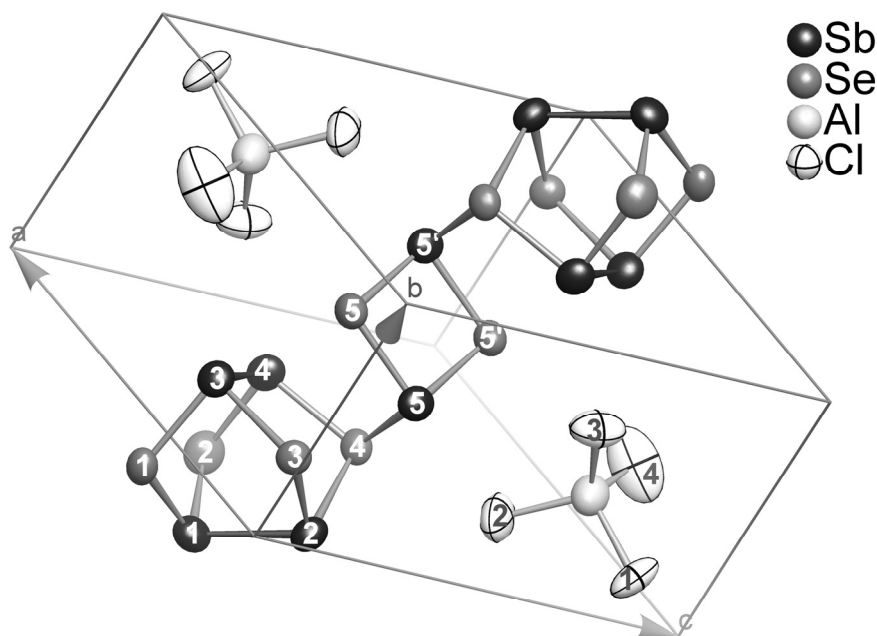


Figure 7.1: Section of the triclinic crystal structure of $(\text{Sb}_{10}\text{Se}_{10})[\text{AlCl}_4]_2$. The ellipsoids represent 90 % probability at 293(2) K. Distances (in pm) are listed in Table 7.2. Angles (in °): Se2–Sb1–Se1 95.99(2), Se2–Sb1–Sb2 100.81(1), Se1–Sb1–Sb2 96.22(1), Se3–Sb2–Se4 88.66(1), Se3–Sb2–Sb1 100.23(1), Se4–Sb2–Sb1 97.12(1), Se1–Sb3–Se3 87.38(1), Se1–Sb3–Sb4 100.99(1), Se3–Sb3–Sb4 97.63(1), Se2–Sb4–Se4 91.07(1), Se2–Sb4–Sb3 100.13(1), Se4–Sb4–Sb3 99.80(1), Se5–Sb5–Se5' 88.96(1), Se5–Sb5–Se4 97.49(1), Se5'–Sb5–Se4 94.61(1), Sb3–Se1–Sb1 104.04(2), Sb4–Se2–Sb1 104.22(2), Sb2–Se3–Sb3 104.28(1), Sb4–Se4–Sb2 102.65(1), Sb4–Se4–Sb5 103.48 (1), Sb2–Se4–Sb5 90.41(1), Sb5–Se5–Sb5' 91.04(1).

The anionic group $[\text{AlCl}_4]^-$ in the title compound has a slightly distorted tetrahedral shape with the Al–Cl distances between 213.2(2) and 222.8(2) pm, and Cl–Al–Cl angles within the 107.1° to 112.9° range.

The shortest Sb⋯Cl interatomic distances are 342.6 pm, and the Se⋯Cl distances start at 346.1 pm. Therefore, these interactions can be considered as non-bonding. To evaluate the degree of interaction between the polycation and the surrounding counter anions, we performed quantum chemical calculations of ground state and geometry optimization for a free $(\text{Sb}_{10}\text{Se}_{10})^{2+}$ polycation (Table 7.2). Bond lengths and angles of the geometry-optimized C_i -symmetrical free $(\text{Sb}_{10}\text{Se}_{10})^{2+}$ show almost no distortion with respect to that observed in

(Sb₁₀Se₁₀)[AlCl₄]₂. The calculations also yield similar bonding energies of -61.7 and -61.3 eV for equilibrium and experimental (single point calculation) molecular shapes. Hence, the polycation and its fragments are almost unstrained by packing or by ionic interactions with the weakly coordinating [AlCl₄]⁻ anions in the crystal structure of (Sb₁₀Se₁₀)[AlCl₄]₂.

The Raman spectrum of a (Sb₁₀Se₁₀)[AlCl₄]₂ crystal showed several bands having reasonable intensity in the characteristic range up to 350 cm⁻¹ (Figure 7.2). Due to the low symmetry of the unit cell, the vibrational spectrum consists of about 80 bands that strongly overlap in the range from 150 to 200 cm⁻¹, which hinders considerably the identification of the bands. Only the band at 345 cm⁻¹ is readily identified as the symmetric stretch mode of [AlCl₄]⁻ anion [177], another weak band at about 160 cm⁻¹ is likely hidden behind the strong bands of the polycation.

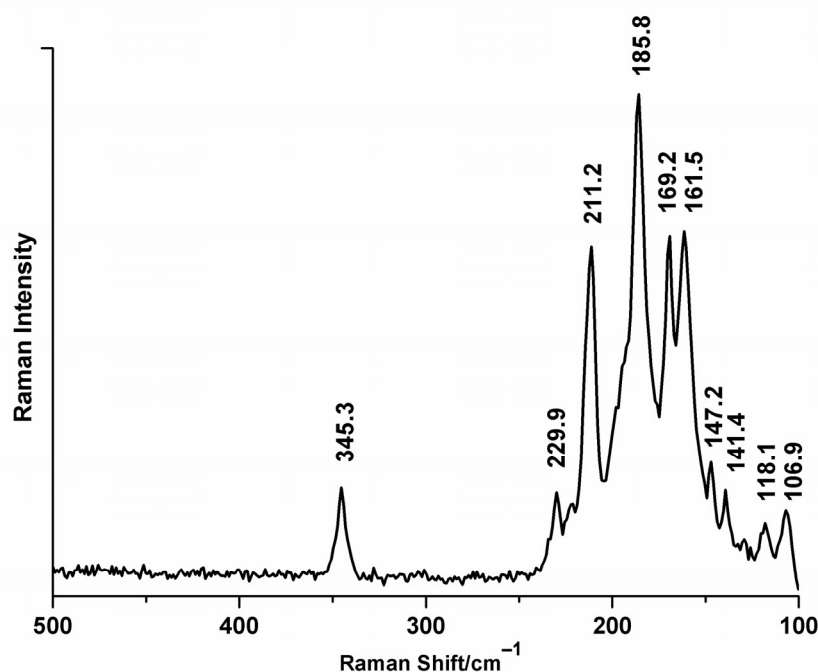


Figure 7.2: Raman spectrum of a single crystal of (Sb₁₀Se₁₀)[AlCl₄]₂.

The extended (8-N)-rule by *Mooser* and *Pearson* [178], which generalizes the ideas of *Zintl* about the bonding in polyanionic compounds, easily rationalizes the connectivity in the polycation. The three-bonded selenium atom, Se⁴⁻, should bear the positive charge, rendering it a pseudo-element of group 15. On the other hand, the electronegativities, which determine the attribution of oxidation states, draw an alternative picture, which is expressed by the extended formula (Sb^{II}₈Sb^{III}₂Se^{-II}₁₀)²⁺. As can be seen from the charge distribution pattern for

$(\text{Sb}_{10}\text{Se}_{10})^{2+}$ in the solid as well as in free space (Table 7.3), quantum theory of atoms in molecules (QTAIM) [154] proposed by *Bader* follows this consideration and attributes negative charges to all selenium atoms, although their values are much lower than is expected for significant ionic interaction. At first glance, a contradictory situation arises for the three-bonded selenium atom, especially as the first ionization potentials of the atoms are not in favor of oxidation of selenium [179]. Empirically, in heteropolyocations of the main group elements, e.g. in $(\text{Bi}_4\text{Se}_4)^{4+}$, $(\text{As}_3\text{S}_5)^+$, or ${}^1[\text{Sb}_2\text{Te}_2]^+$, it is always the electron-rich partner that is oxidized. This results in a structural trend towards the equalization of the connectivity of the atoms.

Since the charge population analysis in the framework of the Bader scheme does not distinguish the three-bonded Se4 from the other selenium atoms, the ELI-D (electron localizability indicator, γ_D), which allows real space interpretation of chemical bonding, was further employed [152]. The ELI-D basin populations and ELIBON values for $(\text{Sb}_{10}\text{Se}_{10})[\text{AlCl}_4]_2$ are summarized in Tables 7.2 and 7.3. A detailed description of different ELI-D basins and bond polarity indices is given in Table 7.8. Within the $(\text{Sb}_{10}\text{Se}_{10})^{2+}$ polycation, covalent bonding is dominant (Figure 7.3).

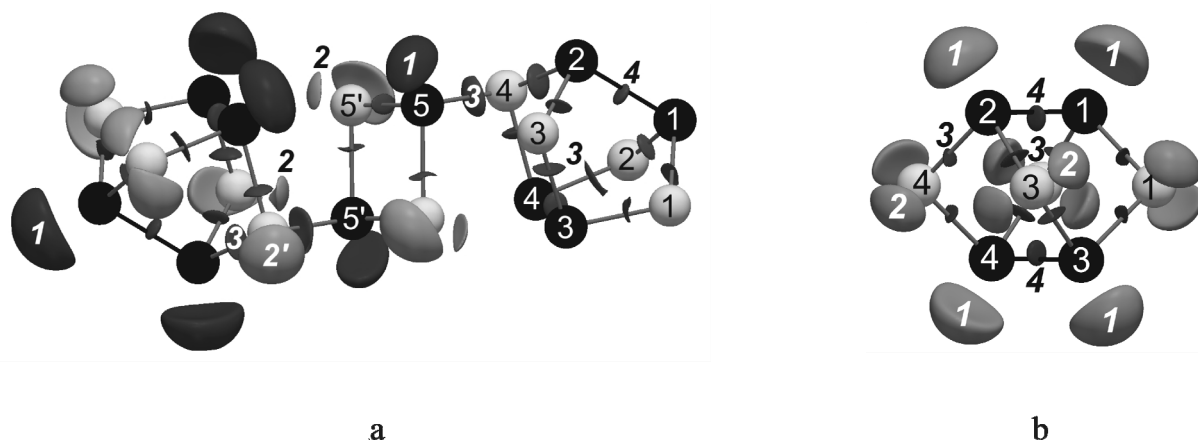


Figure 7.3: (a) Localization domains (*I–4*) calculated for the $(\text{Sb}_{10}\text{Se}_{10})^{2+}$ polycation within the crystal structure of $(\text{Sb}_{10}\text{Se}_{10})[\text{AlCl}_4]_2$. Black atoms depict antimony, light gray depict selenium. *I*: lone pair of antimony (not depicted for the right $[\text{Sb}_4\text{Se}_4]$ realgar-cage in order to enhance readability; $\gamma = 1.455$); *2*: lone pairs of two-bonded selenium ($\gamma = 1.49$); *2'*: lone pair of three-bonded Se4 ($\gamma = 1.455$); *3*: Sb–Se bond ($\gamma \approx 1.31–1.33$); *4*: Sb–Sb bond ($\gamma = 1.315$), (b) ELI-D localization domains for equilibrium geometry of a hypothetical $[\text{Sb}_4\text{Se}_4]$ realgar-type molecule. Black atoms depict antimony, light gray depict selenium (atomic labels corresponds to the ones with atomic coordinates given in Table 7.7). *I*: lone pair of antimony ($\gamma = 1.52$); *2*: lone pair of selenium ($\gamma = 1.52$); *3*: Sb–Se bond ($\gamma = 1.315$); *4*: Sb–Sb bond ($\gamma = 1.315$).

Antimony atoms that are involved in Sb_2 dumbbells share common surfaces with the disynaptic basins [156b], which contain nearly two electrons. In addition, each antimony atom has an electron lone pair that sticks out of the cage, but shows no evidence of interaction with chloride ions. The antimony atoms in the cages are also engaged in covalent bonding with selenium atoms, forming two covalent bonds (ca. 1 to 1.4 electrons in the disynaptic basins). The bond polarity index of these interactions is relatively low, $p(\text{Sb}-\text{Se}) \approx 0.1-0.3$, indicating slightly polar Sb–Se covalent interactions with detectable shift of electron density towards the more electronegative selenium atom. The bonds that involve Se4 show dramatic contrast in their polarity: The calculated ionic fraction of Se4–Sb4 and Se4–Sb2 is about 60 %, while Se4–Sb5 is less polar ($p = 0.26$). The Se5 atom is electronically similar to the selenium atoms of the cage. Within the central $[\text{Sb}_2\text{Se}_2]$ ring, the Sb5–Se5 bonding is nearly non-polar, which is evidenced by a bond polarity index of 0.11.

Neither pure covalent nor ionic treatment is able to explicitly describe the bonding in $(\text{Sb}_{10}\text{Se}_{10})[\text{AlCl}_4]_2$. On equal distribution of the basin population, i.e. in the non-polar approximation, a positive charge is assigned to Se4 (Table 7.3), which supports the application of the Zintl concept to the $(\text{Sb}_{10}\text{Se}_{10})^{2+}$ polycation. Strong electrostatic contribution in bonding may be associated with polarization of the $[\text{Sb}_4\text{Se}_4]$ cage (Table 7.7 for polarity indices in the neutral cage) upon interaction with oxidized Se4 atom that partakes in three covalent bonds.

According to the calculation, the whole polycation bears a total charge of about +2.1 electrons. The unusually low average charge of +0.1 per atom stimulates ideas about a hypothetical uncharged mother compound, which could possibly be accessed under mild conditions. Yet the ratio Sb:Se = 1:1 of the polycation has no correspondence in the binary system. The only known antimony selenide, Sb_2Se_3 , shows a tendency towards higher connectivity (Figure 7.4) [180]. The antimony atoms tend towards square pyramidal coordination, while some of the selenium atoms in Sb_2Se_3 are connected to three antimony atoms, although there is no charge to be allocated. In order to compare bonding scenarios in the title compound and Sb_2Se_3 , we also performed a numerical analysis of ELI-D topology for the latter, using the same computational approach and parameters that were applied to $(\text{Sb}_{10}\text{Se}_{10})[\text{AlCl}_4]_2$. In addition to the above considered polar 2c2e covalent bonding, Sb_2Se_3 also exhibits multicenter antimony–selenium bonding that drastically differs from the above discussed interactions. Although a realgar modification is not known for the binary system,

the geometry optimization accomplished of a hypothetical realgar-type molecule $[\text{Sb}_4\text{Se}_4]$ predicts a stable D_{2d} -symmetrical cage (no imaginary frequencies, bonding energy -30.5 eV) with Sb–Se distances of 257.6 pm, Sb–Sb bond lengths of 300.7 pm, and Sb–Se–Sb, Se–Sb–Sb, and Se–Sb–Se bond angles of 101.3° , 99.0° , and 95.5° , respectively. Data on QTAIM charges, ELI-D basin population analysis and ELIBON of the neutral isolated $[\text{Sb}_4\text{Se}_4]$ cage (Figure 7.3b) are given in the Table 7.7.

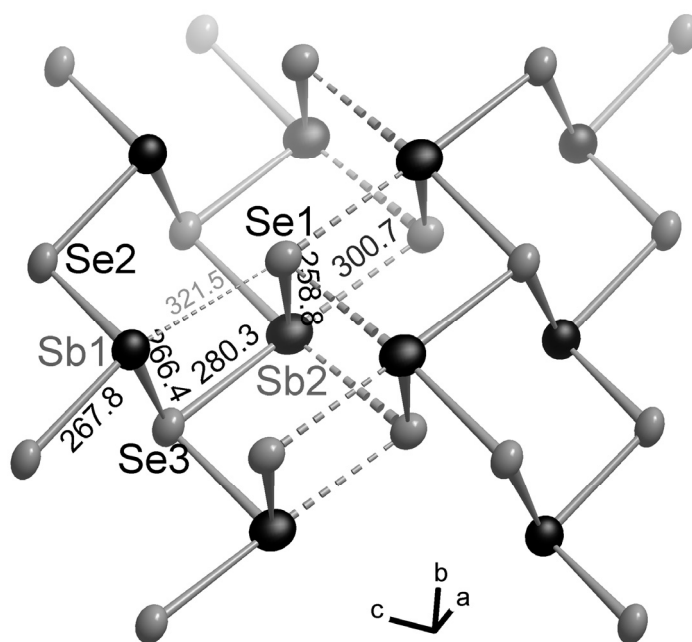


Figure 7.4: Section of the crystal structure of Sb_2Se_3 . Interatomic distances in pm.

The calculated band structure of $(\text{Sb}_{10}\text{Se}_{10})[\text{AlCl}_4]_2$ (Figure 7.5a) corresponds to an indirect semiconductor with a band gap width of about 1.3 eV. Although the band gap is a bit underestimated within LDA, it should be an acceptable approximation since the crystals are black in color. Measurements of the band gap are challengeable due to high air-sensibility of the compound. Small band dispersions reflect very weak intermolecular interactions in the structure. The density of states plot (Figure 7.5b) shows predominant contribution of Sb-5*p*, Se-4*p*, and Cl-3*p* states directly below the Fermi level.

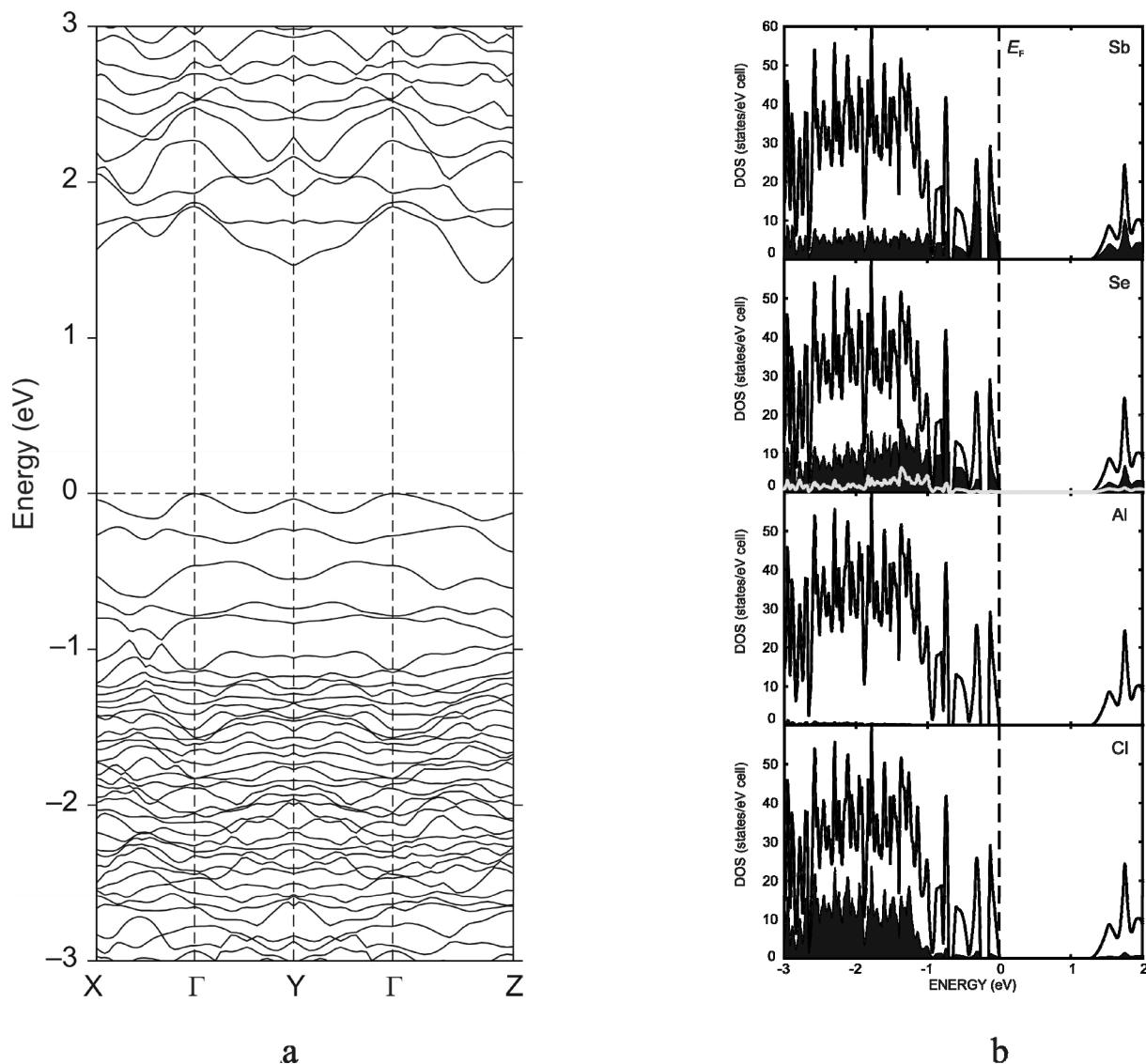


Figure 7.5: (a) Band structure of $(\text{Sb}_{10}\text{Se}_{10})[\text{AlCl}_4]_2$ along the main crystallographic directions (b) Total and partial density of states calculated for $(\text{Sb}_{10}\text{Se}_{10})[\text{AlCl}_4]_2$. The Se5 contribution is outlined by light grey curve.

The contribution of aluminum is negligible, which is in accordance with its positive charge. In view of the small band dispersion, the MO diagram (Figure 7.6) becomes more informative than the DOS. It clearly shows that the HOMO is Sb–Sb bonding, while the LUMO is Sb–Se antibonding. The energy gap for the isolated $(\text{Sb}_{10}\text{Se}_{10})^{2+}$ polycation is 1.89 eV wide.

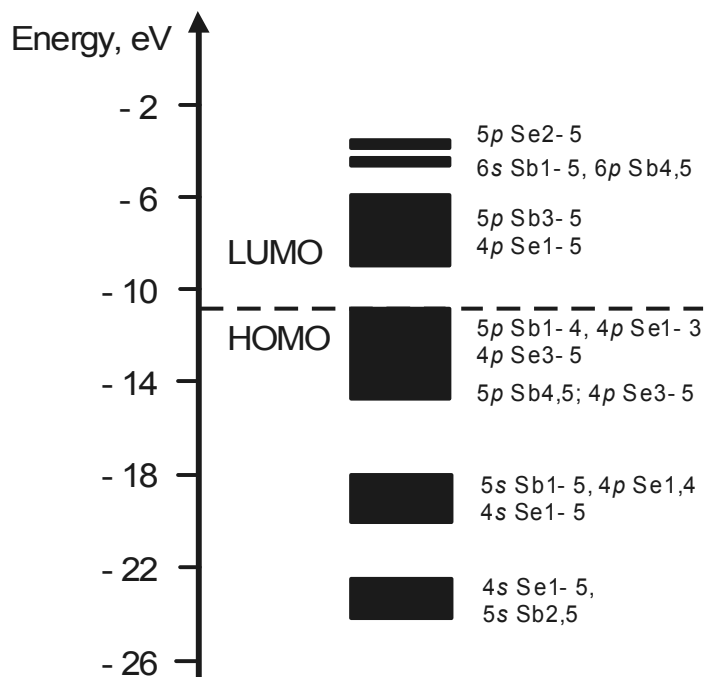


Figure 7.6: MO diagram calculated for the free $(\text{Sb}_{10}\text{Se}_{10})^{2+}$ polycation.

Table 7.1 Coordinates and equivalent isotropic displacement parameters for the atoms in $(\text{Sb}_{10}\text{Se}_{10})[\text{AlCl}_4]_2$. All atoms reside on Wyckoff positions $2i$. U_{eq} (in pm^2) is defined as one third of the trace of the orthogonalized tensor U_{ij} . For tensor coefficients see Table S1 of the Supporting Information.

atom	x	y	z	U_{eq}
Sb1	0.21766(3)	-0.23399(3)	0.06066(3)	314.0(6)
Sb2	0.09425(3)	-0.02625(3)	0.19246(2)	277.3(5)
Sb3	0.42215(3)	0.18764(3)	0.08436(2)	286.0(5)
Sb4	0.57711(3)	0.11972(3)	0.31579(2)	298.1(5)
Sb5	0.29640(3)	0.37791(3)	0.41566(3)	284.1(5)
Se1	0.27776(4)	-0.07734(4)	-0.07802(3)	279.6(7)
Se2	0.49927(5)	-0.16453(5)	0.22704(4)	330.6(8)
Se3	0.15385(4)	0.19512(4)	0.11085(3)	244.9(6)
Se4	0.35867(4)	0.11066(4)	0.40682(3)	240.9(6)
Se5	0.50410(5)	0.48684(4)	0.34323(4)	315.9(8)
Al1	0.0757(2)	0.3785(1)	0.6998(1)	330(2)
Cl1	-0.1711(1)	0.3247(1)	0.6812(1)	362(2)
Cl2	0.0947(2)	0.1980(1)	0.5569(1)	452(3)
Cl3	0.1248(1)	0.5893(1)	0.6697(1)	458(2)
Cl4	0.2335(2)	0.3946(2)	0.8915(1)	674(4)

Table 7.2 Bonding characteristics for the $(\text{Sb}_{10}\text{Se}_{10})^{2+}$ polycation in the solid and for the geometry-optimized free polycation. For atomic coordinates of the optimized molecule, refer to Table 7.6.

Bond	$(\text{Sb}_{10}\text{Se}_{10})^{2+}$, solid		$(\text{Sb}_{10}\text{Se}_{10})^{2+}$, free cation	
	Experi- mental bond length, pm	ELI-D basin population, electrons	Calculated bond length, pm	ELI-D basin population, electrons
Se1–Sb3	257.81(4)	1.05	256.0	1.11
Se1–Sb1	258.50(5)	0.87	257.1	1.16
Se2–Sb1	255.32(5)	0.99	259.4	1.20
Se2–Sb4	254.59(5)	0.77	255.4	1.05
Se3–Sb2	257.57(4)	1.01	258.7	1.38
Se3–Sb3	267.69(4)	0.73	264.2	1.36
Se4–Sb2	268.87(4)	1.42	267.3	1.58
Se4–Sb5	271.05(4)	1.42	274.9	1.67
Se4–Sb4	263.24(4)	1.48	269.4	1.62
Se5–Sb5	255.81(4)	0.93	256.3	0.97
Se5'–Sb5	262.94(5)	1.01	273.5	1.28
Sb1–Sb2	288.03(3)	2.10	300.4	1.92
Sb3–Sb4	287.54(4)	2.22	297.6	2.02

Table 7.3 Atomic charges calculated for $(\text{Sb}_{10}\text{Se}_{10})[\text{AlCl}_4]_2$ and the free $(\text{Sb}_{10}\text{Se}_{10})^{2+}$ polycation by integration of electron density in QTAIM basins or ELI-D basins (partitioning is based on covalent bonding concept for Sb–Se fragment, based on ionic treatment for $[\text{AlCl}_4]^-$).

Atom	$(\text{Sb}_{10}\text{Se}_{10})[\text{AlCl}_4]_2$		$(\text{Sb}_{10}\text{Se}_{10})^{2+}$, free cation	
	QTAIM	ELIBON	QTAIM	ELIBON
Sb1	+0.73	+0.71	+0.68	+0.49
Sb2	+0.79	+0.41	+0.61	+0.22
Sb3	+0.81	+0.71	+0.63	+0.40
Sb4	+0.56	+0.39	+0.59	+0.31
Sb5	+0.77	+0.83	+0.77	+0.43
Se1	–0.64	–0.58	–0.42	–0.48
Se2	–0.41	–0.65	–0.42	–0.46
Se3	–0.69	–0.51	–0.47	–0.13
Se4	–0.43	+0.58	–0.44	+0.75
Se5'	–0.54	–0.73	–0.60	–0.68
Al	+1.95	+2.91		
Cl1	–0.70	–0.87		
Cl2	–0.61	–0.92		
Cl3	–0.76	–1.15		
Cl4	–0.67	–0.99		

Table 7.4 Crystallographic data and details of the structure determination for $(\text{Sb}_{10}\text{Se}_{10})[\text{AlCl}_4]_2$.

Sum formula	$\text{Sb}_{10}\text{Se}_{10}\text{Al}_2\text{Cl}_8$
Crystal system	triclinic
Space group	$P\bar{1}$
Temperature (K)	293(2)
a, b, c (pm)	947.85(2), 957.79(2), 1166.31(3)
α, β, γ (°)	103.622(1), 110.318(1), 99.868(1)
V (10^6 pm^3)	927.04(4)
Formula units per cell	1
Calculated density ($\text{g}\cdot\text{cm}^{-3}$)	4.20
Measurement device	CCD Kappa (Bruker)
Radiation	graphite-monochromated Mo- $K\alpha$ radiation ($\lambda = 71.073 \text{ pm}$)
Measurement range	$-16 \leq h \leq 16, -16 \leq k \leq 16, -20 \leq l \leq 19$
μ (Mo- $K\alpha$) (mm^{-1})	17.6
Measured reflections	34030
Unique reflections ($F_o > 4\sigma(F_o)$)	9426, 7467
$R(\text{int}), R(\sigma)$	0.031, 0.030
$R_I [F_o > 4\sigma(F_o)]$	0.035
R_I (all F_o)	0.049
wR_2 (all F_o^2)	0.082
No. of parameters	136
Goodness of fit	1.33
$\Delta\rho$ (max, min) ($\text{e}\cdot 10^{-6} \text{ pm}^{-3}$)	+3.22, -1.39

Table 7.5 Coefficients (in pm^2) of the displacement tensor U_{ij} for the atoms in $(\text{Sb}_{10}\text{Se}_{10})[\text{AlCl}_4]_2$.

atom	U_{11}	U_{22}	U_{33}	U_{12}	U_{13}	U_{23}
Sb1	333(1)	235(1)	342(1)	59.1(8)	138(1)	47.8(9)
Sb2	251(1)	304(1)	322(1)	78.4(8)	150.6(9)	125.2(9)
Sb3	319(1)	292(1)	272(1)	66.4(8)	139.7(9)	117.1(8)
Sb4	216.0(9)	376(1)	261(1)	60.6(8)	69.8(8)	86.4(9)
Sb5	260(1)	255(1)	347(1)	83.0(8)	144.7(9)	70.1(8)
Se1	250(1)	348(2)	215(1)	77(1)	99(1)	41(1)
Se2	335(2)	353(2)	372(2)	179(2)	150(2)	165(2)
Se3	219(1)	271(2)	237(2)	74(1)	74(1)	89(1)
Se4	278(1)	255(1)	197(1)	78(1)	101(1)	74(1)
Se5	368(2)	280(2)	274(2)	18(1)	173(1)	28(1)
Al	379(6)	302(5)	372(6)	127(5)	196(5)	128(5)
Cl1	302(4)	433(5)	548(6)	139(3)	284(4)	306(4)
Cl2	619(7)	317(4)	554(6)	166(4)	418(6)	73(4)
Cl3	436(5)	297(4)	605(7)	17(4)	189(5)	174(4)
Cl4	944(11)	645(8)	396(6)	486(8)	76(7)	208(6)

Table 7.6 Atomic coordinates (in Å) for equilibrium geometries of the free $(\text{Sb}_{10}\text{Se}_{10})^{2+}$ polycation and a hypothetical Sb_4Se_4 molecule.

$(\text{Sb}_{10}\text{Se}_{10})^{2+}$ polycation				Sb_4Se_4			
Sb1	0.377431	-5.552579	-4.699029	Sb1	1.063100	1.063100	-1.683767
Sb2	-1.720907	-3.955118	-3.260103	Sb2	-1.063100	-1.063100	-1.683767
Se1	1.257973	-3.654796	-6.192555	Se1	0.0	2.696761	0.0
Se2	2.170681	-5.442507	-2.827377	Se2	2.696761	0.0	0.0
Se3	-1.246054	-1.579325	-4.166122	Se3	-2.696761	0.0	0.0
Se4	-0.291529	-3.402704	-1.069472	Se4	0.0	-2.696761	0.0
Sb3	1.354883	-1.632633	-4.626190	Sb3	-1.063100	1.063100	1.683767
Sb4	2.161910	-2.993142	-2.105292	Sb4	1.063100	-1.063100	1.683767
Sb5	-1.311801	-0.849849	-1.054394				
Se5	0.833088	0.439503	-1.606705				
Se5'	-0.833088	-0.439503	1.606705				
Sb5'	1.311801	0.849849	1.054394				
Sb4'	-2.161910	2.993142	2.105292				
Sb3'	-1.354883	1.632633	4.626190				
Se4'	0.291529	3.402704	1.069472				
Se3'	1.246054	1.579325	4.166122				
Se2'	-2.170681	5.442507	2.827377				
Se1'	-1.257973	3.654796	6.192555				
Sb2'	1.720907	3.955118	3.260103				
Sb1'	-0.377431	5.552579	4.699029				

Table 7.7 Numerical analysis of ELI-D topology for a hypothetical $[\text{Sb}_4\text{Se}_4]$ molecule. Upon integration of ELI-D data, bond basin populations have been equally distributed between the atoms according to low values of bond polarity index. QTAIM basin populations: Sb +0.55 and Se -0.51. ELIBON: Sb +0.49 and Se -0.45.

Attribution of ELI-D feature	Basin population q/e^-	Bond polarity index, p
Sb core	45.86	
Sb lone pair (LP)	2.54	
Se core	27.78	
Se LP1	2.76	
Se LP2	2.75	
Se-Sb disynaptic basin	1.16	0.0044
Sb-Sb disynaptic basin	1.90	0.0015

Table 7.8 Numerical analysis of ELI-D topology for $(\text{Sb}_{10}\text{Se}_{10})[\text{AlCl}_4]_2$.

Attribution of ELI-D feature	Basin population q/e^-	Bond polarity index, p Percentage of prevailing contribution
Sb1 core	45.79	
Sb1 lone pair (LP)	2.52	
Sb2 core	45.76	
Sb2 lone pair (LP)	2.57	
Sb3 core	45.80	
Sb3 lone pair (LP)	2.49	
Sb4 core	45.82	
Sb4 lone pair (LP)	2.55	
Sb5 core	45.82	
Sb5 lone pair (LP)	2.67	
Sb1–Sb2 disynaptic basin	2.09	0.09, 54% Sb2
Sb3–Sb4 disynaptic basin	2.22	0.06, 53% Sb4
Se1 core	27.81	
Se1 LP1	2.99	
Se1 LP2	2.82	
Se1–Sb3 disynaptic basin	1.05	0.07, 54% Se1
Se1–Sb1 disynaptic basin	0.87	0.29, 65% Se1
Se2 core	27.81	
Se2 LP1	3.00	
Se2 LP2	2.96	
Se2–Sb1 disynaptic basin	0.99	0.13, 57% Sb1
Se2–Sb4 disynaptic basin	0.77	0.04, 52% Sb4
Se3 core	27.78	
Se3 LP1	3.06	
Se3 LP2	2.80	
Se3–Sb2 disynaptic basin	1.01	0.30, 65% Se3
Se3–Sb3 disynaptic basin	0.73	0.15, 58% Se3
Se4 core	27.84	
Se4 LP	3.42	
Se4–Sb2 disynaptic basin	1.42	0.56, 78% Se4
Se4–Sb5 disynaptic basin	1.42	0.26, 63% Se4
Se4–Sb4 disynaptic basin	1.48	0.56, 78% Se4
Se5 core	27.79	
Se5 LP1	2.64	
Se5 LP2	3.33	
Se5–Sb5 disynaptic basin	0.93	0.11, 56% Sb5
Se5'–Sb5 disynaptic basin	1.01	0.11, 56% Sb5
Al core	10.09	
Cl1 core	10.08	
Cl1 valence shell	7.08	
Al–Cl1 disynaptic basin	0.71	0.57, 78% Cl1
Cl2 core	10.08	
Cl2 valence shell	7.04	
Al–Cl2 disynaptic basin	0.80	0.34, 67% Cl2
Cl3 core	10.11	
Cl3 valence shell	7.32	
Al–Cl3 disynaptic basin	0.72	0.57, 78% Cl3
Cl4 core	10.08	
Cl4 valence shell	7.13	
Al–Cl4 disynaptic basin	0.78	0.33, 66% Cl4

8. Synthesis and Characterization of $\text{Te}_4[\text{Bi}_{0.74}\text{Cl}_4]$

8.1. Synthesis of $\text{Te}_4[\text{Bi}_{0.74}\text{Cl}_4]$

Stoichiometric amounts of Te, TeCl_4 and BiCl_3 (total mass = 250 mg) were added to the Lewis acidic IL $[\text{bmim}]\text{Cl}/\text{AlCl}_3$ (molar ratio = 1:2, volume \approx 1.5 mL), which immediately turned into a dark violet solution. The reaction mixture was left for stirring overnight at room temperature then filtered to separate unreacted material. After two days, air sensitive golden lustrous needles were obtained. Yield: 58 %.

8.2. Results and Discussion

The formation of $\text{Te}_4[\text{Bi}_{0.74}\text{Cl}_4]$ in RTIL can be interpreted as a synproportionation of elemental tellurium and tellurium(IV) to a low-valent intermediate facilitated by the Lewis acid BiCl_3 , which accepts chloride ions from TeCl_4 . According to the weak intensity satellite reflections in the diffraction pattern of single crystals, the crystal structure of $\text{Te}_4[\text{Bi}_{0.74}\text{Cl}_4]$ can be regarded as incommensurately modulated (Figure 8.1). The complete diffraction image can then be indexed based on a primitive tetragonal unit cell with super space group $P4/n(\frac{1}{2}\frac{1}{2}\gamma)q0$, $a = 1206.5(2)$ pm, $c = 352.4(1)$ pm and, modulation wave vector $q = (\frac{1}{2}\frac{1}{2}\gamma)$ with $\gamma = 0.272(1)$ (Tables 8.1 to 8.4). This unit cell setting and modulation wave vector have been chosen for the structure refinement, *vide infra*. Alternatively, the diffraction image can be attributed to a composite of two interpenetrating lattice-periodic substructures that have the same tetragonal basis but are mutually incommensurate along their c axes. The incommensurate composite approach was chosen to develop a structure model of the closely related compound $\text{Te}_4[\text{Bi}_{0.67}\text{Cl}_4]$ [86].

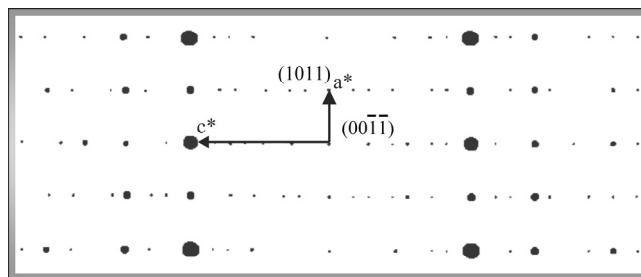


Figure 8.1: Simulated diffraction pattern of the $h0l$ layer of $\text{Te}_4[\text{Bi}_{0.74}\text{Cl}_4]$. Diameter of the spots is scaled with the root of the reflection intensity. The lengths of the vectors a^* and c^* are drawn with respect to the basic cell.

$\text{Te}_4[\text{Bi}_{0.67}\text{Cl}_4]$ was prepared through CVT by reacting Te, TeCl_4 , and BiCl_3 in a glass ampoule, using a temperature gradient (403 to 468 K). $\text{Te}_4[\text{Bi}_{0.67}\text{Cl}_4]$ was best described as a composite of two tetragonal lattices with a common square basis ($a = 1700.9$ pm) but different periodicity along c . One of them describes the Te and Cl part in the superspace group $I4(00\gamma)q$ with modulation vector = $0\ 0\ 0.445(1)$ and $c = 700.7$ pm. The second lattice with $c = 484.9$ pm applies to the Bi part (superspace group $I4_1(00\gamma)q$ with modulation vector = $0\ 0\ 0.307958(1)$).

In the modulated structure of $\text{Te}_4[\text{Bi}_{0.74}\text{Cl}_4]$, the Bi and Cl atoms chemically form a complex sequence of chloridobismuthate(III) anions with average composition $[\text{Bi}_{0.74}\text{Cl}_4]^{1.78-}$, while the Te atoms constitute square polycations, which are stacked eclipsically parallel to the c -axis (Figure 8.2). In the projection along the c direction, a checkerboard pattern of both structural motives results. In the course of the occupancy modulation of Bi, the positions of the Cl atoms vary markedly, which leads to a strong modulation of the Bi–Cl distances (Table 8.3, Figures 8.3, 8.5). Along $[001]$ isolated $[\text{BiCl}_6]^{3-}$ and $[\text{Bi}_2\text{Cl}_{10}]^{4-}$ groups form an aperiodic sequence. The Cl atoms at the edges of neighbouring groups define empty tetrahedra, resembling the situation in $[\text{Bi}_3\text{Ni}]_2[\text{Bi}_{1-8}\text{Br}_{4(-2\delta)}]\text{Br}$ [70j] and $[\text{PdBi}_6][(\text{Bi},\text{Sn})_{1-8}\text{Br}_{4-8}]\text{Br}$ [70g]. The Bi–Cl distances show great variation ranging from 253 to 295 pm.

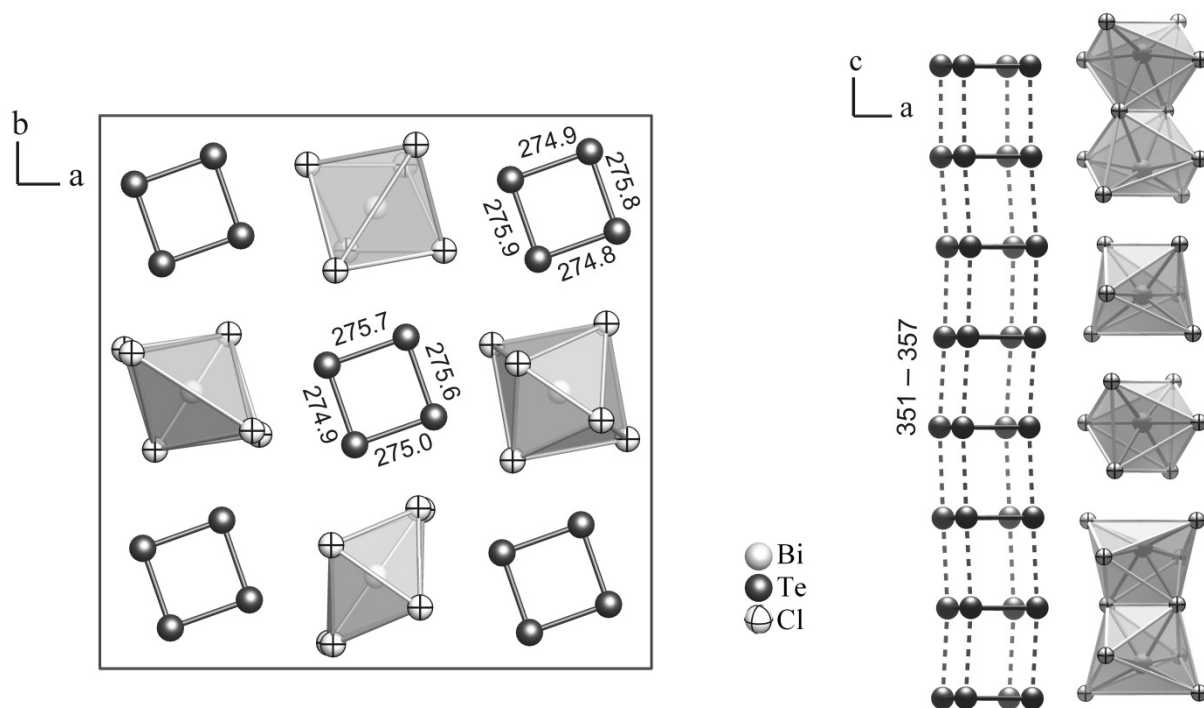


Figure 8.2: The incommensurate modulated structure of $\text{Te}_4[\text{Bi}_{0.74}\text{Cl}_4]$, Left: Projection along the c axis. Right: Sequence of chlorido-bismuthate anions and stack of tellurium polycations running parallel to the c direction. Distances in pm.

The tellurium part of the structure is much more intriguing. Square planar Te_4^{2+} polycations are well known and the typical bond lengths from 265 to 270 pm have been reported [14b, 19]. Because of the modulation, in $\text{Te}_4[\text{Bi}_{0.74}\text{Cl}_4]$ each Te_4 -ring deviates individually from $4/mmm$ symmetry. Still the bond lengths vary only in the narrow range from 274.8(3) to 275.9(3) pm with an average of 275.3(4) pm (Table 8.3, Figures 8.4, 8.5). Hence, besides the irregular distortion also a small overall lengthening of interatomic distances can be stated.

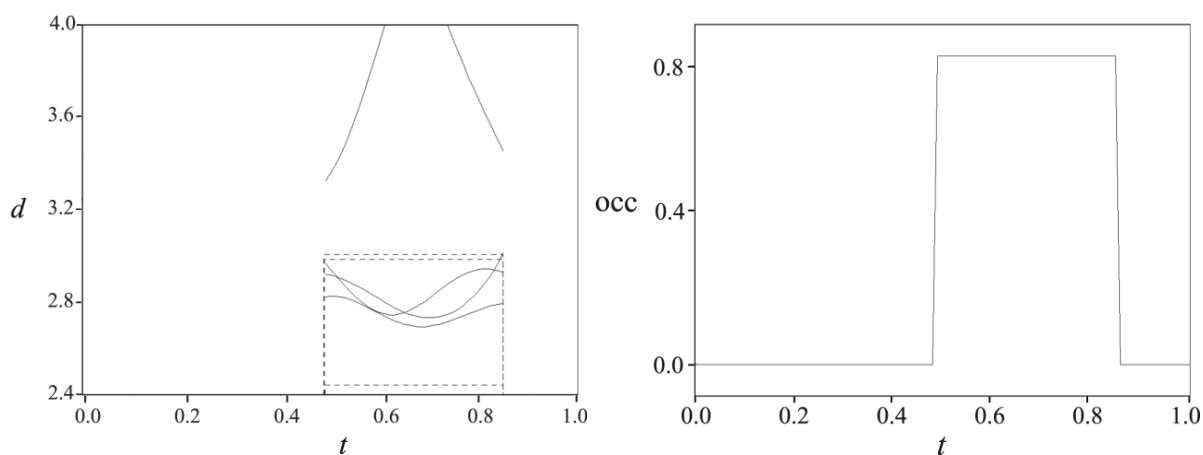


Figure 8.3: Left: t plot of the Bi–Cl distances in the modulated structure of $\text{Te}_4[\text{Bi}_{0.74}\text{Cl}_4]$, Right: t plot of the occupancy modulation for Bi along c .

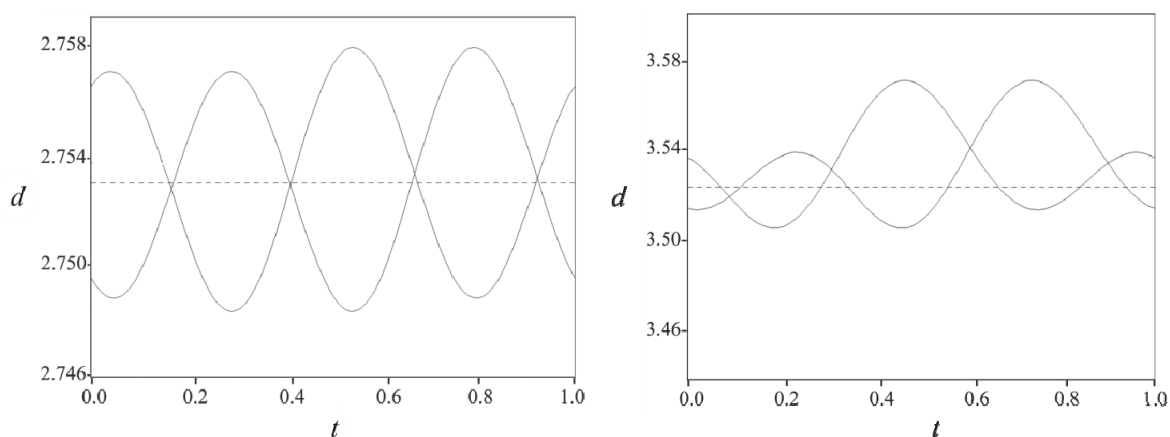


Figure 8.4: t plots of the Te–Te distances in the modulated structure of $\text{Te}_4[\text{Bi}_{0.74}\text{Cl}_4]$.

Disregarding electrostatic repulsion, the tellurium polycations are stacked ecliptically, a structural peculiarity, which can only be rationalized by assuming covalent bonding between rings that exceeds π -stacking interactions known from mainly uncharged aromatic systems. In fact the distance between adjacent rings in the stack range from 351 to 357 pm (average 352.4(1) pm), which is clearly within the sum of the van der Waals radii of 412 pm [181].

The bonding in the Te_4^{2+} polycation has been described by four $2c2e$ σ -bonds, using the $5p_x$ and $5p_y$ atomic orbitals, and an aromatic π -binding system, created by the $5p_z$ orbitals [182]. In accordance with the Hückel scheme, the bonding $5p_z$ and the two degenerate $5p_z$ nonbonding molecular orbitals (MO) are filled with six electrons, while the nonbonding MO remains unoccupied (Figure 8.6). In total, a bond order of $1\frac{1}{4}$ results per Te–Te interaction. The calculated ELI-D basin population equals to 1.44 electrons per each bond.

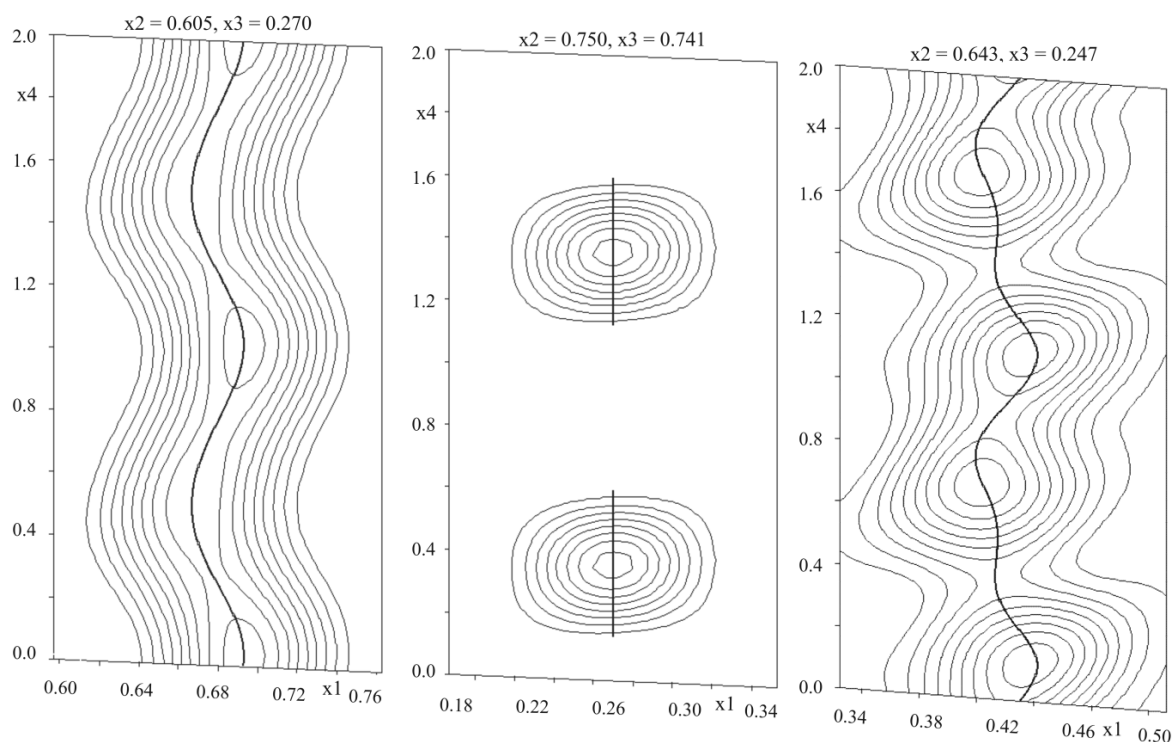


Figure 8.5: Fourier maps for $\text{Te}_4[\text{Bi}_{0.74}\text{Cl}_4]$; Left: Calculated atom modulation functions for Te, Centre: Bi, and Right: Cl.

In $\text{Te}_4[\text{Bi}_{0.74}\text{Cl}_4]$, the Te_4^{2+} polycations are partially reduced (average charge +1.78). In a hypothetical square $\text{Te}_4^{1.8+}$ polycation, the additional electron would populate the antibonding π_z^* MO (Figure 8.7). However, calculations show that upon reduction to Te_4^+ the equilibrium geometry of the ring should change dramatically (Figure 8.6): The square (Te–Te 274 pm) transforms into a rectangle with an elongated bond along x (292 pm) and a shortened bond along y (264 pm). Thereby, the two σ_x^* antibonding states ($5p_x$ and $5p_y$), which belong to the long edges, are lowered in energy and compete with the π_z^* state ($5p_z$). By transferring the electron from the π_z^* to the σ_x^* MO, which is the new highest occupied molecular orbital (HOMO), the σ -bonds along x are weakened by approximately $\frac{1}{4}$ in average (calculated ELI-D basin population equals to 0.26 electrons per bond). Simultaneously, the degeneracy of the formerly nonbonding π_z MO is removed, which stabilizes the π -bonding along the shortened

edge y . As a result, the bonding ELI-D basin of the short dumbbells contains 1.57 electrons, indicating that fractional π -bonding persists. However, in $\text{Te}_4[\text{Bi}_{0.74}\text{Cl}_4]$ such a dramatic distortion is not observed.

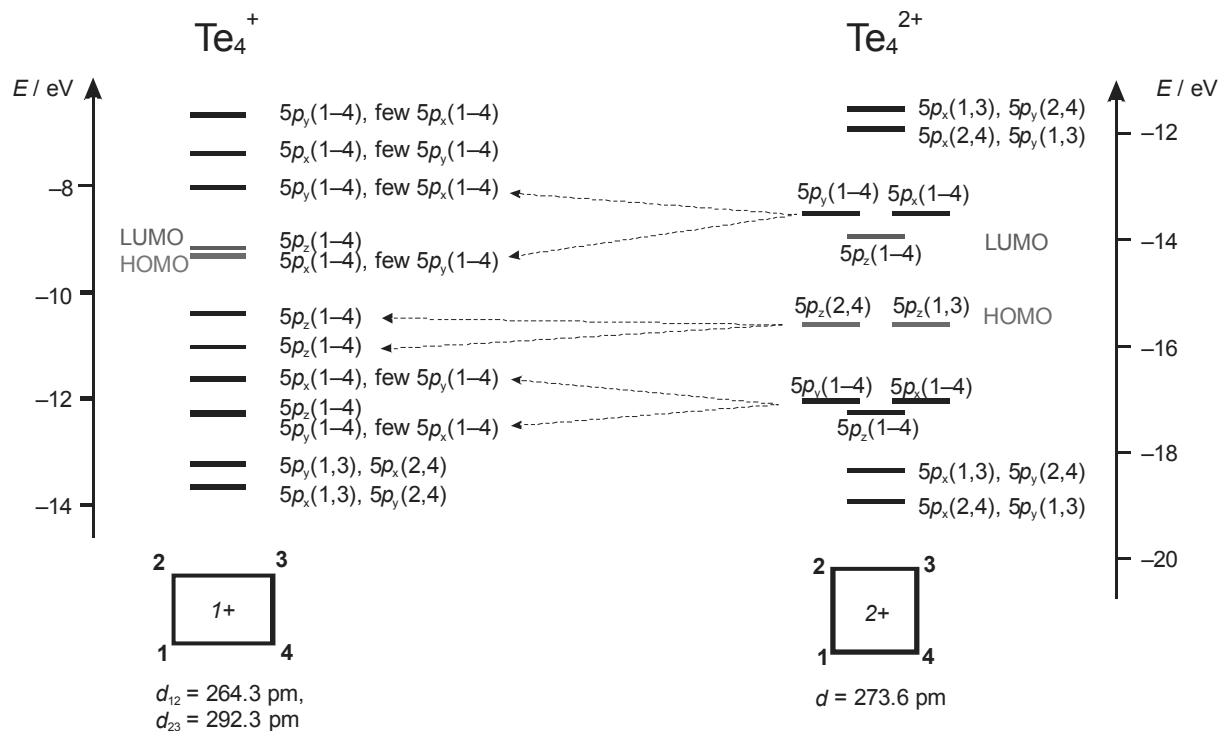


Figure 8.6: The molecular orbital diagram for geometrically optimized Te_4^+ and Te_4^{2+} .

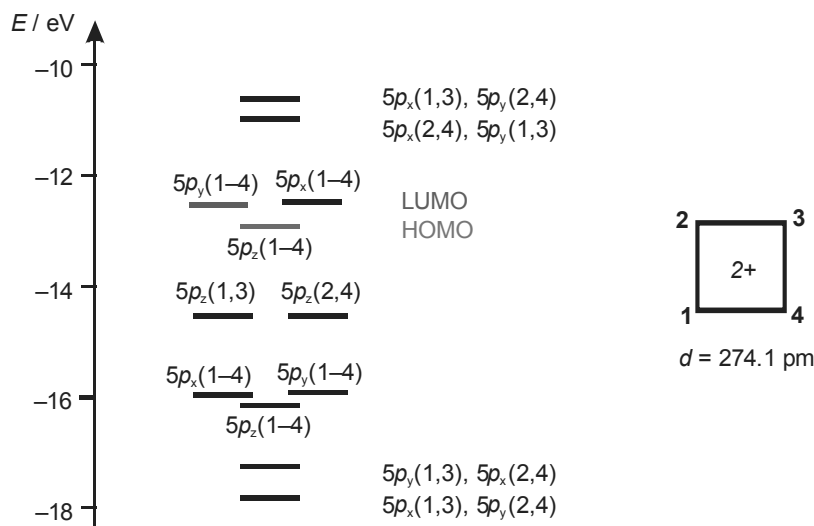


Figure 8.7: The molecular orbital diagram for geometrically optimized $\text{Te}_4^{+1.8}$.

In the periodic stack, the four MO of the π -system form bands in the c^* direction. Within the approximation of regular squares, reduction to $[\text{Te}_4]^{1.78+}$ means that the band formed by the antibonding π_z^* states is partially populated. A one-dimensional metal should result (Figure 8.8).

Band structure calculations (DFT, TB-LMTO-ASA) performed for the crystal structure of $\text{Te}_4[\text{Bi}_{0.74}\text{Cl}_4]$ have confirmed that the compound with the nearly square arrangement of Te_4 -rings demonstrate bands crossing of the Fermi level in the direction of the eclipsed stacking, and should therefore exhibit metallic conductivity (Figure 8.9). The analysis of atomic contributions has revealed that bands in the vicinity of the Fermi level are comprised by $5p$ -Te orbitals.

The analysis of chemical bonding in the stack of “ $\text{Te}_4^{1.78+}$ ” polycations reveals two inert lone pairs at two atoms of each “ $\text{Te}_4^{1.78+}$ ” ring (Figure 8.10a). These two atoms are also involved in two homoatomic covalent bonds with the neighboring tellurium atoms in the ring plane. The two other tellurium atoms in each ring are not only engaged in the homonuclear bonding in the ring plane (Figure 8.10b), but also demonstrate a substantial inter-ring interaction (feature #4 in Figure 8.10b). As a result, these two Te atoms possess only one lone pair each, and the rest of the electron density resides in inter-ring region. This bonding is not visualized as an isolated attractor, but was already encountered and explained by means of decomposition of relative ELI-D Laplacian [183, 184].

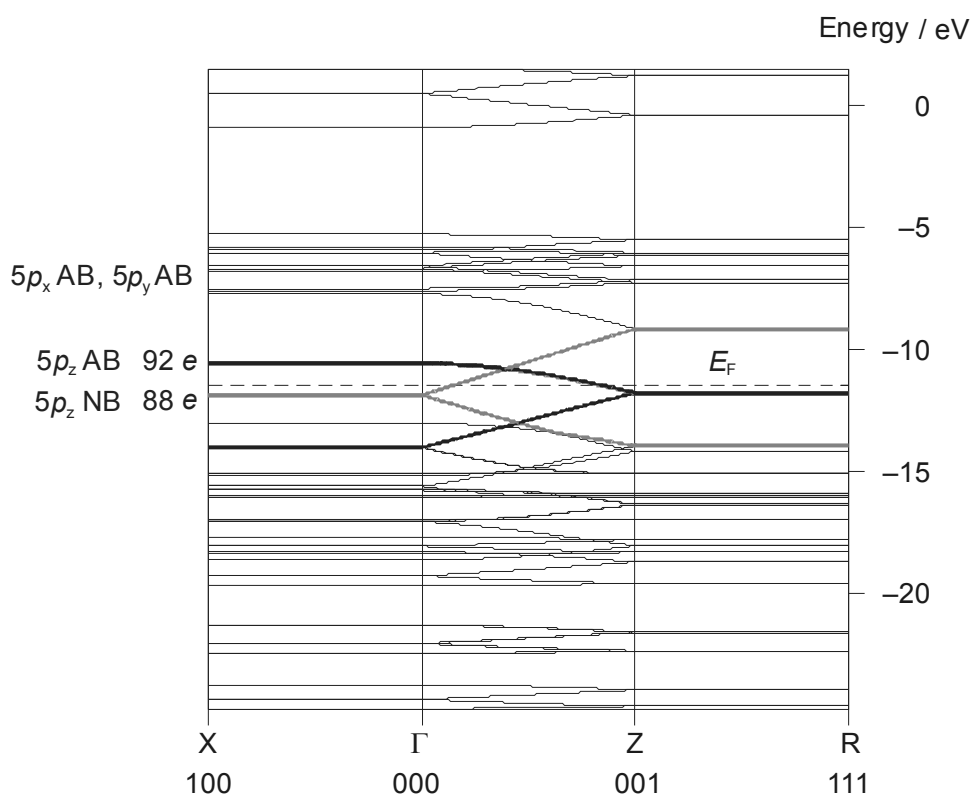


Figure 8.8: The band structure (extended Hückel calculation) of one-dimensional stacking of square Te_4 rings. The bold black band (88 electrons) resides at the Fermi level when the stack is built by Te_4^{2+} rings, the bold grey band (92 electrons) — if the stack comprise Te_4^+ rings. In reality, the Fermi level is somehow in between, which corresponds to metallic properties. NB = nonbonding MO, AB = antibonding MO.

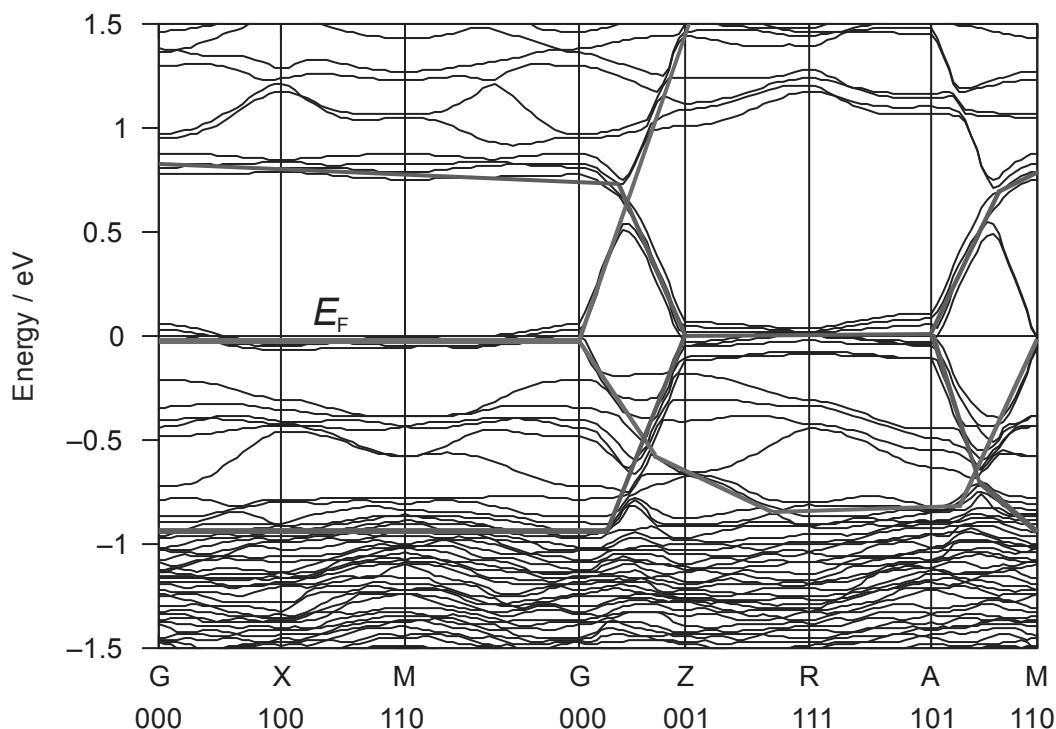


Figure 8.9: The band structure for $\text{Te}_4[\text{Bi}_{0.74}\text{Cl}_4]$ model with square rings. The bands at the Fermi level (at $E = 0$) correspond to respective Te-bands in the isolated $\{\text{Te}_4\}_n$ stack (cf. Figure 8.8).

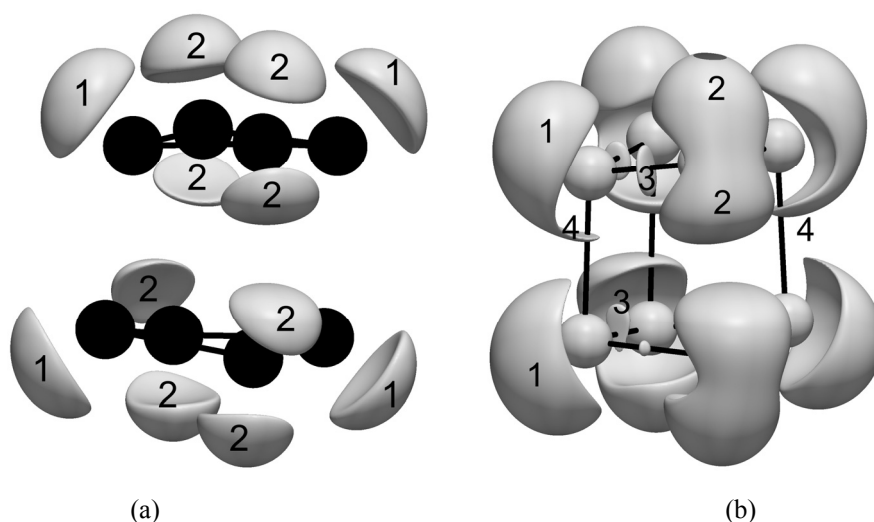


Figure 8.10: Localization domains calculated for two adjacent $[\text{Te}_4]^{1.78+}$ rings within the crystal structure of $\text{Te}_4[\text{Bi}_{0.74}\text{Cl}_4]$: (a) $\mathcal{I} = 1.38$, (b) $\mathcal{I} = 1.26$. **1** – lone pairs of Te bonded in the ring plane, **2** – lone pair of Te bonded in the ring plane and along the c axis, **3** – Te–Te intra-ring bonding attractor, **4** – Te–Te inter-ring bonding attractor.

Quantum chemical calculations predict (Figure 8.11) that the metallic conductivity along the c axis can be effectively hindered upon the Te_4 ring distortion (that may occur, e.g. upon its reduction). In analogy to the isolated polycation, the orthogonal and thus localized σ_x^* antibonding MO compete with the states of the partially filled band. Since the band has

dispersion over an energy range, there will be no binary win–lose situation in the competition for the excess electrons but a distribution, which should depend on temperature by excitation as well as by thermal expansion. In a one-dimensional system, the localization of a small fraction of the conduction electrons in orthogonal states will terminate or at least disturb metallic conductivity. A poor metal or a semiconductor with very small band gap width should result. The experimental observation of $\text{Te}_4[\text{Bi}_{0.67}\text{Cl}_4]$ [86] crystals with the conductivity characteristics of a semiconductor with an estimated band gap of 0.16 eV nicely fits these expectations.

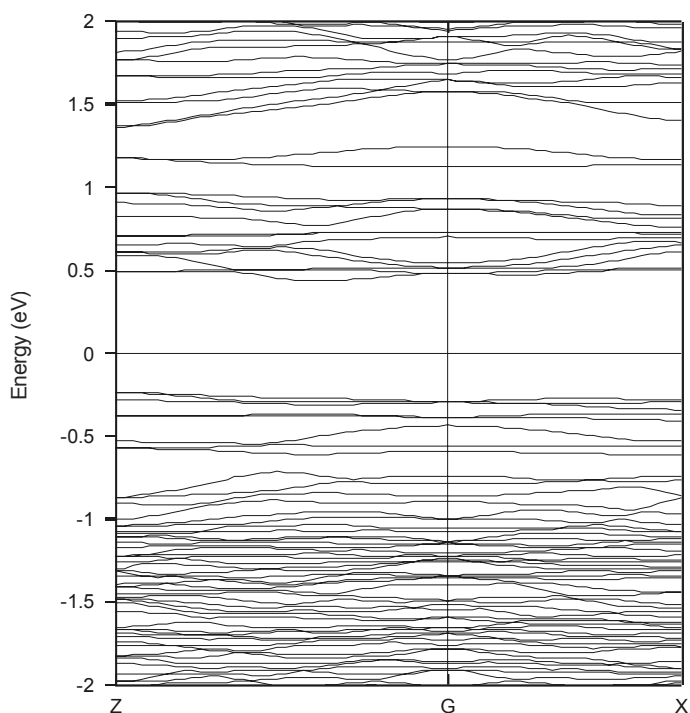


Figure 8.11: The band structure for $\text{Te}_4[\text{Bi}_{0.74}\text{Cl}_4]$ model with rectangular rings.

Yet in the more bismuth-rich compound $\text{Te}_4[\text{Bi}_{0.74}\text{Cl}_4]$, a very good metallic conductivity has been observed: The low room-temperature resistivity is comparable to iron, given that $\text{Te}_4[\text{Bi}_{0.74}\text{Cl}_4]$ is just a one-dimensional conductor (Figure 8.12). The bent on the resistivity curve above the room-temperature is not yet fully understood. Surprisingly, there is a transition to the superconducting state at 7.1 K, which is a very high T_c for a π -stacking. The π -stacking interaction, which led to the first organic conductors, was observed in tetrathiofulvalene–tetracyanoquinomethane (TTF-TCNQ), which exhibits a room temperature conductivity of $10^3 \Omega^{-1}\text{cm}^{-1}$. TTF-TCNQ is a charge-transfer compound with separate stacks of the cations TTF (charge donors) and anions TCNQ (electron acceptors). It has very good

metallic properties down to a temperature of approximately 58 K, where a metal–insulator transition occurs [185].

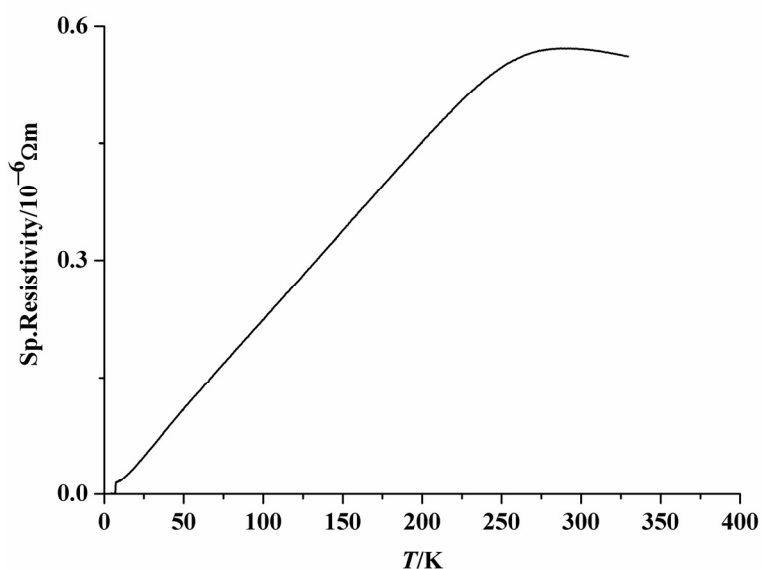


Figure 8.12: Temperature dependence of the specific resistivity of $[\text{Te}_4][\text{Bi}_{0.74}\text{Cl}_4]$.

In the study of the magnetization of $\text{Te}_4[\text{Bi}_{0.74}\text{Cl}_4]$, a Pauli-paramagnetism has been observed with temperature-independent magnetic susceptibility, which indicates very low defect concentration, superimposed by strong diamagnetism [Figure 8.13].

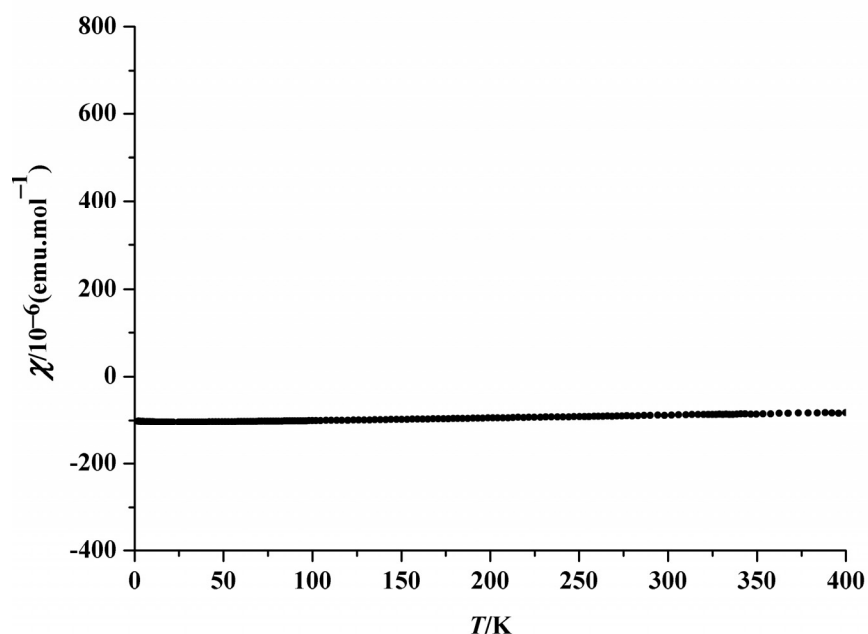


Figure 8.13: Temperature dependence of the reciprocal molar susceptibility of $[\text{Te}_4][\text{Bi}_{0.74}\text{Cl}_4]$ in an external magnetic field of $H = 35$ kOe.

The low field measurement nicely shows a very sharp transition to the superconducting state (Figure 8.14). The almost negligible difference between field cooling (f_c) and zero-field

cooling (*zfc*) susceptibilities hints at a type-I superconductor. The volume fraction of the superconducting phase is at least 50 % of the sample.

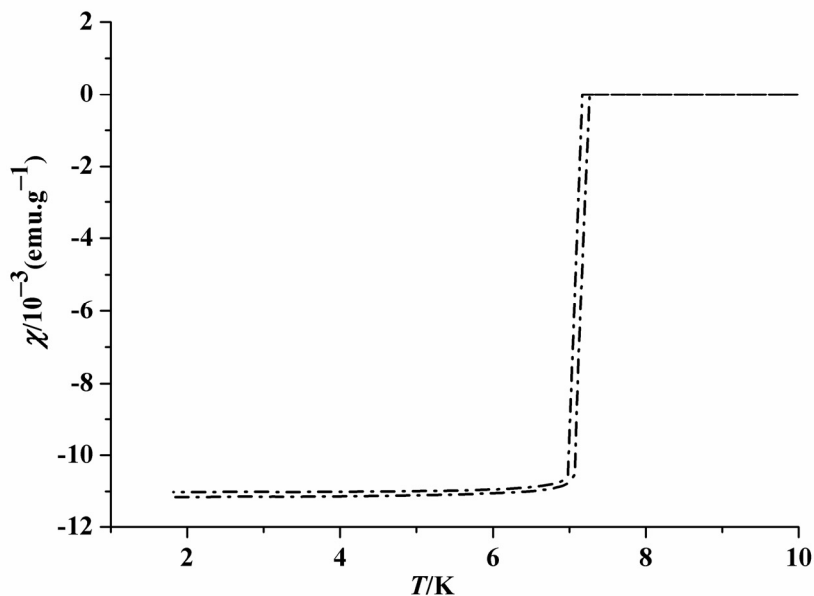


Figure 8.14: Temperature dependence of the reciprocal molar susceptibility of $[\text{Te}_4][\text{Bi}_{0.74}\text{Cl}_4]$ in an external magnetic field of $H = 20$ kOe.

Table 8.1 Coordinates and equivalent displacement parameters for the atoms in $[\text{Te}_4][\text{Bi}_{0.74}\text{Cl}_4]$. U_{eq} (in pm^2) is defined as one third of the trace of the orthogonalized tensor U_{ij} .

Atom	x	y	z	U_{eq}
Te1	0.68007(4)	0.60459(3)	0.26991(1)	451(2)
Bi1	0.25	0.75	0.7411(8)	656(10)
Cl1	0.4120(2)	0.6428(2)	0.2470(7)	508(8)

Table 8.2 Coefficients U_{ij} (in pm^2) of the tensors of the harmonic displacement parameters of the atoms in $[\text{Te}_4][\text{Bi}_{0.74}\text{Cl}_4]$.

Atom	U_{11}	U_{22}	U_{33}	U_{12}	U_{13}	U_{23}
Te1	0.0417(3)	0.0351(3)	0.0583(3)	-0.0042(2)	-0.0005(3)	0.0004(3)
Bi1	0.0356(12)	0.0333(10)	0.1279(11)	-0.0014(12)	0	0
Cl1	0.0362(11)	0.0443(11)	0.0720(15)	0.0029(8)	-0.0030(14)	0.0036(14)

Table 8.3 Comparison of selected interatomic distances (in pm) in $[\text{Te}_4][\text{Bi}_{0.74}\text{Cl}_4]$ and $[\text{Te}_4][\text{Bi}_{0.67}\text{Cl}_4]$.

Distance	$[\text{Te}_4][\text{Bi}_{0.74}\text{Cl}_4]$		$[\text{Te}_4][\text{Bi}_{0.67}\text{Cl}_4]$	
	Average	Range	Average	Range
Te-Te	275.3(4)	274.8(3) – 275.9(3)	275(3)	248(3) – 299(3)
Te-Cl	327(1)	300(1) – 378(1)	343(7)	292(4) – 421(4)
Cl-Cl	358(2)	341(1) – 389(2)	381(4)	321(6) – 558(6)
Bi-Cl	274(2)	253(2) – 295(2)	262(3)	257(4) – 290(2)

Table 8.4 Crystallographic data and details of the structure determination for $\text{Te}_4[\text{Bi}_{0.74}\text{Cl}_4]$.

Chemical formula	$\text{Te}_4[\text{Bi}_{0.74}\text{Cl}_4]$
Crystal systems	tetragonal
Superspace groups	$P4/n(\frac{1}{2}\frac{1}{2}\gamma)q0$
a, c (pm); V (10^6 pm^3)	1206.6(2), 352.4(1); 513.0(2)
Modulation wave vector	$(\frac{1}{2}\frac{1}{2}\gamma)$, $\gamma = 0.272(2)$
Temperature (K)	293(2)
Formula units per cell	2
Calculated density ($\text{g}\cdot\text{cm}^{-3}$)	5.24
Measurement device	imaging plate diffractometer IPDS-II (Stoe)
Radiation	graphite-monochromated Mo- $K\alpha$ radiation
Wavelength (pm)	71.073
Range of indices	$-13 \leq h, k \leq 13, -4 \leq l \leq 4, -2 \leq m \leq 2$
$\mu(\text{Mo-}K\alpha)$ (mm^{-1})	24.8
Transmission(max, min)	0.685, 0.221
$R(\text{int}), R(\sigma)$	0.112, 0.026
No. of parameters	84
Refinement on	F^2
Measured reflections	16420
Unique reflections	1698
Reflections with $F_o > 3\sigma(F_o)$	759
All reflections: $R_I[F_o > 3\sigma(F_o)]$	0.031
R_I (all F_o)	0.094
wR_2 (all F_o^2)	0.070
Main reflections	341
Reflections with $F_o > 3\sigma(F_o)$	241
$R_I [F_o > 3\sigma(F_o)]$	0.020
R_I (all F_o)	0.031
wR_2 (all F_o^2)	0.048
First-order satellites	682
Reflections with $F_o > 3\sigma(F_o)$	394
$R_I [F_o > 3\sigma(F_o)]$	0.035
R_I (all F_o)	0.072
wR_2 (all F_o^2)	0.065
Second-order satellites	675
Reflections with $F_o > 3\sigma(F_o)$	124
$R_I [F_o > 3\sigma(F_o)]$	0.073
R_I (all F_o)	0.308
wR_2 (all F_o^2)	0.135
Goodness of fit (all)	1.30
$\Delta\rho(\text{max, min})$ ($\text{e}\cdot 10^{-6} \text{ pm}^{-3}$)	+1.79, -2.03

9. Conclusion and Outlook

Main group polycations and transition metal clusters had traditionally been synthesized via high-temperature routes by performing reactions in melts or by CTR, at room-temperature or lower temperature by using so-called superacid solvents, and at room-temperature in benzene–GaX₃ media. Considering the major problems associated with higher temperature routes (e.g. long annealing time, risk of product decomposition, and low yield) and taking into account the toxicity of benzene and liquid SO₂ in room-temperature or lower temperature synthesis, a soft and sustainable chemical approach has been developed, employing a Lewis-acidic IL [bmim]Cl/AlCl₃. This new alternative reaction medium has proven to be an excellent solvent system for the single-step synthesis of main group polycations and transition metal clusters. X-ray diffraction and Raman spectroscopy have been used for the structural characterization of the isolated compounds. Physical properties and quantum chemical calculations of some of the compounds have also been carried out.

This new synthetic scheme is based on the extraordinarily high solubility of metal halogenides in Lewis acidic systems, which renders pseudo-melt behavior to the saturated solution. Thus, it has been possible to repeat, at room temperature, several of the reactions previously performed in melts or by CTR at substantially higher temperature. Although, in the beginning, it was quite challenging to isolate the desired products from highly viscous IL and only spectroscopic studies could be performed to identify different species in colored solutions. The successive efforts proved that salting out or the use of excess AlCl₃ could facilitate the growth of single crystals in only few days. The additional advantages of this synthetic route over other methodologies include:

- Low temperature synthesis eliminates the risk of product decomposition.
- Pure inorganic cluster compounds can be synthesized. Organic components of the IL are not included in the final products.
- IL render stability to the ionic intermediates.
- Unlike for solid-state methods or gas phase deposition, reactions in IL are fast; crystal growth requires only few days rather than weeks and the overall product yield can be high.

An IL based room temperature synthesis facilitated the crystallization of several transition metal and post-transition metal cluster compounds [Table 9.1]. The mild reaction

conditions in IL obviously allow preparing new solid phases, which seem to be not accessible via high temperature routes.

Table 9.1 Compounds containing main group polycations and transition metal clusters, synthesized and isolated from IL at room-temperature.

Compounds with polycations	Compounds with transition metal clusters
$[\text{Mo}_2\text{Te}_{12}]\text{I}_6$	$\text{Bi}[\text{Mo}_5\text{Cl}_{13}]\text{Cl}$
$\text{Te}_4[\text{Bi}_{0.74}\text{Cl}_4]$	$\text{BiCl}[\text{Mo}_6\text{Cl}_{14}]$
$\text{Te}_4[\text{AlCl}_4]_2$	$\text{Sn}[\text{SnCl}][\text{W}_3\text{Cl}_{13}]$
$\text{Te}_4[\text{Bi}_6\text{Cl}_{20}]$	$\text{BiCl}[\text{W}_6\text{Cl}_{14}]$
$\text{Te}_6[\text{WOCl}_4]_2$	
$\text{Te}_8[\text{Bi}_4\text{Cl}_{14}]$	
$\text{Bi}_5[\text{AlCl}_4]_3$	
Bi_6Cl_7	
Bi_6Br_7	
$\text{Te}_4[\text{AlCl}_4]_2$	
$(\text{Sb}_{10}\text{Se}_{10})[\text{AlCl}_4]_2$	

The binuclear complex salt $[\text{Mo}_2\text{Te}_{12}]\text{I}_6$, which contains the heteropolycationic $[\text{Mo}_2\text{Te}_{12}]^{6+}$ cluster, was obtained by the direct reaction of the elements at room temperature in only three days. This nicely demonstrates the versatility of IL in inorganic synthesis: The homeotypic $[\text{Mo}_2\text{Te}_{12}]\text{Br}_6$ has been synthesized previously through CVT at about 300 °C within four weeks yielding less product. Moreover, the CVT synthesis of the iodide complex failed completely. Contrary to the weak temperature-independent paramagnetism found in $[\text{Mo}_2\text{Te}_{12}]\text{Br}_6$, coupling of the magnetic moments was not observed in $[\text{Mo}_2\text{Te}_{12}]\text{I}_6$ (paramagnetic effective moment = 3.53 μ_{B}/Mo). In the present case the complex is a diradical with seventeen electrons per central atom.

For the synthesis of the trinuclear tungsten compound $\text{Sn}[\text{SnCl}][\text{W}_3\text{Cl}_{13}]$, Sn was proved to be a very effective reductant for the convenient room-temperature preparation of a new polynuclear cluster compound from WCl_6 in high overall yield. The crystallographic point group of the $[\text{W}_3\text{Cl}_{13}]^{3-}$ cluster anions is C_3 , but pseudo-symmetry C_{3v} is observed within double standard deviation. The Sn(II) cations, which are in trigonal pyramidal and in distorted trigonal-antiprismatic coordination by apical chloride ions, connect the clusters into layers that are stacked according to the 6_3 screw axis. The pronounced polarity of the crystal structure creates huge deviations from Friedel's law in the diffraction pattern.

The pentanuclear molybdenum cluster compound $\text{Bi}[\text{Mo}_5\text{Cl}_{13}]\text{Cl}$ was synthesized by the reduction of MoCl_5 with elemental Bi at room temperature. The structure is a defect variant of the $\text{Pb}[\text{Mo}_6\text{Cl}_{14}]$ type; in statistical distribution one of the molybdenum atoms is missing in the cluster core. With respect to the paramagnetic behavior of $\text{Bi}[\text{Mo}_5\text{Cl}_{13}]\text{Cl}$, a hypothetical alternative structure model, basing on the statistical missing of each sixth complete octahedron, is ruled out. The experimental effective magnetic moment of $1.67 \mu_{\text{B}}$ suggests pure spin magnetism of an unpaired electron ($S = 1/2$; $g \approx 2$). In fact the $[\text{Mo}_5\text{Cl}_{13}]^{2-}$ anion comprises the odd number of 19 electrons in molybdenum based cluster orbitals.

The first mixed antimony/selenium polycation $(\text{Sb}_{10}\text{Se}_{10})^{2+}$ was obtained by reacting Sb, Se, and SeCl_4 at room temperature. In the salt-like compound $(\text{Sb}_{10}\text{Se}_{10})[\text{AlCl}_4]_2$, the centrosymmetric polycyclic cation $(\text{Sb}_{10}\text{Se}_{10})^{2+}$ consists of two realgar-like $[\text{Sb}_4\text{Se}_4]$ cages, which are connected through positively charged, three-bonded selenium atoms with a central $[\text{Sb}_2\text{Se}_2]$ ring. Quantum chemical calculations predict semiconducting behavior of the compound and indicate primarily covalent bonding with varying ionic contribution within the $[\text{Sb}_{10}\text{Se}_{10}]^{2+}$ polycation, while the interactions between the polycation and the $[\text{AlCl}_4]^-$ anions are predominantly ionic.

In the modulated structure of $\text{Te}_4[\text{Bi}_{0.74}\text{Cl}_4]$, the Bi and Cl atoms chemically form a complex sequence of chloridobismuthate(III) anions with average composition $[\text{Bi}_{0.74}\text{Cl}_4]^{1.78-}$, while the Te atoms constitute square polycations, which are stacked eclipsed parallel to the c -axis. Along $[001]$ isolated $[\text{BiCl}_6]^{3-}$ and $[\text{Bi}_2\text{Cl}_{10}]^{4-}$ groups form an aperiodic sequence. Because of the modulation, in $\text{Te}_4[\text{Bi}_{0.74}\text{Cl}_4]$ each Te_4 -ring deviates individually from $4/mmm$ symmetry. The MO diagram analysis reveals competition of intermolecular interactions with σ and π -bonding in the rings. In a case of nearly non-distorted square $[\text{Te}_4]^{1.78+}$ rings, metallic conductivity along the one-dimensional stack is predicted by quantum chemical calculations, which has been confirmed by the electrical conductivity experiment. In the more bismuth-rich compound $\text{Te}_4[\text{Bi}_{0.74}\text{Cl}_4]$, a very good metallic conductivity has been observed. The low room-temperature resistivity is comparable to iron, given that $\text{Te}_4[\text{Bi}_{0.74}\text{Cl}_4]$ is just a one-dimensional conductor. Surprisingly, there is a transition to the superconducting state at 7.1 K, which is a very high T_c for the π -stacking. The almost negligible difference between field cooling (fc) and zero-field cooling (zfc) susceptibilities hints at a type-I superconductor.

The new alternative facile route has the potential to flourish and promote the richness of the transition metals and main group cluster chemistry. The observation that different mixtures of elements in ILs specifically generate new cluster species yield spirit for new combinations not yet employed. Moreover, ILs offer a promising synthetic strategy towards new chalcogenide species with cationic character rather than the more familiar anionic nature. The different functions of the IL (as solvent or structural component) further extend the applicability of this method and open the opportunity to create a diversity of metal complexes and clusters with interesting structures and compositions.

These features make IL based synthetic methods convenient chemical procedures that are versatile and general routes for the development of polycations or clusters of high nuclearity. Finally, compared to other low-temperature synthetic routes, which make use of cancer causing or toxic organic and inorganic substances like benzene, SO₂, and AsF₅, IL are more convenient, economical and environmental friendly solvents.

10. Acknowledgment

I would like to express my profound gratitude to Prof. Michael Ruck for assigning me this fascinating project, his excellent supervision, encouragement, and fruitful discussion.

Prof. Johannes Beck (Universität Bonn), Prof. Thomas Straßner (TU Dresden) and Prof. Arnold Guloy (University of Houston, USA) are gratefully acknowledged for the valuable discussions, suggestions, and effective cooperation.

I am deeply indebted to Dr. Thomas Doert for his technical assistance especially with regards to crystallographic problems and Dr. Anna Isaeva for the quantum chemical calculations.

I am thankful to Christoph Ziegler and Ellen Kern (Physikalische Chemie, TU Dresden) for performing Raman spectroscopy and EDX analysis respectively, Dr. Walter Schnelle (Max Planck Institute for Chemical Physics of Solids, Dresden) for magnetization and electrical conductivity experiments.

Jutta Krug and Gudrun Kadner are appreciatively acknowledged for their continuous experimental assistance.

Ilona Salzmann is thanked for her administrative support.

I express my appreciation to all my colleagues of AK Ruck, especially Dr. Andreas Heerwig for his constant support in solving the tricky structures and Daniel Köhler for his regular help regarding all matters inside and outside the institute.

Finally, I would like to pay thanks to all my students for their excellent contribution in synthesis, my family for their constant prayers, and my wife for her great care and patience.

The generous financial support from *the Higher Education Commission of Pakistan* (HEC), *the German Academic Exchange Service* (DAAD), and *the Max Planck Society* (MPG) is gratefully acknowledged.

11. References

- [1] M. H. Klaproth, *Phil. Mag.* **1798**, *1*, 78–82.
- [2] R. J. Gillespie, J. Passmore in: H. J. Emeleus, A. G. Sharpe (eds.), *Advances in Inorganic Chemistry and Radiochemistry*, Academic Press Inc, London **1975**, vol. *15*, pp. 49–88.
- [3] N. J. Bjerrum, G. P. Smith, *J. Am. Chem. Soc.* **1968**, *90*, 4472–4473.
- [4] a) J. Barr, R. J. Gillespie, R. Kapoor, C. Malhotra, *Can. J. Chem.* **1968**, *49*, 149–159; b) J. Barr, R. J. Gillespie, R. Kapoor, G. P. Pez, *J. Am. Chem. Soc.* **1968**, *90*, 6855–6856.
- [5] a) N. Bartlett, D. H. Lohmann, *Proc. Chem. Soc.* **1962**, 115–116; b) N. Bartlett, D. H. Lohmann, *J. Chem. Soc.* **1962**, 5253–5261.
- [6] A. Hershaft, J. D. Corbett, *Inorg. Chem.* **1963**, *2*, 979–985.
- [7] a) R. M. Friedman, J. D. Corbett, *Inorg. Chem.* **1973**, *12*, 1134–1139; b) R. M. Friedman, J. D. Corbett, *Inorg. Chim. Acta* **1973**, *7*, 525–527.
- [8] a) R. C. Paul, K. K. Paul, K. C. Malhotra, *J. Chem. Soc. D.* **1970**, 453b–454; b) R. C. Paul, J. K. Puri, K. C. Malhotra, *J. Chem. Soc. D.* **1971**, 1031; c) R. C. Paul, J. K. Puri, K. K. Paul, R. D. Sharma, K. C. Malhotra, *Inorg. Nucl. Chem. Lett.* **1971**, *7*, 725–728.
- [9] a) P. A. W. Dean, R. J. Gillespie, *J. Chem. Soc. D.* **1970**, 853; b) R. J. Gillespie, O. C. Vaidya, *J. Chem. Soc., Chem. Commun.* **1972**, 40–41.
- [10] a) A. Vij, W. W. Wilson, V. Vij, F. S. Tham, J. A. Sheehy, K. O. Christe, *J. Am. Chem. Soc.* **2001**, *123*, 6308–6313; b) M. Lindsjö, A. Fischer, L. Kloo, *Angew. Chem.* **2004**, *116*, 2594–2597; *Angew. Chem. Int. Ed.* **2004**, *43*, 2540–2543.
- [11] a) R. J. Gillespie, J. Passmore, *Acc. Chem. Res.* **1971**, *4*, 413–419; b) R. J. Gillespie, *Chem. Soc. Rev.* **1979**, *8*, 315–352.
- [12] a) M. Binnewies, R. Glaum, M. Schmidt, P. Schmidt, *Chemische Transportreaktionen*, de Gruyter, Berlin **2011**; b) H. Schäfer, *Chemische Transportreaktionen*, Verlag Chemie, Weinheim **1962**.
- [13] a) J. Beck, *Angew. Chem.* **1994**, *106*, 172–182; *Angew. Chem. Int. Ed. Engl.* **1994**, *33*, 163–172; b) J. Beck, *Coord. Chem. Rev.* **1997**, *163*, 55–70.
- [14] a) J. D. Corbett, *Inorg. Chem.* **1968**, *7*, 198–208; b) T. W. Couch, D. A. Lokken, J. D. Corbett, *Inorg. Chem.* **1972**, *11*, 357–362; c) J. D. Corbett, *Prog. Inorg. Chem.* **1976**, *21*, 129–158.
- [15] M. Ruck, F. Steden, *Z. Anorg. Allg. Chem.* **2007**, *633*, 1556–1562.

- [16] a) M. Lindsjö, L. Kloo, *Acta Crystallogr.* **2005**, *E61*, i18–i19; b) A. N. Kuznetsov, B. A. Popovkin, K. Ståhl, M. Lindsjö, L. Kloo, *Eur. J. Inorg. Chem.* **2005**, 4907–4913; c) M. Lindsjö, A. Fischer, L. Kloo, *Eur. J. Inorg. Chem.* **2005**, 670–675.
- [17] E. Ahmed, D. Köhler, M. Ruck, *Z. Anorg. Allg. Chem.* **2009**, *635*, 297–300.
- [18] E. Ahmed, M. Groh, M. Ruck, *Eur. J. Inorg. Chem.* **2010**, 5294–5297.
- [19] E. Ahmed, E. Ahrens, M. Heise, M. Ruck, *Z. Anorg. Allg. Chem.* **2010**, *636*, 2602–2606.
- [20] a) E. Ahmed, E. Ahrens, M. Heise, M. Ruck, *Z. Anorg. Allg. Chem.* **2010**, *636*, 2053; b) E. Ahmed, E. Ahrens, M. Heise, M. Ruck, *Z. Anorg. Allg. Chem.* **2011**, *637*, 961–964.
- [21] Q. Zhang, I. Chung, J. I. Jang, J. B. Ketterson, M. G. Kanatzidis, *J. Am. Chem. Soc.* **2009**, *131*, 9896–9897.
- [22] K. Biswas, Q. Zhang, I. Chung, J. H. Song, J. Androulakis, A. J. Freeman, M. G. Kanatzidis, *J. Am. Chem. Soc.* **2010**, *132*, 14760–14762.
- [23] D. Freudenmann, C. Feldmann, *Dalton Trans.* **2011**, *40*, 452–456.
- [24] N. Burford, J. Passmore, J. C. P. Sanders, in: J. F. Liebman, A. Greenberg (eds.), *From Atoms to Polymers: Isoelectronic Analogies*, New York **1989**, vol. *11*, pp. 53–108.
- [25] S. Brownridge, I. Krossing, J. Passmore, H. D. B. Jenkins, H. K. Roobottom, *Coord. Chem. Rev.* **2000**, *197*, 397–481.
- [26] S. Ulvenlund, L. Bengtsson-Kloo in: P. Braunstein, L. A. Oro, P. R. Raithby (eds), *Metal Clusters in Chemistry*, Wiley-VCH, Weinheim **1999**, vol. *1*, pp. 561–662.
- [27] M. Ruck, *Angew. Chem.* **2001**, *113*, 1222–1234; *Angew. Chem. Int. Ed.* **2001**, *40*, 1182–1193.
- [28] I. Krossing in: M. Driess, H. Nöth (eds), *Molecular clusters of the main group elements*, Wiley-VCH, Weinheim **2004**, pp. 209–229.
- [29] W. S. Sheldrick in: M. Driess, H. Nöth (eds), *Molecular clusters of the main group elements*, Wiley-VCH, Weinheim **2004**, pp. 230–245.
- [30] T. A. O'Donnell, *Chem. Soc. Rev.* **1987**, *16*, 1–43.
- [31] I. D. Brown, D. B. Crump, R. J. Gillespie, *Inorg. Chem.* **1971**, *10*, 2319–2323.
- [32] J. Passmore, G. Sutherland, P. S. White, *J. Chem. Soc., Chem. Commun.* **1980**, 330–331.
- [33] G. Cardinal, R. J. Gillespie, J. F. Sawyer, J. E. Vekris, *J. Chem. Soc., Dalton Trans.* **1982**, 765–779.

- [34] M. J. Rothman, L. S. Bartell, C. S. Ewig, J. R. van Wazer, *J. Comput. Chem.* **1980**, *1*, 64–68.
- [35] R. C. Burns, R. J. Gillespie, W. C. Luk, D. R. Slim, *Inorg. Chem.* **1979**, *18*, 3086–3094.
- [36] G. W. Drake, G. L. Schimek, J. W. Kolis, *Inorg. Chem.* **1996**, *35*, 1740–1742.
- [37] C. G. Davies, R. J. Gillespie, J. J. Park, J. Passmore, *Inorg. Chem.* **1971**, *10*, 2781–2784.
- [38] M. J. Collins, R. J. Gillespie, J. F. Sawyer, *Acta Crystallogr.* **1988**, *C44*, 405–409.
- [39] R. K. McMullan, D. J. Prince, J. D. Corbett, *J. Chem. Soc. D.* **1969**, 1438–1439.
- [40] R. C. Burns, W. L. Chan, R. J. Gillespie, W. C. Luk, J. F. Sawyer, D. R. Slim, *Inorg. Chem.* **1980**, *19*, 1432–1439.
- [41] R. C. Burns, R. J. Gillespie, J. F. Sawyer, *Inorg. Chem.* **1980**, *19*, 1423–1432.
- [42] R. C. Burns, R. J. Gillespie, W. C. Luk, *Inorg. Chem.* **1978**, *17*, 3596–3604.
- [43] a) P. Boldrini, I. D. Brown, M. J. Collins, R. J. Gillespie, E. Maharajh, D. R. Slim, J. F. Sawyer, *Inorg. Chem.* **1985**, *24*, 4302–4307; b) M. J. Collins, R. J. Gillespie, J. F. Sawyer, G. J. Schrobilgen, *Inorg. Chem.* **1986**, *25*, 2053–2057.
- [44] a) R. C. Burns, M. J. Collins, S. M. Eicher, R. J. Gillespie, J. F. Sawyer, *Inorg. Chem.* **1988**, *27*, 1807–1813; b) R. J. Gillespie, W. C. Luk, E. Maharajh, D. R. Slim, *Inorg. Chem.* **1977**, *16*, 892–896.
- [45] M. J. Collins, R. J. Gillespie, J. F. Sawyer, *Inorg. Chem.* **1987**, *26*, 1476–1481.
- [46] R. Faggiani, R. J. Gillespie, J. E. Vekris, *J. Chem. Soc., Chem. Commun.* **1988**, 902–904.
- [47] P. Boldrini, I. D. Brown, R. J. Gillespie, P. R. Ireland, W. C. Luk, D. R. Slim, J. E. Vekris, *Inorg. Chem.* **1976**, *15*, 765–770.
- [48] a) B. H. Christian, R. J. Gillespie, J. F. Sawyer, *Inorg. Chem.* **1981**, *20*, 3410–3420; b) R. J. Gillespie, J. P. Kent, J. F. Sawyer, D. R. Slim, J. D. Tyrer, *Inorg. Chem.* **1981**, *20*, 3799–3812; c) A. J. Banister, P. J. Dainty, A. C. Hazell, R. G. Hazell, J. G. Lomborg, *J. Chem. Soc. D.* **1969**, 1187; d) A. J. Banister, H. G. Clarke, I. Rayment, H. M. M. Shearer, *Inorg. Nucl. Chem. Lett.* **1974**, *10*, 647–654; e) C. Knapp, A. Mailman, G. B. Nikiforov, J. Passmore, *J. Fluorine Chem.* **2006**, *127*, 916–919.
- [49] a) Y. C. Leung, J. Waser, S. van Houten, A. Vos, G. A. Wiegers, E. H. Wiebenga, *Acta Crystallogr.* **1957**, *10*, 574–582; b) R. Gleiter, M. C. Böhm, M. Eckert-Maksic, W. Schäfer, M. Baudler, Y. Aktalay, G. Fritz, K. D. Hoppe, *Chem. Ber.* **1983**, *116*, 2972–2982.

- [50] a) B. Krebs, M. Mummert, C. Brendel, *J. Less-Common Met.* **1986**, *116*, 159–168; b) B. Krebs, M. Hucke, C. J. Brendel, *Angew. Chem.* **1982**, *94*, 453–454; *Angew. Chem. Int. Ed.* **1982**, *21*, 445–446; c) J. Beck, C. J. Brendel, L. Bengtsson-Kloo, B. Krebs, M. Mummert, A. Stankowski, S. Ulvenlund. *Chem. Ber.* **1996**, *129*, 1219–1226.
- [51] a) M. Ruck, *Z. Anorg. Allg. Chem.* **2000**, *626*, 14–22; b) M. Ruck, V. Dubenskyy, T. Söhnel, *Angew. Chem.* **2003**, *115*, 3086–3090; *Angew. Chem. Int. Ed.* **2003**, *42*, 2978–2982; c) V. Dubenskyy, M. Ruck, *Z. Anorg. Allg. Chem.* **2004**, *630*, 2458–2462; d) B. Wahl, L. Kloo, M. Ruck, *Angew. Chem.* **2008**, *120*, 3996–3999; *Angew. Chem. Int. Ed.* **2008**, *47*, 3932–3935; e) B. Wahl, M. Erbe, A. Gerisch, L. Kloo, M. Ruck, *Z. Anorg. Allg. Chem.* **2009**, *635*, 743–752; f) B. Wahl, M. Ruck, *Z. Anorg. Allg. Chem.* **2008**, *634*, 2267–2275.
- [52] a) N. J. Bjerrum, C. R. Boston, G. P. Smith, H. L. Davis, *Inorg. Nucl. Chem. Lett.* **1965**, *1*, 141–143; b) N. J. Bjerrum, C. R. Boston, G. P. Smith, *Inorg. Chem.* **1967**, *6*, 1162–1172; c) N. J. Bjerrum, G. P. Smith, *Inorg. Chem.* **1967**, *6*, 1968–1972.
- [53] a) M. Ruck, *Z. Anorg. Allg. Chem.* **1998**, *624*, 521–528; b) M. Ruck, S. Hampel, *Polyhedron* **2002**, *21*, 651–656.
- [54] S. Hampel, M. Ruck, *Z. Anorg. Allg. Chem.* **2006**, *632*, 1150–1156.
- [55] a) J. Beck, T. Hilbert, *Eur. J. Inorg. Chem.* **2004**, 2019–2026; b) A. N. Kuznetsov, B. A. Popovkin, *Z. Anorg. Allg. Chem.* **2002**, *628*, 2179.
- [56] a) A. Hershaft, J. D. Corbett, *J. Chem. Phys.* **1962**, *36*, 551–552; b) H. von Benda, A. Simon, W. Bauhofer, *Z. Anorg. Allg. Chem.* **1978**, *438*, 53–67; c) A. N. Kuznetsov, A. V. Shevel'kov, S. I. Troyanov, B. A. Popovkin, *Russ. J. Inorg. Chem.* **1996**, *41*, 920–923; d) A. N. Kuznetsov, A. V. Shevel'kov, B. A. Popovkin, *Russ. J. Coord. Chem.* **1998**, *24*, 861–866; e) V. Dubenskyy, M. Ruck, *Z. Anorg. Allg. Chem.* **2003**, *629*, 375–380; f) A. N. Kuznetsov, P. I. Naumenko, B. A. Popovkin, L. Kloo, *Russ. Chem. Bull.* **2003**, *52*, 2100–2104; g) S. Hampel, P. Schmidt, M. Ruck, *Z. Anorg. Allg. Chem.* **2005**, *631*, 272–283; h) B. Wahl, M. Ruck, *Z. Anorg. Allg. Chem.* **2008**, *634*, 2873–2879.
- [57] a) B. Wahl, M. Ruck, *Z. Anorg. Allg. Chem.* **2010**, *636*, 337–342; b) A. Gerisch, M. Ruck, *Z. Anorg. Allg. Chem.* **2010**, *636*, 2033.
- [58] J. Beck, T. Hilbert, *Z. Anorg. Allg. Chem.* **2000**, *626*, 837–844.
- [59] a) J. Beck, *Chem. Ber.* **1995**, *128*, 23–27; b) J. Beck, M. Kasper, A. Stankowski, *Chem. Ber.* **1997**, *130*, 1189–1192.
- [60] A. Baumann, J. Beck, *Z. Anorg. Allg. Chem.* **2004**, *630*, 2078–2082.

- [61] a) J. Beck, *Angew. Chem.* **1991**, *103*, 1149–1151; *Angew. Chem. Int. Ed. Engl.* **1991**, *30*, 1128–1130; b) J. Beck, *Z. Anorg. Allg. Chem.* **1993**, *619*, 237–242; c) J. Beck, G. Bock, *Z. Anorg. Allg. Chem.* **1994**, *620*, 1971–1975.
- [62] J. Beck, *Angew. Chem.* **1990**, *102*, 301–302; *Angew. Chem. Int. Ed. Engl.* **1990**, *29*, 293–295.
- [63] J. Beck, K. Müller-Buschbaum, *Z. Anorg. Allg. Chem.* **1997**, *623*, 409–413.
- [64] a) J. Beck, A. Stankowski, *Z. Naturforsch.* **2001**, *56b*, 453–457; b) J. Beck, A. Fischer, *Z. Anorg. Allg. Chem.* **2002**, *628*, 369–372.
- [65] J. Beck, G. Bock, *Angew. Chem.* **1995**, *107*, 2739–2741; *Angew. Chem. Int. Ed. Engl.* **1995**, *34*, 2559–2561.
- [66] R. K. McMullan, D. J. Prince, J. D. Corbett, *Inorg. Chem.* **1971**, *10*, 1749–1753.
- [67] J. Beck, A. Fischer, A. Stankowski, *Z. Anorg. Allg. Chem.* **2002**, *628*, 2542–2548.
- [68] J. Beck, J. Wetterau, *Inorg. Chem.* **1995**, *34*, 6202–6204.
- [69] H. Braunschweig, P. Cogswell, K. Schwab, *Coord. Chem. Rev.* **2011**, *255*, 101–117.
- [70] a) M. Ruck, *Angew. Chem.* **1997**, *109*, 2059–2062; *Angew. Chem. Int. Ed. Engl.* **1997**, *36*, 1971–1973; b) M. Ruck, *Z. Anorg. Allg. Chem.* **1997**, *623*, 1535–1541; c) M. Ruck, *Z. Anorg. Allg. Chem.* **1997**, *623*, 1583–1590; d) M. Ruck, *Z. Anorg. Allg. Chem.* **1997**, *623*, 1591–1598; e) M. Ruck, R. M. Heich, *Z. Anorg. Allg. Chem.* **2000**, *626*, 2449–2456; f) A. Günther, F. Steden, M. Ruck, *Z. Anorg. Allg. Chem.* **2008**, *634*, 423–430; g) B. Wahl, L. Kloo, M. Ruck, *Z. Anorg. Allg. Chem.* **2009**, *635*, 1979–1985; h) M. Ruck, *Solid State Sci.* **2001**, *3*, 369–376; i) R. B. King, *Dalton Trans.* **2003**, 395–397; j) R. B. King, *Inorg. Chem.* **2003**, *42*, 8755–8761; k) B. U. Wahl, T. Doert, T. Söhnel, M. Ruck, *Z. Anorg. Allg. Chem.* **2005**, *631*, 457–467.
- [71] a) J. Beck, M. Dolg, S. Schlüter, *Angew. Chem.* **2001**, *113*, 2347–2350; *Angew. Chem. Int. Ed.* **2001**, *40*, 2287–2290; b) J. Beck, S. Schlüter, N. Zotov, *Z. Anorg. Allg. Chem.* **2004**, *630*, 2512–2519.
- [72] J. Beck, S. Schlüter, *Z. Anorg. Allg. Chem.* **2005**, *631*, 569–574.
- [73] J. Beck, T. Schlörb, *Phosphorus Sulfur Silicon Relat. Elem.* **1997**, *124*, *125*, 305–313.
- [74] J. Beck, S. Schlüter, N. Zotov, *Z. Anorg. Allg. Chem.* **2005**, *631*, 2450–2456.
- [75] S. Ulvenlund, K. Ståhl, L. Bengtsson-Kloo, *Inorg. Chem.* **1996**, *35*, 223–230.
- [76] a) A. Apblett, T. Chivers, J. F. Fait, *J. Chem. Soc., Chem. Commun.* **1989**, 1596–1598; b) U. Thewalt, K. Berhalter, P. Müller, *Acta Crystallogr.* **1982**, *B38*, 1280–1282; c) C. Knapp, E. Lork, T. Borrmann, W.-D. Stohrer, R. Mews, *Z. Anorg. Allg. Chem.* **2005**,

- 631, 1885–1892; d) J. Åkerstedt, R. Zaffaroni, L. Kloo, *Dalton Trans.* **2010**, 39, 8132–8134.
- [77] J. Wright, *Environmental Chemistry*, Taylor & Francis, New York **2003**, pp. 74, 208.
- [78] a) P. Wasserscheid, T. Welton, *Ionic Liquids in Synthesis*, Wiley-VCH, Weinheim **2007**; b) P. Wasserscheid, W. Keim, *Angew. Chem.* **2000**, 112, 3926–3945; *Angew. Chem. Int Ed.* **2000**, 39, 3772–3789.
- [79] T. P. Lodge, *Science* **2008**, 321, 50–51.
- [80] P. J. Dyson, T. J. Geldbach, *Metal Catalysed Reactions in Ionic Liquids*, Springer, Heidelberg **2005**.
- [81] G. Clavel, J. Larionova, Y. Guari, C. Guérin, *Chem. Eur. J.* **2006**, 12, 3798–3804; b) H. Zhu, J. F. Huang, Z. Pan, S. Dai, *Chem. Mater.* **2006**, 18, 4473–4477.
- [82] a) A. M. Guloy, R. Ramlau, Z. Tang, W. Schnelle, M. Baitinger, Yu. Grin, *Nature* **2006**, 443, 320–323; b) A. M. Guloy, Z. Tang, R. Ramlau, B. Böhme, M. Baitinger, Yu. Grin, *Eur. J. Inorg. Chem.* **2009**, 2455–2458.
- [83] R. E. Morris, *Angew. Chem.* **2008**, 120, 450–452; *Angew. Chem. Int. Ed.* **2008**, 47, 442–444.
- [84] E. Ahmed, M. Ruck, *Coord. Chem. Rev.* **2011**, in print.
- [85] T. Keilhauer, *Bachelor Thesis*, Dresden University of Technology, Dresden **2010**.
- [86] S. J. Eck, *Doctoral Thesis*, University of Bonn, Bonn **2010**.
- [87] E. Ahmed, A. Isaeva, A. Fiedler, M. Haft, M. Ruck, *Chem. Eur. J.* **2011**, 17, 6847–6852.
- [88] a) H. T. Sun, Y. Sakka, H. Gao, Y. Miwa, M. Fujii, N. Shirahata, Z. Bai, J. G. Li, *J. Mater. Chem.* **2011**, 21, 4060–4063; b) H. T. Sun, Y. Sakka, M. Fujii, N. Shirahata, H. Gao, *Opt. Lett.* **2011**, 36, 100–102.
- [89] K. R. Seddon, *J. Chem. Technol. Biotechnol.* **1997**, 68, 351–356.
- [90] W. M. Reichert, J. D. Holbrey, K. B. Vigour, T. D. Morgan, G. A. Broker, R. D. Rogers, *Chem. Commun.* **2006**, 4767–4779.
- [91] J. D. Holbrey, K. B. Vigour, W. M. Reichert, G. A. Broker, R. D. Rogers, *J. Chem. Cryst.* **2006**, 36, 799–804.
- [92] K. Jin, X. Huang, L. Pang, J. Li, A. Appel, S. Wherland, *Chem. Commun.* **2002**, 2872–2873.
- [93] A. Babai, A. V. Mudring, *Chem. Mater.* **2005**, 17, 6230–6238.
- [94] a) S. Tang, A. Babai, A. V. Mudring, *Angew. Chem.* **2008**, 120, 7743–7746; *Angew. Chem. Int. Ed.* **2008**, 47, 7631–7634; b) A. Babai, A. V. Mudring, *Inorg. Chem.* **2006**,

- 45, 4874–4876; c) A. Getsis, S. Tang, A. V. Mudring, *Eur. J. Inorg. Chem.* **2010**, 2172–2177.
- [95] A. Babai, A. V. Mudring, *J. Alloys Compd.* **2006**, 418, 122–127.
- [96] A. Babai, A. V. Mudring, *Z. Anorg. Allg. Chem.* **2006**, 632, 1956–1958.
- [97] A. E. Visser, R. P. Swatloski, W. M. Reichert, R. Mayton, S. Sheff, A. Wierzbicki, J. H. Davis, R. D. Rogers, *Environ. Sci. Technol.* **2002**, 36, 2523–2529.
- [98] F. Endres, M. Bukowski, R. Hempelmann, H. Natter, *Angew. Chem.* **2003**, 115, 3550–3552; *Angew. Chem. Int. Ed.* **2003**, 42, 3428–3430.
- [99] N. Papageorgiou, Y. Athanassov, M. Armand, P. Bonhôte, H. Pettersson, A. Azam, M. Grätzel, *J. Electrochem. Soc.* **1996**, 143, 3099–3108.
- [100] K. Lunstroot, K. Driesen, P. Nockemann, C. Görrler-Walrand, K. Binnemans, S. Bellayer, J. L. Bideau, A. Vioux, *Chem. Mater.* **2006**, 18, 5711–5715.
- [101] P. Nockemann, B. Thijs, N. Postelmans, K. Van Hecke, L. Van Meervelt, K. Binnemans, *J. Am. Chem. Soc.* **2006**, 128, 13658–13659.
- [102] Y. Yoshida, J. Fujii, G. Saito, T. Hiramatsu, N. Sato, *J. Mater. Chem.* **2006**, 16, 724–727.
- [103] I. J. B. Lin, C. S. Vasam, *J. Organomet. Chem.* **2005**, 690, 3498–3512.
- [104] M. Hasan, I. V. Kozhevnikov, M. R. H. Siddiqui, A. Steiner, N. Winterton, *Inorg. Chem.* **1999**, 38, 5637–5641.
- [105] a) R. E. D. Sesto, T. M. McCleskey, A. K. Burrell, G. A. Baker, J. D. Thompson, B. L. Scott, J. S. Wilkes, P. Williams, *Chem. Commun.* **2008**, 447–449; b) S. Pitula, A. V. Mudring, *Chem. Eur. J.* **2010**, 16, 3355–3365; c) B. Mallick, B. Balke, C. Felser, A. V. Mudring, *Angew. Chem.* **2008**, 120, 7747–7750; *Angew. Chem. Int. Ed.* **2008**, 47, 7635–7638.
- [106] a) F. W. Koknat, J. A. Parsons, A. Vongvusharintra, *Inorg. Chem.* **1974**, 13, 1699–1702; b) Y. Park, M. G. Kanatzidis, *Chem. Mater.* **1991**, 3, 781–783; c) J. Beck, M. Hengstmann, *Z. Anorg. Allg. Chem.* **1998**, 624, 433–437; d) M. Ruck, *Z. Anorg. Allg. Chem.* **1995**, 621, 2034–2042.
- [107] R. D. Adams, J. E. Babin, M. Tasi, *Angew. Chem.* **1987**, 99, 691–692; *Angew. Chem. Int. Ed. Engl.* **1987**, 26, 685–686; b) M. M. Olmstead, P. P. Power, *J. Am. Chem. Soc.* **1984**, 106, 1495–1496.
- [108] a) G. Schmid, N. Klein, L. Korste, U. Kreibig, D. Schönauer, *Polyhedron* **1988**, 7, 605–608; b) F. W. Vergeer, P. Matousek, M. Towrie, P. J. Costa, M. J. Calhorda, F. Hartl, *Chem. Eur. J.* **2004**, 10, 3451–3460.

- [109] a) E. J. Welch, N. R. M. Crawford, R. G. Bergman, J. R. Long, *J. Am. Chem. Soc.* **2003**, *125*, 11464–11465; b) S. Cordier, K. Kirakci, D. Méry, C. Perrin, D. Astruc, *Inorg. Chim. Acta* **2006**, *359*, 1705–1709.
- [110] a) H.-J. Meyer, *Z. Anorg. Allg. Chem.* **1995**, *621*, 921–924; b) B. Jung, G. Meyer, *Z. Anorg. Allg. Chem.* **1992**, *610*, 15–19; c) X. Zhao, Y. G. Li, Y. H. Wang, E. B. Wang, *Transition Met Chem.* **2008**, *33*, 323–330; d) S. Chang, Y. F. Qi, E. B. Wang, Z. Zhang, *Inorg. Chim. Acta* **2009**, *362*, 453–457.
- [111] C. L. Hussey, *Pure & Appl. Chem.* **1988**, *60*, 1763–1772.
- [112] C. L. Hussey, R. Quigley, K. R. Seddon, *Inorg. Chem.* **1995**, *34*, 370–377.
- [113] P. A. Barnard, I. W. Sun, C. L. Hussey, *Inorg. Chem.* **1990**, *29*, 3670–3674.
- [114] R. Quigley, P. A. Barnard, C. L. Hussey, K. R. Seddon, *Inorg. Chem.* **1992**, *31*, 1255–1261.
- [115] C. E. Runyan, T. Hughbanks, *J. Am. Chem. Soc.* **1994**, *116*, 7909–7910.
- [116] Y. Tian, T. Hughbanks, *Inorg. Chem.* **1995**, *34*, 6250–6254.
- [117] J. D. Harris, T. Hughbanks, *J. Am. Chem. Soc.* **1997**, *119*, 9449–9459.
- [118] a) D. Sun, T. Hughbanks, *Inorg. Chem.* **1999**, *38*, 992–997; b) D. Sun, T. Hughbanks, *Inorg. Chem.* **2000**, *39*, 1964–1968.
- [119] J. B. Willems, H. W. Rohm, C. Geers, M. Köckerling, *Inorg. Chem.* **2007**, *46*, 6197–6203.
- [120] H. Sakamoto, Y. Watanabe, T. Saito, *Inorg. Chem.* **2006**, *45*, 4578–4579.
- [121] P. J. Dyson, *Transition Met Chem.* **2002**, *27*, 353–358.
- [122] a) P. J. Dyson, *Coord. Chem. Rev.* **2004**, *248*, 2443–2458; b) T. J. Geldbach, G. Laurenczy, R. Scopelliti, P. J. Dyson, *Organometallics* **2006**, *25*, 733–742.
- [123] a) P. Nockemann, B. Thijs, K. Van Hecke, L. Van Meervelt, K. Binnemans, *Cryst. Growth Des.* **2008**, *8*, 1353–1363; b) P. Nockemann, B. Thijs, K. Lunstroot, T. N. Parac-Vogt, C. Görrler-Walrand, K. Binnemans, K. Van Hecke, L. Van Meervelt, S. Nikitenko, J. Daniels, C. Hennig, R. Van Deun, *Chem. Eur. J.* **2009**, *15*, 1449–1461.
- [124] a) P. Nockemann, R. Van Deun, B. Thijs, D. Huys, E. Vanecht, K. Van Hecke, L. Van Meervelt, K. Binnemans, *Inorg. Chem.* **2010**, *49*, 3351–3360; b) P. Nockemann, B. Thijs, T. N. Parac-Vogt, K. Van Hecke, L. Van Meervelt, B. Tinant, I. Hartenbach, T. Schleid, V. T. Ngan, M. T. Nguyen, K. Binnemans, *Inorg. Chem.* **2008**, *47*, 9987–9999.
- [125] K. Binnemans, *Chem. Rev.* **2007**, *107*, 2592–2614.

- [126] a) V. A. Cocalia, K. E. Gutowski, R. D. Rogers, *Coord. Chem. Rev.* **2006**, *250*, 755–764; b) W. R. Pitner, A. E. Bradley, D. W. Rooney, D. Sanders, K. R. Seddon, R. C. Thied, J. E. Ratter, *Green Ind. Appl. Ionic Liquids.* **2003**, *92*, 209–226; c) P. R. V. Rao, K. A. Venkatesan, T. G. Srinivasan, *Prog. Nucl. Energy.* **2008**, *50*, 449–455.
- [127] T. Kanatani, K. Matsumoto, R. Hagiwara, *Eur. J. Inorg. Chem.* **2010**, 1049–1055.
- [128] Z. Fei, D. Zhao, R. Scopelliti, P. J. Dyson, *Organometallics* **2004**, *23*, 1622–1628.
- [129] H. Schäfer, H. G. Schnering, *Angew. Chem.* **1964**, *76*, 833–849.
- [130] A. B. Bourlinos, K. Raman, R. Herrera, Q. Zhang, L. A. Archer, E. P. Giannelis, *J. Am. Chem. Soc.* **2004**, *126*, 15358–15359.
- [131] P. G. Rickert, M. R. Antonio, M. A. Firestone, K. A. Kubatko, T. Szreder, J. F. Wishart, M. L. Dietz, *J. Phys. Chem. B.* **2007**, *111*, 4685–4692.
- [132] H. Li, Z. Hou, Y. Qiao, B. Feng, Y. Hu, X. Wang, X. Zhao, *Catal. Commun.* **2010**, *11*, 470–475.
- [133] H. Li, Y. Qiao, L. Hua, Z. Hou, B. Feng, Z. Pan, Y. Hu, X. Wang, X. Zhao, Y. Yu, *ChemCatChem.* **2010**, *2*, 1165–1170.
- [134] W. Huang, W. Zhu, H. Li, H. Shi, G. Zhu, H. Liu, G. Chen, *Ind. Eng. Chem. Res.* **2010**, *49*, 8998–9003.
- [135] Y. Leng, J. Wang, D. Zhu, X. Ren, H. Ge, L. Shen, *Angew. Chem.* **2009**, *121*, 174–177; *Angew. Chem. Int. Ed.* **2009**, *48*, 168–171.
- [136] A. Corma, S. Iborra, F. X. L. Xamena, R. Montón, J. J. Calvino, C. Prestipino, *J. Phys. Chem. C.* **2010**, *114*, 8828–8836.
- [137] L. Dai, S. Yu, Y. Shan, M. He, *Eur. J. Inorg. Chem.* **2004**, 237–241.
- [138] G. Brauer, *Handbuch der Präparativen Anorganischen Chemie*, Ferdinand Enke, Stuttgart, **1975**, p. 432.
- [139] J. S. Wilkes, J. A. Levisky, R. A. Wilson, C. L. Hussey, *Inorg. Chem.* **1982**, *21*, 1263–1264.
- [140] a) X-RED32, *Data Reduction Program*, Version 1.01, Stoe & Cie GmbH, Darmstadt, **2001**; b) SAINT v7.XXA, Bruker AXS Inc., Madison (WI, USA), v2010.9–1.
- [141] a) X-SHAPE, *Crystal Optimisation for Numerical Absorption Correction Program*, Version 1.06, Stoe & Cie GmbH, Darmstadt, **1999**; b) APEX2 v2010.1, Bruker AXS Inc., Madison (WI, USA), **2010**.
- [142] a) G. M. Sheldrick, *SHELXL97, Programs for crystal structure determination*, Univ. of Göttingen, **1997**; b) G. M. Sheldrick, *Acta. Crystallogr.* **2008**, *A64*, 112–122.

- [143] K. Brandenburg, *Diamond 3.2g, Crystal and Molecular Structure Visualization*, Crystal Impact GbR, Bonn, **2010**.
- [144] L. Palatinus, G. Chapuis, *J. Appl. Crystallogr.* **2007**, *40*, 786–790.
- [145] a) V. Petříček, M. Dušek, L. Palatinus, *Jana2006, The Crystallographic Computing System*. Institute of Physics, Praha, **2006**; b) V. Petříček, V. A. van der Lee, M. Evain, *Acta Crystallogr.* **1995**, *A51*, 529–535.
- [146] O. Jepsen, A. Burkhardt, O. K. Andersen, *The Program TB–LMTO–ASA*, Version 4.7, Max Planck Institute for Solid State Research, Stuttgart, **1999**.
- [147] a) U. Barth, L. Hedin, *J. Phys. C* **1972**, *5*, 1629–1642; b) J. P. Perdew, J. A. Chevary, S. H. Vosko, K. A. Jackson, M. R. Pederson, D. J. Singh, C. Fiolhais, *Phys. Rev. B.* **1992**, *46*, 6671–6687; c) A. D. Becke, *J. Chem. Phys.* **1992**, *97*, 9173–9177.
- [148] T. Williams, C. Kelley, *Gnuplot 4.4: an interactive plotting program*, **2010**. <http://gnuplot.sourceforge.net/>.
- [149] C. Fonseca Guerra, O. Visser, J. G. Snijders, G. te Velde, E. J. Baerends, in *Methods and Techniques for Computational Chemistry*, METECC–5, STEF, Cagliari, pp. 303–395, **1995**; *Amsterdam Density Functional*, Vrije Universiteit Amsterdam, Amsterdam, **2003**.
- [150] a) A. D. Becke, *Phys. Rev. A* **1988**, *38*, 3098–3100; b) J. P. Perdew, *Phys. Rev. B* **1986**, *33*, 8822–8824.
- [151] a) E. van Lenthe, E. J. Baerends, J. G. Snijders, *J. Chem. Phys.* **1993**, *99*, 4597–4610; b) E. van Lenthe, *The ZORA equation*, Vrije Universiteit Amsterdam, Amsterdam, **1996**.
- [152] a) M. Kohout, *Faraday Discuss.* **2007**, *135*, 43–54; b) M. Kohout, *Int. J. Quantum Chem.* **2004**, *97*, 651–658.
- [153] M. Kohout, *DGrid 4.6*, Radebeul, **2009**.
- [154] R. F. W. Bader, *Atoms in Molecules*, Oxford University Press, Oxford **1990**.
- [155] Sandia National Labs, Kitware Inc, Los Alamos National Labs, *Paraview: Parallel visualization application*. <http://paraview.org>, **2008**.
- [156] a) I. Veremchuk, T. Mori, Yu. Prots, W. Schnelle, A. Leithe-Jasper, M. Kohout, Yu. Grin, *J. Solid State Chem.* **2008**, *181*, 1983–1991; b) B. Silvi, A. Savin, F. R. Wagner in: B. Silvi, P. D'Arco (eds.), *Modelling of Minerals and Silicated Materials*, Kluwer Academic, New York **1997**, pp. 179–199; c) S. Raub, G. Jansen, *Theor. Chem. Acc.* **2001**, *106*, 223–232.
- [157] J. Beck, *J. Solid State. Chem.* **1996**, *125*, 165–170.

- [158] J. Beck, private communication.
- [159] V. Kolesnichenko, J. J. Luci, D. C. Swenson, L. Messerle, *J. Am. Chem. Soc.* **1998**, *120*, 13260–13261.
- [160] M. Weisser, S. Tragl, H.-J. Meyer, *Z. Anorg. Allg. Chem.* **2006**, *632*, 1885–1889.
- [161] J. M. Bijvoet, *Nature* **1954**, *173*, 888–891.
- [162] a) H. G. von Schnering, H. G. Wöhrle, H. Schäfer, *Naturwissenschaften* **1961**, *48*, 159; b) M. Ströbele, J. Glaser, A. Lachgar, H.-J. Meyer, *Z. Anorg. Allg. Chem.* **2001**, *627*, 2002–2004; c) T. Duraisamy, A. Lachgar, *Inorg. Chem.* **2003**, *42*, 7747–7751; d) J. R. Kennedy, P. Adler, R. Dronskowski, A. Simon, *Inorg. Chem.* **1996**, *35*, 2276–2282.
- [163] H. V. R. Dias, W. Jin, *Inorg. Chem.* **1996**, *35*, 6546–6551.
- [164] N. E. Brese, M. O’Keeffe, *Acta Crystallogr.* **1991**, *B47*, 192–197.
- [165] K. Jödden, H. G. Schnering, H. Schäfer, *Angew. Chem.* **1975**, *87*, 594–595; *Angew. Chem. Int. Ed.* **1975**, *14*, 570–571.
- [166] K. Jödden, H. Schäfer, *Z. Anorg. Allg. Chem.* **1977**, *430*, 5–22.
- [167] T. C. Zietlow, H. B. Gray, *Inorg. Chem.* **1986**, *25*, 631–634.
- [168] S. Bösch, H.-L. Keller, *Z. Kristallogr.* **1992**, *200*, 305–315.
- [169] J. D. Franolic, J. R. Long, R. H. Holm, *J. Am. Chem. Soc.* **1995**, *117*, 8139–8153.
- [170] M. Ströbele, H.-J. Meyer, *Z. Anorg. Allg. Chem.* **2010**, *636*, 62–66.
- [171] J. Beck, S. Benz, *Z. Anorg. Allg. Chem.* **2010**, *636*, 928–935.
- [172] R. Blachnik, B. Jaschinski, H. Reuter, G. Kastner, *Z. Kristallogr.* **1997**, *212*, 874–877.
- [173] H. Meissner, D. V. Korol’kov *Z. Anorg. Allg. Chem.* **1983**, *496*, 175–185.
- [174] a) B. D. Sharma, D. J. Donohue, *Acta Crystallogr.* **1963**, *16*, 891–897; b) T. Ito, N. Morimoto, R. Sadanaga, *Acta Crystallogr.* **1952**, *5*, 775–782; c) E. J. Porter, G. M. Sheldrick, *J. Chem. Soc., Dalton Trans.* **1972**, 1347–1349; d) P. Goldstein, A. Paton, *Acta Crystallogr.* **1974**, *B30*, 915–920.
- [175] L. Balázs, H. J. Breunig, *Coord. Chem. Rev.* **2004**, *248*, 603–621.
- [176] a) G. Cordier, R. Cook, H. Schäfer, *Angew. Chem.* **1980**, *92*, 310; *Angew. Chem. Int. Ed. Engl.* **1980**, *19*, 324–325.
- [177] a) G. Herzberg, *Molecular Spectra and Molecular Structure II. Infrared and Raman spectra of polyatomic molecules*, D. Van Nostrand Company, Princeton, **1959**; b) G. L. Carlson, *Spectrochim. Acta* **1963**, *19*, 1291–1307.
- [178] E. Mooser, W. B. Pearson, *Phys. Rev.* **1956**, *101*, 1608–1609.

-
- [179] a) G. C. Rodrigues, P. Indelicato, J. P. Santos, P. Patte, F. Parente, *At. Data Nucl. Data Tab.* **2004**, *86*, 117–233; b) F. J. Gálvez, E. Buendia, P. Maldonado, A. J. Sarsa, *Eur. Phys. J. D* 2008, *46-49*, 229–235.
- [180] N. W. Tideswell, F. H. Kruse, J. D. McCullough, *Acta Crystallogr.* **1957**, *10*, 99–102.
- [181] A. Bondi, *J. Phys. Chem.* **1964**, *68*, 441–451.
- [182] S. Schlüter, *Doctoral Thesis*, University of Bonn, Bonn **2004**.
- [183] F. R. Wagner, M. Kohout, Yu. Grin. *J. Phys. Chem. A.* **2008**, *112*, 9814–9828.
- [184] A. Günther, M. Heise, F. R. Wagner, M. Ruck, *Angew. Chem.* **2011**, *in print*.
- [185] M. J. Cohen, L. B. Coleman, A. F. Garito, A. J. Heeger, *Phys. Rev. B.* **1974**, *10*, 1298–1307.

12. Publications

This thesis is based on the following publications:

Journal Publications:

- 1) “*Chemistry of Polynuclear Transition Metal Complexes in Ionic Liquids*”
E. Ahmed, M. Ruck, *Dalton Trans.* **2011**, 40, 9347–9357.
- 2) “*Homo- and Heteroatomic Polycations of Groups 15 and 16. Recent Advances in Synthesis and Isolation Using Room Temperature Ionic Liquids*”
E. Ahmed, M. Ruck, *Coord. Chem. Rev.* **2011**, 255, 2892–2903.
- 3) “*[Sb₁₀Se₁₀]²⁺, a Heteronuclear Polycyclic Polycation from a Room Temperature Ionic Liquid*”
E. Ahmed, A. Isaeva, A. Fiedler, M. Haft, M. Ruck, *Chem. Eur. J.* **2011**, 17, 6847–6852.
- 4) “*An Ionic Liquid Based Single Step Room Temperature Route for the Synthesis of Molybdenum Cluster Compounds*”
E. Ahmed, E. Ahrens, M. Heise, M. Ruck, *Z. Anorg. Allg. Chem.* **2011**, 637, 961–964.
- 5) “*Room-Temperature Synthesis of the Highly Polar Cluster Compound Sn[SnCl][W₃Cl₁₃]*”
E. Ahmed, M. Groh, M. Ruck, *Eur. J. Inorg. Chem.* **2010**, 5294–5297.
- 6) “*A Facile Route for the Synthesis of Polycationic Tellurium Cluster Compounds: Synthesis in Ionic Liquid Media and Characterization by Single-Crystal X-Ray Crystallography and Magnetic Susceptibility*”
E. Ahmed, E. Ahrens, M. Heise, M. Ruck, *Z. Anorg. Allg. Chem.* **2010**, 636, 2602–2606.
- 7) “*Raumtemperatursynthese von BiCl[Mo₅Cl₁₃] in Ionischer Flüssigkeit*”
E. Ahmed, E. Ahrens, M. Heise, M. Ruck, *Z. Anorg. Allg. Chem.* **2010**, 636, 2053.
- 8) “*Room-Temperature Synthesis of Bismuth Clusters in Ionic Liquid and Crystal Growth of Bi₅(AlCl₄)₃*”
E. Ahmed, D. Köhler, M. Ruck, *Z. Anorg. Allg. Chem.* **2009**, 635, 297–300.

Conference Publications:

- 1) “*Synthesis of Inorganic Materials using Room Temperature Ionic Liquids: a Green Chemistry Approach*” (oral presentation).

E. Ahmed, M. Ruck, *Book of Abstracts*, 9th Green Chemistry Conference. 14-16 September, 2011 Madrid, Spain.

2) “*Raumtemperatursynthese von BiCl[Mo₅Cl₁₃] in Ionischer Flüssigkeit*” (poster presentation).

E. Ahmed, E. Ahrens, M. Heise, M. Ruck, *Book of Abstracts*, 15th Conference on Solid State Chemistry and Material Research. 20-22 September, 2010 Berlin, Germany.

3) “*Low-Temperature Synthesis of Inorganic Materials from Ionic Liquids: Soft and Sustainable Chemistry*” (oral presentation).

E. Ahmed, M. Ruck, *Book of Abstracts*, 3rd European Chemistry Congress. 29 Aug-02 September, 2010 Nürnberg, Germany.

4) “*Synthesis of Bismuth and Tellurium Sub-valent Cluster Compounds at Room-Temperature*” (poster presentation).

E. Ahmed, D. Köhler, M. Ruck, *Book of Abstracts*, 6th International Conference on Inorganic Materials. 28-30 September, 2008 Dresden, Germany.

5) “*Synthesis and Characterization of Main Group Sub-valent Cluster Compounds*” (oral presentation)

E. Ahmed, D. Köhler, M. Ruck, *Book of Abstracts*, 6. Mitteldeutsches Anorganiker-Nachwuchs-Symposium. 22 September, 2008 Freiberg, Germany.

Versicherung

Hiermit versichere ich, dass ich die vorliegende Arbeit ohne unzulässige Hilfe Dritter und ohne Benutzung anderer als der angegebenen Hilfsmittel angefertigt habe; die aus fremden Quellen direkt oder indirekt übernommenen Gedanken sind als solche kenntlich gemacht. Die Arbeit wurde bisher weder im Inland noch im Ausland in gleicher oder ähnlicher Form einer anderen Prüfungsbehörde vorgelegt.

Die vorliegende Arbeit wurde am Institut für Anorganische Chemie der Technischen Universität Dresden unter wissenschaftlicher Betreuung von Herrn Prof. Dr. Michael Ruck im Zeitraum von April 2007 bis Juni 2011 angefertigt.

Es haben keine früheren erfolglosen Promotionsverfahren stattgefunden. Hiermit erkenne ich die Promotionsordnung der Fakultät Mathematik und Naturwissenschaften der Technischen Universität Dresden vom 23.02.2011 an.

Dresden, den 22. Jun 2011

Ejaz Ahmed

Curriculum Vitae

Ejaz Ahmed

^a Department of Chemistry and Food Chemistry

Dresden University of Technology Dresden, Germany

^b Max-Planck Institute for Chemical Physics of Solids Dresden, Germany

ejazsaab@yahoo.com

Tel: +49 351-46333649

Personal Data

Name	Ejaz Ahmed
Date of Birth	06/07/1978
Email	ejazsaab@yahoo.com
Nationality	Pakistani
Religion	Islam
Current Address	Budapester Strasse 39, 01069 Dresden, Germany

Education

2007 - 2011	PhD (Inorganic Chemistry) Dresden University of Technology Dresden, Germany
2004 - 2006	M.Phil (Analytical chemistry/Inorganic Chemistry) Quaid-i-Azam University Islamabad, Pakistan
2002 - 2004	M.Sc (Analytical Chemistry/Inorganic Chemistry) Quaid-i-Azam University Islamabad, Pakistan

Work Experience

2007 – 2011	Research Assistant Chair of Inorganic Chemistry II Dresden University of Technology, Germany
2004 - 2006	Research Assistant Department of Inorganic and analytical Chemistry Quaid-i-Azam University Islamabad, Pakistan
2004 - 2006	Lecturer Shah Institute of Sciences Rawalpindi, Pakistan